Department of Precision and Microsystems Engineering

Optical fibre precision positioning at cryogenic conditions

Rudi Smits

Report no : 2023.084 Coach : H. Kooiman
Professor : Dr. N. Bhattacharya
Specialisation : MSD

Type of report : Master Thesis

: Friday 29th September, 2023 Date







Optical fibre precision positioning at cryogenic conditions

For the degree of Master of Science in High-Tech Engineering at Delft University of Technology

Rudi Smits

Friday 29th September, 2023

Student number: 4653319

Project duration: December 2022 - September 2023

Thesis committee: Dr. N. Bhattacharya TU Delft

M.K. Ghatkesar TU Delft

H. Kooiman Single Quantum

Faculty of Mechanical, Maritime and Materials Engineering (3mE) · Delft University of Technology

Cover: Single Quantum 24 channel system, by Single Quantum

An electronic version of this thesis is available at http://repository.tudelft.nl/.



Preface

This report is the master thesis on the design and testing of a cryogenic precision actuator. It has been written to obtain the master degree of Mechanical Engineering at the TU Delft. This setup was designed for and in cooperation with Single Quantum. I was researching, designing and testing the setup from December 2022 to September 2023.

During my master I discovered that working on something with a practical application interested me a lot more than theoretical topics. This is the reason why I wanted to do my master thesis at a company. Mechanical systems interested me the most during my study, so I was really happy that Single Quantum has a mechanical issue that I could tackle as my master thesis. They wanted to continue their research on actively positioning the optical fibre with respect to the detector. This required the design of a cryogenic actuator with a positioning resolution in the nano meter range, which should fit inside the small space of their radiation shield.

The readers who are interested in the background of the final design can read chapter 2 to chapter 4. And chapter 5 and chapter 6 are interesting for the readers who want to know about the result of the test.

And thank you for your interest in my thesis. I hope you enjoy your reading.

Rudi Smits Delft, September 2023

Abstract

Single photon detectors are an important optical sensing tool in many industries. However, these highly efficient detectors suffer from variations in the size of an optical cavity when cooling down to 3K. An active positioning system is therefore required to correct the relative position of the fibre to the detector, so an optimal and reproducible cavity size can be achieved, thereby maximizing their efficiency. The literature study performed on cryogenic precision actuators showed that a stepper motor in combination with a motion reduction mechanism is the most feasible design. A stepper motor and a precision screw were two fundamental components of the preliminary design, so their lubrication was removed and were proven to work cryogenically. The rest of the design was based around these fundamental components. Room temperature tests were done to show the functionality of the design and it showed a positioning resolution between 10 nm and 30nm with just a 100nm loss of motion when unloading and loading the system. Cryogenic tests achieved similar results and it showed that the reflected power of a detector was reduced from 8.8% to 3.6%, indicating that the maximum achievable detector efficiency increased from 91.2% to 96.4%.

Acknowlegdement

This endeavor would not have been possible without all the resources that Single Quantum made available to me. They provided materials and personal assistance. The latter especially from my daily supervisor Hugo who was always willing to help out if needed. Also many thanks to Ron who helped out with metalworking and wiring. I am deeply indebted to Nandini Bhattacharya for her guidance and tips, which made the whole process go smoothly and without stress.

I am also grateful for others at Single Quantum for helping out with issues I've encountered and other pressing questions. Special thanks to Harmen, Jorgis and Emil for helping out in the lab. Thanks should also go to Andreas and Sander for allocating budget to the project, making the setup possible. Also many thanks to Walter for making my life so much easier in controlling the Arduino and stepper motor

I would be remiss in not mentioning the PhD's Ali Amoozandeh Nobaveh and Inge van der Knijff for discussing the general direction of the Thesis with me. I'd also like to acknowledge Lyuben Davidov for his input on interferometry. Lastly I'd like to mention Sophia for having put up with my struggles and complaints for the past 10 months.

Contents

Pro	Preface						
AŁ	Abstract						
No	Nomenclature vii						
1	Introduction 1						
2	Background 2.1 Working Principles of SNSPD's 2.1.1 Cryostat 2.1.2 Driver 2.1.3 Superconducting Nanowire 2.2 Challenges of Fibre Positioning 2.2.1 Optical Cavity 2.2.2 Assembly Process 2.2.3 Movement of Ferrule 2.3 State of the Art 2.3.1 Know Fibre Alignment Techniques 2.3.2 System Requirements 2.3.3 Cryogenic Precision Actuators 2.3.4 Motion Transmission 2.3.5 Positing Feedback 2.3.6 James Web Space Telescope Nanoactuator 2.3.7 Previous Experiments by Single Quantum 2.4 Conclusion on the State of the Art	3 3 3 4 4 5 5 6 6 7 8 8 9 14 16 17 18 20 20 20 20 20 20 20 20 20 20 20 20 20					
_	2.5 Design Objective	20					
3	Testing of Crucial Components 3.1 Making a Cryogenic Stepper Motor 3.1.1 Hardware Selection 3.1.2 Wiring 3.1.3 Arduino Code 3.1.4 Modifying and Testing Process 3.1.5 Position Feedback 3.1.6 Cleaning the Bearings 3.1.7 Issues that Occurred 3.2 Making a Cryogenic Precision Screw 3.2.1 Production Tolerances 3.2.2 Issues that occurred 3.3 Speeding up Design Iterations 3.4 Expert Meeting	22 22 24 24 25 26 28 29 30 31 32 32 32					
4	Design Process 4.1 Worm Gear Selection	33 34 35 36 37 39 40 43					

Contents

	4.8		15
	4.9	1 0	1 5
		U	1 5
		o	17
			17
	4.10		18
			18
			18
		J	19
			1 9
			50
	4.11		50
		O .	50
			50
			51
	4.12	Design Process Discussion and Evaluation	51
5	Syst	em Testing at Room Temperature	53
	5.1	About the Setup	53
	5.2	Determining the Fibre Position	54
	5.3	First Warm System Test	55
	5.4	1	56
	5.5		57
			59
	5.6	1	50
	5.7		50
			60
		11	51
		1 1	62
	5.8	Hysteresis and Backlash	54
6	Syst	rem Testing at 3K	66
	6.1		66
	6.2	Plotting Absorption	66
	6.3	Cryogenic Issues	57
	6.4	First Cold System Test	68
			58
		6.4.2 Second Positioning Experiment	59
		6.4.3 Third Positioning Experiment, Efficiency Test	71
	6.5		71
		O	71
		0	72
	6.6	Reducing the Temperature	73
7	Disc	cussion	74
0			7.0
8	Con	clusion	76
Re	feren	ices	77
A	Rese	earch Plan	32
	A.1	Plan 1	32
			33
B	D ₇ , ₄ L	on and Arduino Codo	34
ע	B.1		34 34
	B.2		54 34
	B.3	O Company of the comp	35
	B.4	1	35 35
	B.5		33 37
	···		/ 1

Contents

C	B.6 Direct motor control V1.0 B.7 ByteArray B.8 Direct motor control V1.1 Mail contact C.1 Mail Send to Thorlabs C.2 Reply from Thorlabs	90 93 93
	C.3 Mail received to Amatec	94 94 95
D	ISO 2768 Tolerances	96
Е	Fibre PositionE.1Second Warm TestE.2Third Warm Test 1E.3Third Warm Test 2E.4First Cold System Test, Test 1 Motor InputsE.5First Cold System Test, Test 2 Motor Inputs	98 99
F	Quick User Manual of System	104
G	CAD Drawings	106

Nomenclature

Abbreviations

Abbreviation	Definition			
SNSPD	Superconducting Nanowire Single Photon Detector			
SQ	Single Quantum			
PCB	Printed Circuit Board			
DBR	Distributed Bragg Reflector			
SDE	System Detection Efficiency			
PZT	Lead Zirconate Titanate			
MEMS	Micro-ElectroMechanical Systems			
VCA	Voice Coil Actuators			
HPR	High Precision Reducers			
JWST James Web Space Telescope				
LVDT Linear Variable Displacement Transformer				
RT	Room Temperature			
LN	Liquid Nitrogen			
FEM	Finite Element Method			
DOF	Degree Of Freedom			
PTFE	Polytetrafluoroethylene			
MoS2	Molybdenum Disulfide			
DBTT	Ductile to Brittle Transition Temperature			
SMP Sub miniature push-on (connector)				
SMA	SubMiniature version A (connector)			
CTO	Chief Technical Officer			

\int

Introduction

The utilization of Superconducting Nanowire Single Photon Detectors (SNSPDs) has become indispensable in various applications such as bio-imaging, lidar, and quantum communication.[1] It allows for deeper measurements in biological samples, and for reading encoded information on the different degrees of freedom of the photon, including polarization, momentum, time and energy. SNSPDs can measure disturbances in the superconductive state of the nanowire by incoming photons with high count rates and low jitter and dark counts.[2] One of the companies leading in this field is Single Quantum. They were among the first companies to design and commercialize SNSPDs. The performance of the detectors used depends on maintaining a cavity of 1/4 of the wavelength between the detector and the end face of the optical glass fibre, preventing destructive interference. However, changes occur in the optical cavity size during the cooldown from room temperature to 3 K. These changes cause a drop in efficiency of 15% which is significant for high-end detectors now reaching efficiencies of 99.5%.[3] This is especially relevant for quantum communication where multiple entangle photons need to be detected. When for example 8 entangled photons are detected with a detector with an efficiency 85%, that means for measuring all the photons there is a total system efficiency of 27% is achieved. This significantly increases to a total system efficiency of 43% of the detector has an efficiency of 90%. However, these highly efficient detectors are hard to reproduce due to the uncertain movement. Passive forms of maintaining the fibre position have already been tried, like gluing, clamping and spacers. None of these solutions was able to make the fibre position predictable enough. Therefore, there is the wish to actively position the fibre.

That sets the aim of this thesis on design a cryogenic precision actuator which is able to correct for deviations of the fibre position. It should have nanometer positioning resolution and fit inside the 3K radiation shield. Such a position system will take away the uncertainties during the cooldown, thereby drastically speeding up the production and assembly process with reproducible highly efficient detectors. Single Quantum already tried to position a fibre, but this actuator wasn't scalable due to its tremendous costs. An important focus of the design is thus its cost effectiveness. This means reworking common parts to make them work cryogenically.

To get feedback on if the actuator is moving the fibre according, the absorption and reflection properties of the detector can be used. The detector should have maximum absorption at a wavelength at 1550 nm when the fibre is in its optimal position. This also means that there is a minimum in reflected power at this wavelength. When projecting a broadband laser on the detector and analyzing the reflected light, there should be a minimum visible at 1550 nm since more light should be reflected at different wavelengths. A simulation of the optimal position is shown in Figure 1.1a. This shows the relative absorption, transmission and reflection over the wavelength range of 1200 nm to 1700 nm. There is an absorption peak at 1550nm and the reflection shown by the red line shows a minimum. This reflected power is something that can be measured, and changes for different fibre positions. When the fibre is too close the reflected spectra is more a plateau with a higher reflected power as can be seen

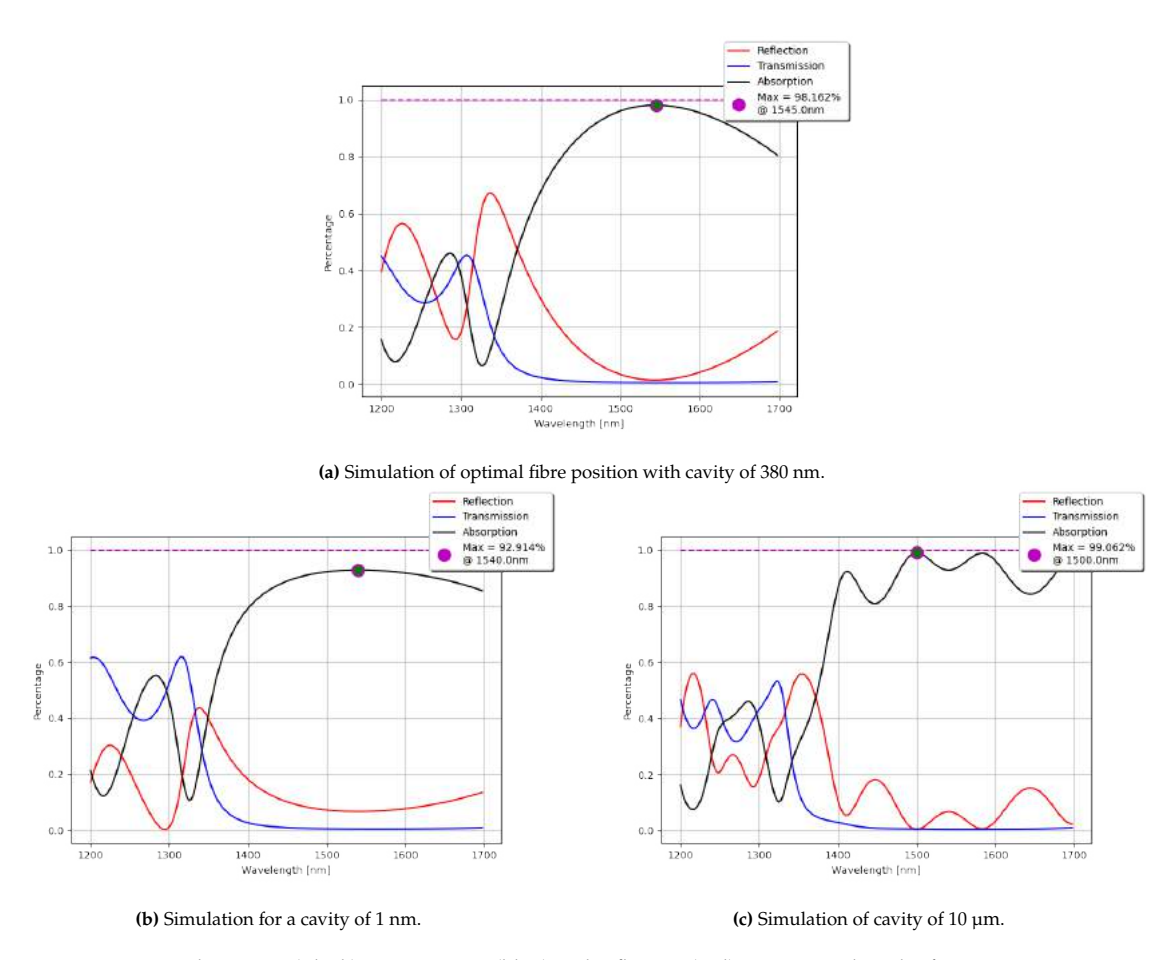


Figure 1.1: Absorption (Black), transmission (blue) and reflection (red) over a wavelength of 1200-1700 nm.

in Figure 1.1b. When the fibre is too far away, a sinusoidal can be observed where a higher frequency corresponds to a larger distance between the fibre and the detector. A simulation with a cavity size of 10 micron is shown in Figure 1.1c which shows that the maximum absorption is no longer at 1550 nm. The shape of the reflected power can tell a lot about the fibre position and if and how the fibre is moving. This represents the primary method for obtaining feedback on the fiber's position during system testing.

This thesis is set out as follows. First, chapter 2 gives background information on working principles of SNSPD's, the issue of fibre positioning, and it covers the current state of the art of cryogenic positioning. Next in chapter 3 the most essential components are cryogenically tested to show their functionality. The rest of the design is designed around these components and the design process is described in chapter 4. First the design is tested at room temperature and the results are reported in chapter 5. Next in chapter 6 the results of the cryogenic test are described. The design process and results are discussed in chapter 7 and in chapter 8 the thesis is concluded. At the end of the report are the appendices for further reading and extra background info.

2

Background

The usage of Superconducting Nanowire Single Photon Detectors (SNSPDs) has become an essential tool for bio-imaging, lidar and quantum communication.[1] It allows for deeper measurements in biological samples, and for reading encoded information on the different degrees of freedom of the photon, including polarization, number stage, momentum, time and energy. SNSPDs can measure disturbances in the superconductive state of the nanowire by incoming photons with high count rates and low jitter and dark counts.[2] One of the companies leading in this field is Single Quantum. They were among the first companies to design and commercialize SNSPDs. The performance of the detectors used depends on maintaining a cavity of 1/4 of the wavelength between the detector and the end face of the optical glass fibre, preventing destructive interference. However, changes occur in the optical cavity size during the cooldown from room temperature to 3 K. These changes cause a drop in efficiency of 15% which is significant for high-end detectors now reaching efficiencies of 99.5%.[3] The industry is asking for highly efficient detectors, but these detectors are hard to reproduce due to the uncertain movement. Passive forms of maintaining the fibre position have already been tried, like glueing, clamping and spacers. None of these solutions was able to make the fibre position predictable enough. Therefore there is the wish to actively position the fibre.

This research aims to investigate the current state of the art high precision positioning systems to lay the foundation for further work on such a system to correct the fibre position. Such a position system will take away the uncertainties during the cooldown, thereby drastically speeding up the production and assembly process with a reproducible highly efficient detectors. This literature review goes in-depth into the state of the art of the different parts of a nanopositioning system.

First are the working principles of SNSPD's discussed in section 2.1 to lay out the background knowledge about SNSPD's. Thereafter, section 2.2 discusses the specifics of the problem at hand showing what kind of system is needed. Knowing this, the related state of the art is discussed in section 2.3 ending with the objective of the research in section 2.5.

2.1. Working Principles of SNSPD's

To be able to detect single photons, one must create a very low disturbance environment, and have the hardware to be able to count and measure the disturbance from a single photon, also while minimizing the timing jitter and the dark counts.

The system that can perform this task is the EOS system from Single Quantum, shown in Figure 2.1a. It comprises of the cryostat and the driver. These convert the weak optical signal to an electrical.

2.1.1. Cryostat

The cryostat has a FC/PC optical attachment points on the front panel. One of these inputs would lead to a Printer Circuit Board (PCB) inside the cryostat, with a coax cable for the output signal. Older EOS versions shown in Figure 2.1a had 8 of these so-called 'channels' with current systems having 24. These optical glass fibres lead the optical signal directly into the vacuum chamber of the cryostat and attach to the PCB on the 3 K cold finger as seen in Figure 2.1b. On the PCB's there is a sleeve which couples precisely to the ferrule of the optical glass fibre. This cancels out any X and Y error with an accuracy of

a few μm , and leaves the attachment with two degrees of freedom, which is generally well clamped due to its press fit. A closeup of one PCB can be seen in Figure 2.1c. The glass fibre has a diameter in the range of 10 μm , which is placed above the SNSPD. The core and the cladding of the fibre usually have a misalignment of 1 μm causing some misalignment in the X and Y axis but won't cause significant problems.[4] The incoming photon disrupts the superconducting state of the nanowire, of which the electrical signal can be read via a coax cable running from the PCB to the output ports of the cryostat. This can in turn be hooked up to the driver.







(a) 8 channel system.

(b) 8 detectors inside cryostat.

(c) PCB closeup.

Figure 2.1: EOS System of Single Quantum.

2.1.2. Driver

The driver translates the output signal of the cryostat to one that can be read by the computer. It converts the signal first to voltage 'clicks'. Each photon thus creates its own voltage pulse. If it exceeds a certain set threshold of the driver, it is counted by the counting electronics. The system can count these clicks at 50-80 MHz. The counts from all these clicks are then converted to a signal that can be read by the computer program, and the photon counts can be seen real time on the screen. The driver is not able to accurately measure the jitter. These measurements are done with an oscilloscope to achieve picosecond accuracy.[4, 5]

2.1.3. Superconducting Nanowire

The physics happening in the nanowire makes the detection of single photons possible. It is built up on a wafer layer by layer. A schematic of an overview of a SNSPD can be seen in Figure 2.2a. The starting point is a silicon wafer, on which the distributed bragg reflector (DBR) is deposited. This optimizes the absorption for a set wavelength. Metal reflectors are also possible.[2] Next, the nanowire is deposited on top of the DBR. This nanowire has usually a thickness of 5-10 nm and a width of around 80 nm. A TEM image of the top layers of the chip can be seen in Figure 2.2b with a closeup of the nanowire in Figure 2.2c.

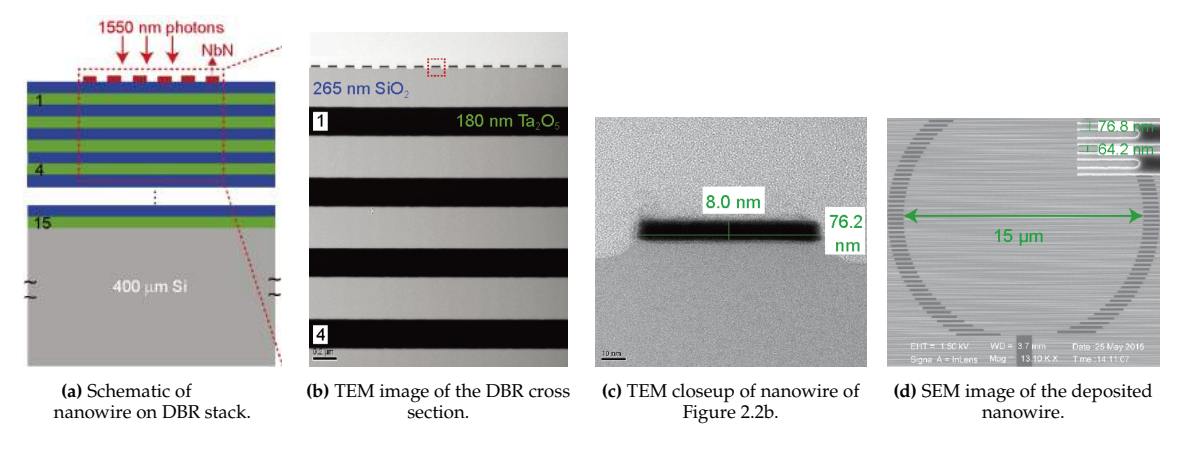


Figure 2.2: Overview of nanowire design and layers[6].

The chip is covered with a close meander of the nanowires to maximize the surface area of the nanowire. The industry often uses a meander pitch of around twice the width of the nanowire. A circle

filled with meanders is created to make an active area with diameters in the range of $10-20 \mu m$, as seen in Figure 2.2d. A larger area would mean more dark counts and a longer recovery time due to it being limited by the kinetic inductance. [2, 7]

Figure 2.3 shows 6 steps of the detection mechanism. The nanowire is in a steady superconducting state (SS), with a direct current, the bias current, flowing through the wire. The current bias is just below the critical current. A (near) infrared photon impacts the wire (I) and leads to the formation of a normal-conducting part of the strip (III). The current is redirected, and the wire can restore to its superconducting state (IV). The current returns (V) and eventually restores to its steady state. The recovery time is usually in the order of tens of nanoseconds, with some detectors having a very fast recovery time (1<ns).[2, 7]

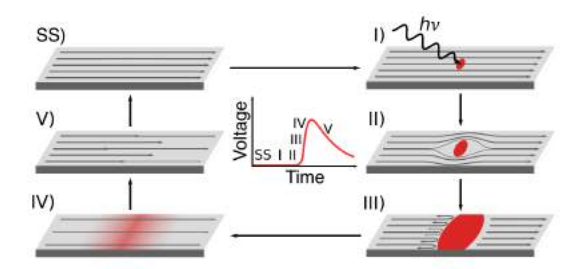


Figure 2.3: Local heating do to impacting photon [2].

A surrounding magnetic field can also influence the superconducting state. The nanowire will fall out of its superconducting state when either the temperature is above the critical temperature, or the magnetic field exceeds the critical magnetic field, as seen in Figure 2.4.[8] When using an alloy, there is not a sharp transition, but rather a transition region with a mixture of normal and superconducting. The impact of an electric field is not researched yet, but it is known that there was an increase in dark counts during experiments with the Attocube as will be discussed in subsection 2.3.7. It could have also originated from the shared ground with the detector.

The lesson here is to keep magnetic and electrical sources close to the nanowire to a minimum.

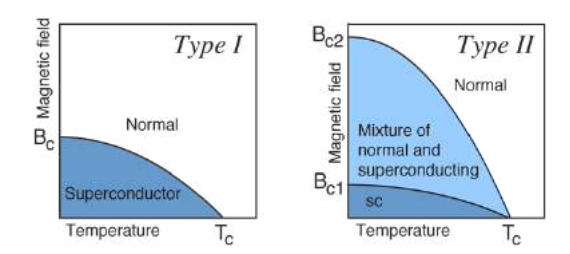


Figure 2.4: Critical Magnetic Field [8].

2.2. Challenges of Fibre Positioning

SNSPDs have been extremely optimized in the past decade. An optical cavity was introduced to get better absorption. This solved one problem but introduced another. Here the optical cavity and the assembly process are briefly discussed. subsection 2.2.3 elaborates on the unwanted movement in the current design and comes up with a hypothesis of the relative moment.

2.2.1. Optical Cavity

The introduction of an optical cavity improved the efficiency, which was limited by reflection from and transmission through the device.[9] It used a cavity behind the nanowire, with a mirror reflecting the lost light back onto the nanowire. The current design of the cavity is to have a gap between the fibre and the nanowire, with a DBR stack below the nanowire as discussed in subsection 2.1.3, as seen in Figure 2.2a. The size of the optical cavity is one-fourth of the wavelength to prevent destructive interference. One of the current designs to maintain the cavity size is with spacers as seen in Figure 2.5a. Next to the SNSPD a spacer is deposited to maintain the optimized cavity for the chosen wavelength.

If one assembles the system, the fibre presses against the spacer and a constant distance is achieved, theoretically.

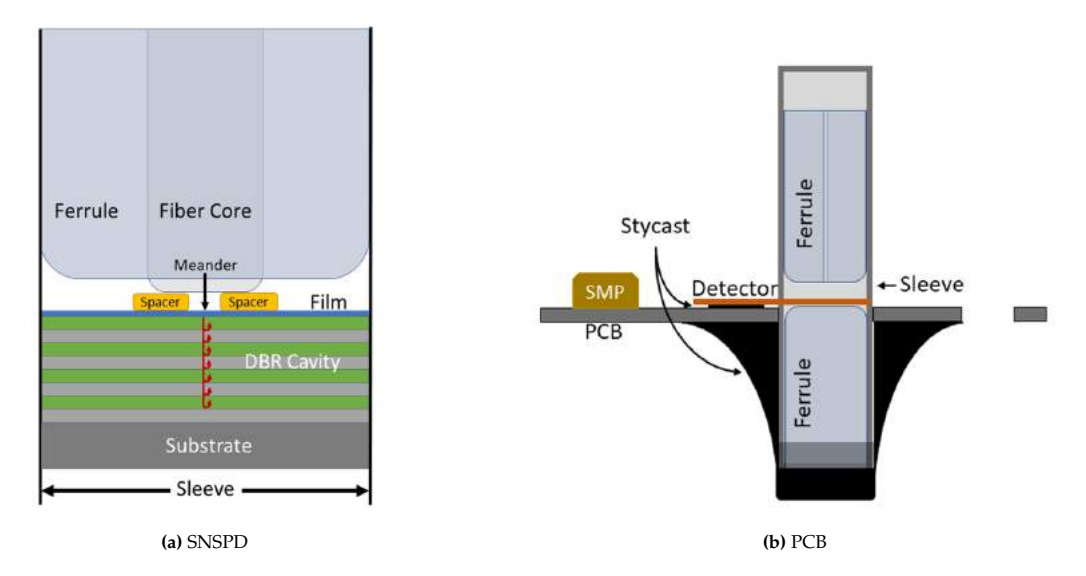


Figure 2.5: Schematics of cross section.

2.2.2. Assembly Process

The way the PCB is assembled is important in understanding the problems that will arise later in the process. A zirconia sleeve is inserted into the PCB. Two zirconia Ferrules are inserted on either side of the sleeve, with the SNSPB in between the two ferrules. The bottom ferrule is glued into place with STYCAST[10], a conductive epoxy. The SNSPD is glued by the tip with a small amount of STYCAST and is then soldered to the PCB. The top ferrule is removed, and the PCB is ready for assembly. The ferrule with the fibre is later on in the assembly process plugged in. A schematic of this can be seen in Figure 2.5b

2.2.3. Movement of Ferrule

The System Detection Efficiency (SDE) of high-end systems are usually around 85-95%. After the first tests of high performing detectors, it is common for them to have a lower efficiency. This reduction in efficiency could eventually be explained by a shift of the optical cavity. The fibre distance relative to the detector would change, shifting the optimal wavelength for the cavity. The distance between the fibre and the SNSPD can be estimated by looking at the absorption spectrum, as seen in Figure 2.6. The optimal peak shifts to a different wavelength. Usually, the system is operated at a set wavelength, so it would reduce the efficiency by 10-20%. N.B. the system still has a relatively high efficiency peak, however not at the desired frequency. This makes it relatively easy to increase the system efficiency by tuning the tuneable laser to the optimal frequency. This explains some lucky cases with extremely high efficiencies where the optimal laser wavelength was chosen for a certain PCB.[3] The reality is however that the frequency of the system is fixed, and that the SDE peak should be as close as possible.

The gap inbetween the film and the fibre is the only thing that is not fixed, so a likely cause of the movement. During many experiments was the absolute distance derived from the spectra measured. The initial distance (W1) was compared to the cold distance (C1), but also to the distance after the warmup (W2). The data showed almost in all cases positive cold shift (W1 - C1), so the fibre would come closer to the detector. The warm shift (W2 - W1) was predominately positive, but also negative cases occurred. These cases were largely uncorrelated. When the system was cycled another time, it showed that the second warm shift (W2 - W3) had a much smaller spread and was more predictable. It was however uncorrelated to the reprehensibility of the cold distance and vice versa. However, the cold distance itself became very reproducible (C1 = C2).

With the data from this experiment was a hypothesis formed. When cooling down, the cavity decreases in size, with a larger increase after the warmup. When the sleeve shrinks over de cooldown, the fibre and the ferrule presses down on the spacer, resulting in a normal force F_{spacer} upwards with an

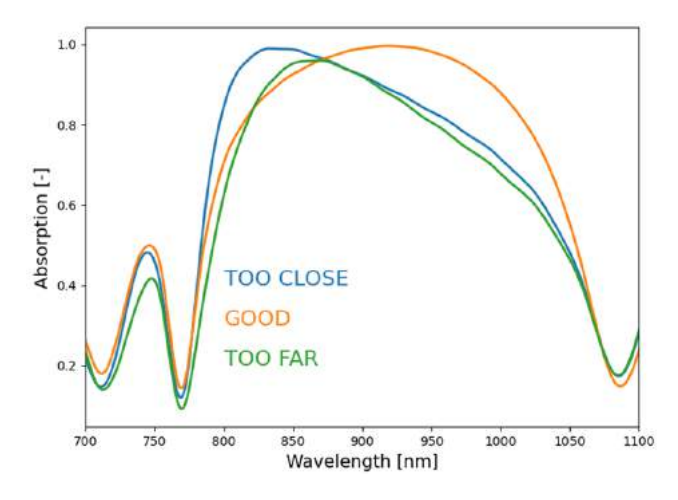


Figure 2.6: Absorption at different wavelengths.

equal and opposite force F_{fibre} . This force is transferred to the walls of the sleeve via the friction force $F_{friction}$ with the opposite reaction force F_{slip} . When this force exceeds the maximum force $F_{frictionMAX}$, the ferrule slips in the sleeve. After the warmup, this leads to an increased warm distance (W2 > W1). This is shown schematically in Figure 2.7

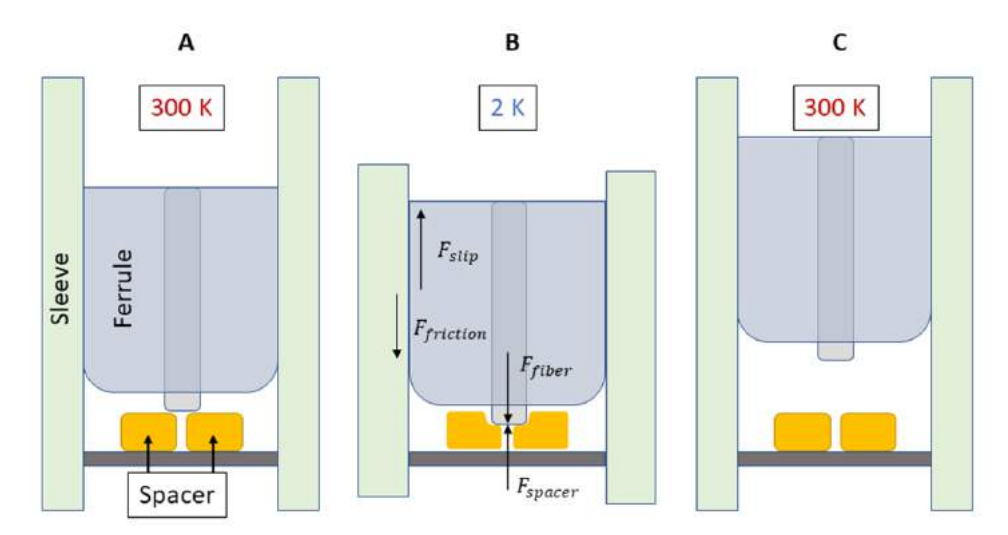


Figure 2.7: Hypothesis ferrule movement.

The hypothesis doesn't unfortunately cover all cases. There are a handful of cases where the warm distance decreased, but also where the cold distance is significantly smaller than the gold spacer which elastically deformation and thermal shrinkage cannot account for.[11] But the key takeaway still holds. The ferrule moves in the sleeve, making the cold distance hard to predict, in turn influencing the efficiency.

Therefore, there is a wish to actively control the fibre distance to the detector, to get better control and reproducibility of the cold distance and get rid of the largely uncorrelated behaviour between *W*1 and *C*1.

2.3. State of the Art

Nanopositioning systems are not limited to one design. There are many different actuators, combined with different motion transmission and feedback devices. The goal is to find the optimal combination of these parts. To start, the known fibre alignment techniques are discussed with thereafter the general system requirements of the actuator. This makes it possible to evaluate the performance of different actuators, motion transfer mechanisms and positioning feedback sensors. Thereafter, the example of the

James Web Space Telescope nanoactuator is discussed, and the previous experiments on active fibre positioning are discussed. Lastly, an outlook is given for the future direction of this project.

2.3.1. Know Fibre Alignment Techniques

The technique of coupling photons to an SNSPD with an optical fibre is an obvious choice, but it comes with several drawbacks. It is challenging to focus the optical spot on the SNSPD active area of around $10 \times 10 \, \mu m$. It is possible to use single-mode fibres[12, 13] or lenses for optical coupling.[14, 15] These methods are however sensitive to temperature differences which can cause optical misalignment.[1] To limit these uncertainties, one could actively align the optical fibre with the active area. Back in 2006 there were already experiments to actively align fibres with micro-actuators to the SNSPD.[9]

In 2011 the industry adopted a new technique to align a single-mode optical fibre to the SNSPD.[16] The design, fabrication, and demonstration of a low-loss, cryogenic-compatible, low-cost, easy, and reproducible solution was presented by Shigehito et al.(2011)[17]. There was no patent on the design, so the industry quickly adapted it. Single Quantum also uses this coupling technique with a zirconia sleeve.[18, 19]

Parallel to that there were also different experiments with optical cavities to increase the coupling efficiency. A cavity behind the nanowire with a reflective surface behind it was demonstrated.[9, 20] Also, the functionality of an optical cavity between the fibre and the nanowire was demonstrated.[15]

In 2020 the previous was all combined in one design.[21] It used a single-mode fibre with an optical cavity between the fibre and the nanowire. New in this design was the fibre spacers on either side of the active area, as can be seen in Figure 2.8, and is patented by Single Quantum.[22]

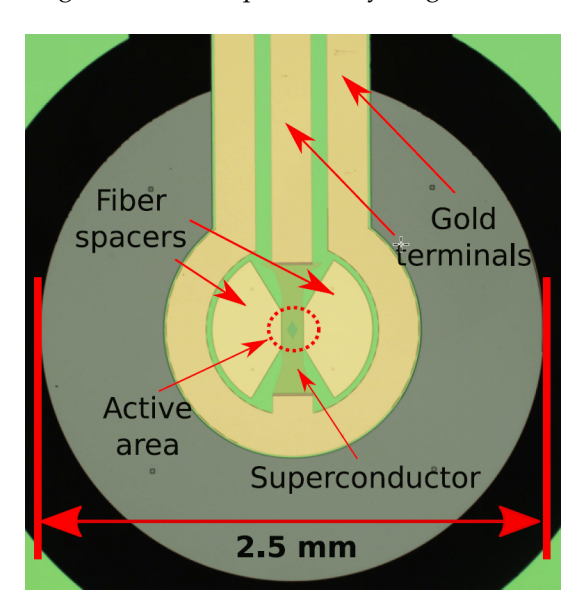


Figure 2.8: SNSPD Top view, reprinted from [21].

2.3.2. System Requirements

Here are the systems requirements elaborated, to get to know which actuators and mechanisms could work. It should first of all be as compact as possible. The more actuated systems fit in the cryostat, the better. It should also have a low heat load to comply with the cryogenic environment since it will be operated at 3 K. The actuation force needs to be around 20 N, as will be discussed later in subsection 2.3.7. The stroke should be large enough to stay within the assembly and cooldown inaccuracies. The positioning resolution should be 10 nm. The actuator should be fixated after tuning and should not drift more than 10 nm per 10.000h, to prevent tuning during continuous operation. Lastly, the system needs to control just one degree of freedom, with a low unit cost of the total system.

- Compact (max 79 mm x 39^ø mm)
- Low continuous heat loading (< 15 mW)
- Cryogenic capabilities (3 K)

- High force (>20 N)
- $Range_{min}$ (>5 µm)
- $Range_{optimal}$ (>50 µm)
- Positioning accuracy (10 nm)
- Low drift (< 10 nm / 10.000 h)
- 1 degree of freedom
- Low unit costs

A leading requirement is the positioning resolution of the system. This largely depends on how sensitive the efficiency is to a shift in position. The efficiency of the system as a function of the relative fibre position and wavelength is plotted in Figure 2.9a for a $1/4\lambda$ wavelength. Note that this simulation uses a cavity of 1/4th of the wavelength and a gold mirror to reflect the light back to the light sensitive meander. The efficiency goes multiple times near to unity for different gap sizes of a certain wavelength. The light diverges however when leaving the fibre, so the peak at the lowest gap gives the highest efficiency, which is at 1/4 of the wavelength. This showed that a positioning resolution of 10 nm is required.

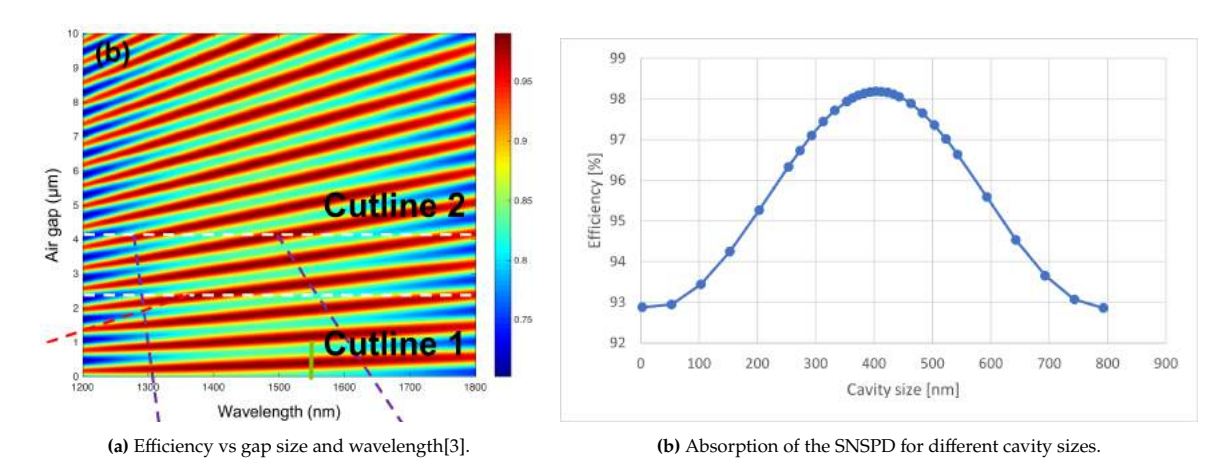


Figure 2.9

The required positioning resolution was extra researched to know the acceptable positioning resolution. Single Quantum has a simulation software which simulated the light on the SNSPD. Different materials and layer thicknesses of the SNSPD can be simulated with this tool to optimize the absorption of the SNSPD. The optical cavity is also included in the tool. This made it possible to make a 2D plot of the cavity size vs the absorption, which is shown in Figure 2.9b. This is thus a cross section of a small part in Figure 2.9a shown with the green line at 1550 nm running from 0 to 0.8 micron.

Putting the values in a Table 2.1 showed that the top part of the bell curve is around 100 nm wide, with a loss of absorption of a maximum of half a percent. It is preferred that the loss doesn't go above this level, setting the minimum positing resolution of 100 nm.

The default cavity size was set to 393 nm, and this was used as a baseline for the other values. Note that the peak is actually at 403 nm in this simulation.

Efficiency versus Absorption It needs to be noted that there is a clear distinction between efficiency and absorption. Figure 2.9a shows the efficiency for different cavity sizes and Figure 2.9b shows the absorption for different cavities. There is a small distinction between the two. The efficiency is partially determined by absorption, but also by the characteristics of the detector. An absorbed photon still needs to be able to be detected. The efficiency is thus limited by the absorption of the detector, but is not equal to it.

2.3.3. Cryogenic Precision Actuators

There are many different actuators which can theoretically achieve the required positioning resolution. The actuators' force and stroke can be exchanged with the help of transmission mechanisms. So,

Cavity [nm]	Absorption @1550 [%]	Δ %
333	97.716	0.456
353	97.936	0.236
363	98.021	0.151
373	98.089	0.083
383	98.14	0.032
393	98.172	0
403	98.186	-0.014
413	98.181	-0.009
423	98.158	0.014
433	98.117	0.055

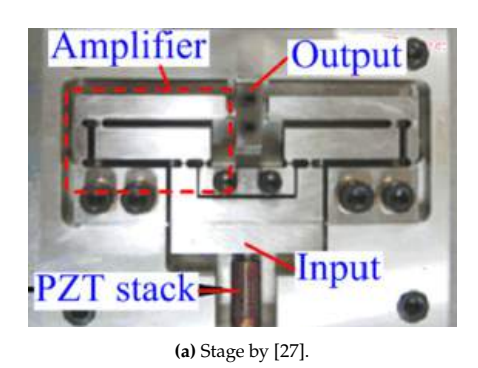
Table 2.1: Absorption for different cavity sizes.

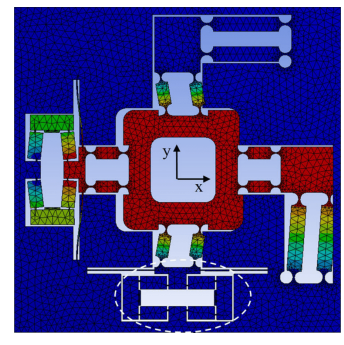
one needs to evaluate an actuator in combination with the right mechanisms on if it will meet the requirements. For the actuators holds in general, that if they are compact enough and can operate at cryogenic conditions with nanometer precision, they will be able to meet most requirements. Actuators which have this possibility are piezoelectric actuators, Micro-electromechanical systems (MEMS), or electrical motors. All actuator types and their subcategories will be looked into and evaluated.

Piezoelectric Actuators

Piezoelectric actuators utilize the piezoelectric effect of the noncentrosymmetric crystal of lead zirconate titanate(PZT). The crystalline structure of this material strains when a voltage is applied. These actuators have displacements in the µm-range with forces ranging from mN to kN and cryogenic operational capabilities. Their stroke at cryogenic temperatures is however just 10% of its stroke at room temperature.[23] PTZ are open loop and require an encoder, and they do however suffer from hysteresis, which needs to be designed for.[24, 25] They are nonetheless suitable for the application in mind. There are several different actuator types which use piezoelectric actuators.

Direct Drive Piezoelectric Actuators are often the combination which includes a monolithic compliant mechanism and one or several PZT stacks. This design can either have a motion amplification or not. An example of a system with an amplifier is shown in Figure 2.10a. This specific system can achieve a resolution of 20 nm. An older example is the 2 degree of freedom actuator with a resolution of 2 nm, a range of 50 μ m with a load capacity of 1 kg.[26] Another example is the compact X-Y stage with a motion range of 120 μ m to 3 nm as seen in Figure 2.10b. It is however challenging to have a stiff enough mechanism, so all amplified stroke is not directly lost in its elastic bending.[4]





(b) Stage by [28].

Figure 2.10: Examples of direct drive mechanisms.

Inertial Piezoelectric Actuators use a coarse and a fine movement to achieve high accuracy over a large range of motion. It uses a piezoelectric actuator to slowly move the output (end effector) which is held in place by friction. To achieve a large stroke, the actuator makes small steps. It does so by rapidly

retracting the piezoelectric actuators, overcoming the friction, and causing them to slip. Repeating this movement creates a stepping motion, which is used to 'walk' the actuator over larger distances. A schematic of this is shown in Figure 2.11a. The movement is relatively inaccurate with an inconsistent coarse step size. The fine range of motion is the movement of the piezoelectric actuator itself. It can achieve an accuracy of 8 nm with a maximum output force of 5 N[27]. A higher force would overcome the friction in the actuator.

The largest benefit of this design is the simplicity of its structure and control.[29] It is often used in industry with different suppliers like Thorlabs[30] and Physik Instrumente[31].

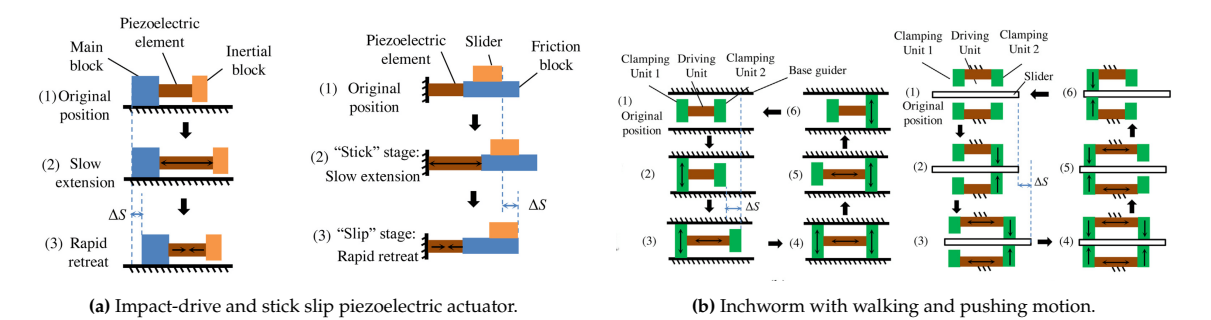


Figure 2.11: Stepping piezoelectric actuators[29].

Inchworm Piezoelectric Actuators use the walking principle of an inchworm. Its movement consists of 6 steps as shown in Figure 2.11b. From its initial position (1), get the rear clamp power (2), followed by the extension of the driving unit (3). Next, is the front clamp actuated (4) and the rear clamp deactivated (5). Afterwards, the driving unit retracts to its original length (6) with the retraction of the rear clamp restoring it to its original system (1).

Experiments have shown that this system shows a maximum driving force of 13.2 N with a long stroke. It is however a complex design with multiple piezoelectric actuators, resulting in difficulties in manufacturing assembly and control.[29]

Parasitic Piezoelectric Actuators use the parasitic motion of a flexing cantilever beam as in Figure 2.12a. The Δx is used to move the end effector forward, and the Δy is used to create the clamping force, as shown in Figure 2.12b. The system has proven to have a position resolution up to 10 nm with a maximum output force of 1.58 N.[29] Other designs are also limited at around 1 N.[32]

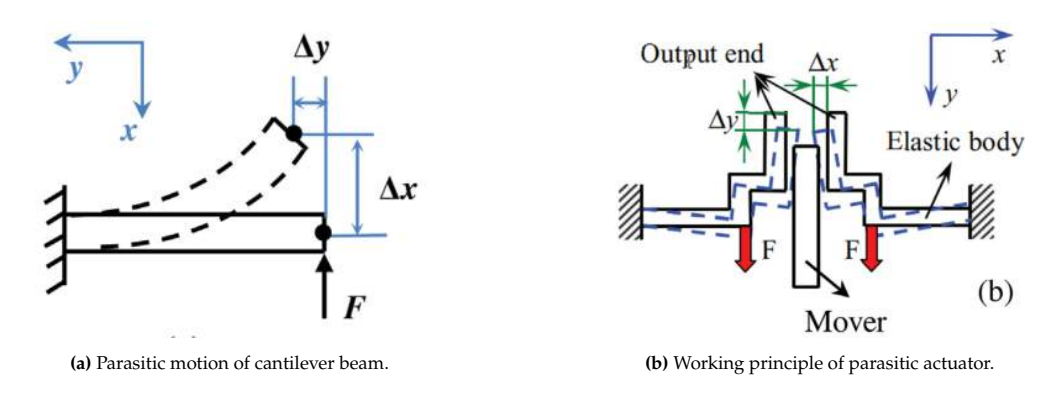
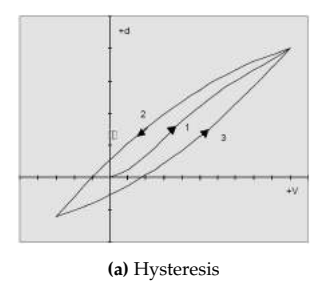


Figure 2.12: Parasitic piezoelectric actuators[29].

Ultrasonic Piezoelectric Actuators are the category of piezoelectric actuators which are actuated at a frequency above the human hearing level of 16 kHz. These actuators mostly use an inertial drive design as explained above. There are several designs for linear and rotational actuators. These actuators have a high travel speed with a positing accuracy in the nanometer range but have a low driving force of a

few Newtons.[25] Due to the high speed, heat generation and wear also become an issue for ultrasonic actuators.[29]

Hysteresis, creep and ageing of piezoelectric actuators can become an issue with controlling the system and needs to be taken into account. Hysteresis is defined as the difference between the forward and backward path when the actuator is cycled, as seen in Figure 2.13a. This uncertainty makes it necessary to use an encoder for piezoelectric actuators. There is also the issue of creep. When the actuator is actuated and moves from point A to point C along the hysteresis graph as seen in Figure 2.13b, it will slowly creep from the initial stop point C to point F over the period of a few minutes.[33] There are strategies on how to reduce the impact of these effects by charge control.[34] It uses the physical properties of PZT stacks to its advantage, without using position sensors or complicated models. Lastly, there is ageing, which refers to the depoling process of the PZT. This can be an issue for sensors of charge-generating applications, but not so much for actuators, since repoling occurs when an electric field is applied.[35]



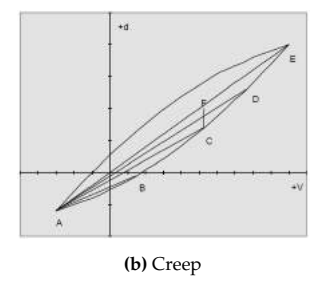


Figure 2.13: Hysteresis and creep in piezoelectric actuators.[33]

Micro-ElectroMechanical Systems (MEMS)

Technically, it is also possible to use a MEMS device. These are highly accurate micro actuators on chips with many different actuation principles, like thermal or electrostatic.[36] One could also control the optical cavity by moving the nanowire closer or further from the fibre. This can be done by placing the nanowire on a MEMS out-of-plane actuator. There are designs for a vertical displacement with a stroke of 6 μ m.[37] These however struggle with manufacturing tolerances, with large differences in spring stiffness due to a 22% thickness variation. In another work, an out-of-plane actuator showed a static displacement of 3.09 μ m,[38] but due to the design is one side of the platform always more actuated than the other, resulting in unwanted inaccuracies.

It is possible to put a DBR with a nanowire on the MEMS actuator. However, it is already difficult to create the current SNSPD. The number of production steps and its complexity would increase significantly if it would be made on the actuator, so this design would not be recommended.[39] Besides that, the MEMS actuator is too large to be able to fit in the current system. So a redesign of the actuator or SNSPD would be required.

Electrical Actuators

There are many types of electrical actuators. However, a select number of these actuators can operate at cryogenic conditions, are compact enough, and can deliver enough power to move the fibre. The two types of actuators that could work are stepper motors or voice coil actuators and their state of the art is discussed below.

Stepper Motors are brushless DC motors which have a discrete number of steps for each rotation. The stators and rotors have teeth which determine the position when different sets of stators are energized by in sequence. A simple schematic of the rotor and stator can be seen in Figure 2.14a. Stepper motors are suitable for open loop position control since the position of the rotor is known due to the constant step angle. It can however lose the step count if the variation in the load torque is fast.[40] It is nonetheless a good compact cryogenic compatible actuator, as was also demonstrated on the James Web Space Telescope.[41] More on this is in subsection 2.3.6. Current cryogenic stepper motors achieve a rotational resolution of 1.8 ° with an accuracy of +-5% with a minimal output force of 2.5 mN m as shown in

Table 2.3. It is also possible to prepare existing stepper motors for cryogenic operations by replacing parts with polished metallic surfaces to prevent outgassing and replacing the bearings for special dry cryogenic bearings. This can reduce the costs of an actuator by an order of 10.[42]

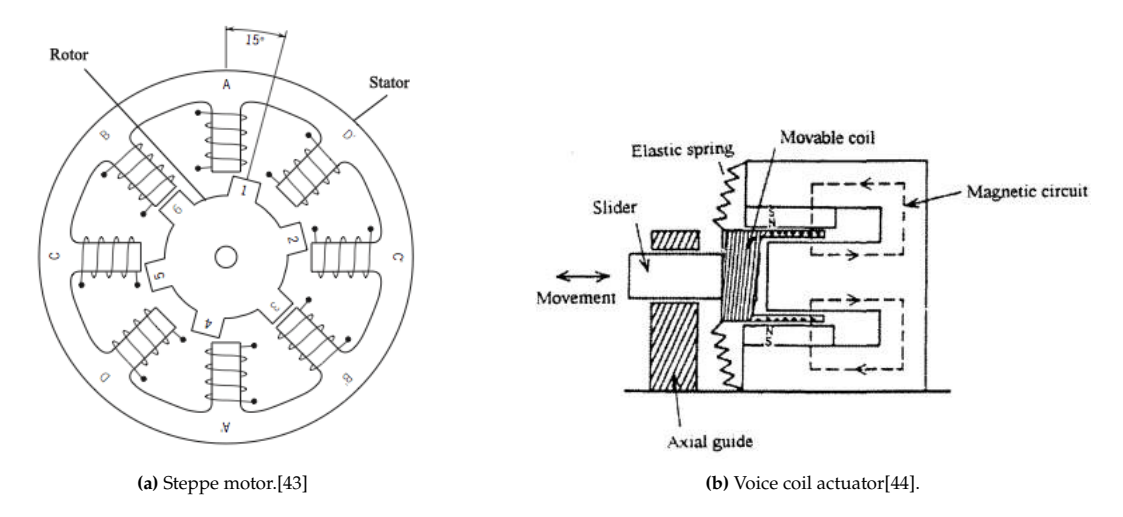


Figure 2.14: Electrical actuator working principle.

Voice Coil Actuators or VCA operate on the principle of the Lorentz force, which states that a force will act upon a current-carrying conductor in a magnetic field. A schematic of this type of actuator is shown in Figure 2.14b. VCA suffer less from drawbacks like hysteresis, nonlinear and thermal sensitive properties, in comparison to piezoelectric actuators.[45] They are optimal for high speed and high accuracy applications, with a position resolution of a few nanometers, as shown in Table 2.2. The current is directly proportional to the force, giving some sense of control, however, a feedback device and controller are still required.[46]

Off the shelf actuators examples

The working principles for different actuator types are used by companies to make off the shelf actuators. An overview of cryogenic nanopositioners is shown below. Table 2.2 shows linear actuators, and Table 2.3 shows rotational actuators. All these actuators can operate at 3 K in a vacuum. Each actuator has a certain positioning resolution, needing a specific transmission ratio to achieve the required positioning resolution. Sometimes the transmission ratio is also limited by the required force of 20 N.

Actuator	Force	Stroke	Res.	Transm.	Volume [mm]	Heat Load	Encoder
VCA[47]	8N	6mm	-	-	30 x 27 ^ø	19mW	Yes
Stepper [48]	10N	13mm	<10um	1:1000	116.5x28 ^ø	1.58W	No
Piezo[49]	60N	6-12mm	1-3nm	3:1	$43.6 \times 22^{\%}$	0,05mJ/step	Yes
Piezo[50]	200g(2N)	12mm	0.8um	1:80	24x24x32	$0.01-1$ m \overline{W}	Yes
Piezo[51]	-	5mm	-	-	24x24x32	-	Yes

Table 2.2: Linear actuator overview.

Table 2.3: Rotational actuator overview.

Actuator	Torque	Resolution	Transm.	Volume [mm]	Heat Load	Encoder
Stepper[52]	2.5mNm	1.8 deg+-5%	1:31400	26.5x19x19	0-0,15W	No
Stepper[52]	92mNm	1.8 deg+-5%	1:31400	54x42x42	0-60W	No
Piezo[53]	15mNm	0,1-0,62mrad	1:350	$43.7 \times 40^{\circ}$	0,14mj/step	Yes
Piezo[54]	6mNm	0,003mrad	1:3	$18 \times 22^{\varnothing}$	-	Yes

	St	iffness	Motion	Max.
Flexures	In-plane	Out-of-plane	Accuracy	Stress
Circular	High	High	High	High
Corner-filleted	Low	Low	Low	Low-med
Elliptical	Low-med	Low-med	Med-high	Low
Parabolic	Med-high	Med-high	Med-high	Med
Hyperbolic	High	High	High	Med-high

Table 2.4: Comparison of flexure types[57].

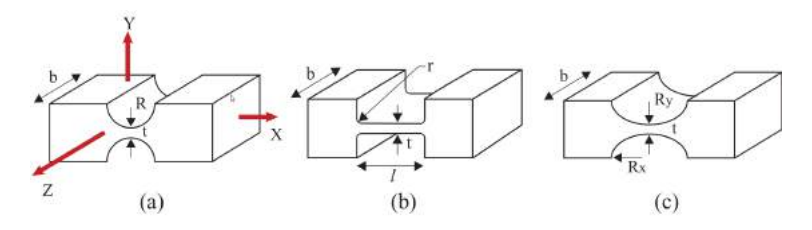


Figure 2.15: Types of flexures: a; Circular b; Corner-filleted c; Elliptical [57].

Superconducting Winding

It is also interesting to mention that it is possible to modify existing actuator winding with superconducting winding.[55, 56] This reduces the generated heat of the actuator. Bugeat et. al. (1987) created a VCA with a superconducting winding with a heat load of lower than 1 mW.[56] Both researchers used a voice coil, so it is uncertain if it will also work on other actuator types.

2.3.4. Motion Transmission

The force, motion and energy of the actuator need to be transferred to the fibre. The two main categories for this are compliant mechanisms which transfer it via elastic deformation with flexures or rigid mechanisms which use prismatic and rotational kinematic joints. Besides that, there is the option of motion transmission from a linear actuator to a linear motion of the fibre, and a motion transformation of a rotational actuator to a linear motion. Different types of motion transmission and transformation are discussed here.

Compliant Mechanism Designs

Compliant mechanisms are flexible mechanisms which transfers motion and force with the help of elastic deforming elements. It can be made from one part, getting rid of the assembly process. The large benefits are that there is no friction and backlash, making it an accurate and repeatable movement. Some energy is however lost in the elastic deformation.

There are different types of flexure hinges to create flexure mechanisms. The different types are shown in Figure 2.15. Circular flexures have a high out-of-plane bending stiffness and are good for accurate positioning over a relatively small range. The corner-filleted flexure is a leaf flexure and is great for large stroke applications. Elliptical flexures are similar, but have a lower maximum stress at the same deflection, resulting in a longer fatigue life. Lastly, there are also parabolic and hyperbolic flexures. All their relative properties are shown in Table 2.4.[57]

There are two common types of compliant amplification mechanisms. These are the arm design shown in Figure 2.16a and the bridge design shown in Figure 2.16b. There are also hybrid designs using both

The arm amplifier is the simplest design. The input stroke is amplified by the arm. The output stroke does not only depend on the input. The stiffness of the amplifier and connected external mechanisms also have their influence.[58] The out-of-plane stiffness is usually large enough to be neglected, however, not for all systems. The bridge amplifier creates a purely linear motion, unlike the arm amplifier. The design is compacter with the same amplification ratio. Its later stiffness is however lower.

The stiffness in compliant mechanisms is a large factor in the design. The mechanical stiffness in the desired axis of freedom should be designed carefully. This can be done by substituting each flexure hinge with a torsional spring, and assuming the links between the hinges are rigid.

Also, the out-of-plane stiffness design of the flexure is important. This can cause unwanted deflections if it is not stiff enough. The out-of-plane stiffness can be increased in several ways. It can be done by increasing the number of flexures that are used in parallel, decreasing the flexure length, and the thickness of the centre section of the flexure, creating effectively a double-hinged flexure.[57] As a rule of thumb, its stiffness-to-mass ratio should be higher than that of the actuator ratio k_x/m_x .

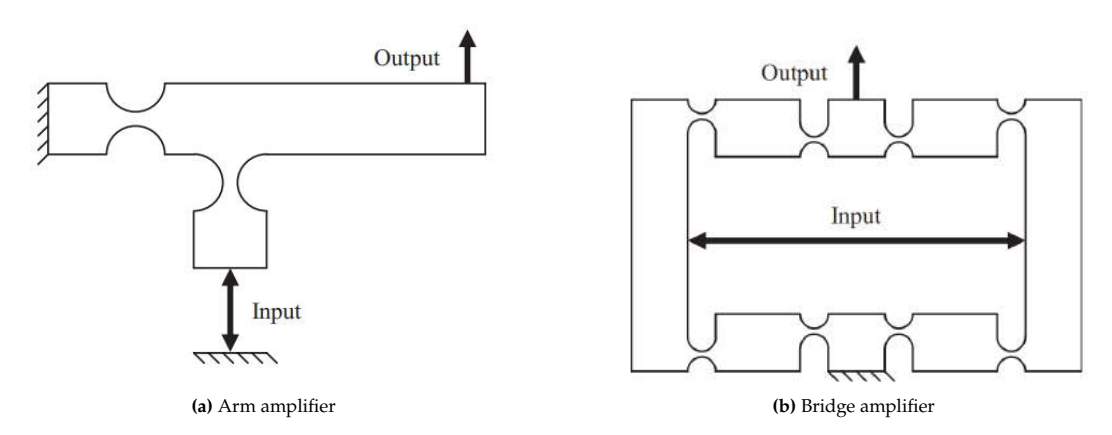


Figure 2.16: Schematics of compliant amplification mechanisms[58].

Rigid Mechanisms

High Precision Reducers (HPRs) play a key role in the manufacturing field. HPRs are often used in aerospace, robotics and machine tools.[59] There are 3 common HPRs used in the industry, which are the planetary reducer, cyclical pinwheel reducer, and the harmonic drive.[60] The application of these HPRs are often limited to relatively large machinery, and are not suitable to fit inside a compact cryostat.

There is a working 6 degree of freedom cryogenic precision mechanism using a planetary reducer in its gearbox.[61] The input of a stepper motor is greatly reduced, which consequently drives a preloaded ball nut to transfer the motion to a linear motion, achieving a positioning resolution of around 300 nm. This motion moves the collimator of the secondary mirror focus unit of their sensor test facility. This system is however also significantly larger than the cryostat.

Also, the design of the James Web Space Telescope is a relevant source of inspiration. It also uses a stepper motor and a set of reduction gears, to finally move a complaint mechanism achieving a 10 nm positioning resolution. This interesting example will be elaborately discussed in subsection 2.3.6.

The design is not limited to these relatively large HPRs. A more compact first design can be made off the shelf gears produced by MÄDLER[62] or Precipart[63] for the higher end of the offer. The design needs to be cryogenic compatible. Besides that, there are also four other important performance parameters for HPR. The first is torsional rigidity. This is the ability to resist torsional deformation. It will never be zero, due to its hysteresis resulting from elastic deformations, and the backlash, which originates from the clearance between parts. Getting rid of these clearances reduces backlash, but in term increases its friction and wear.[64] The second is transmission accuracy. This is all about the relation of the angular displacement of the input and the output, which error mostly originates from thermal expansion and manufacturing errors. Third, the transmission efficiency is the ratio of the input and output power, mostly influenced by the friction in the system. And lastly, there are its dynamic characteristics, which directly influenced the positioning accuracy. Vibrations are a common parameter for presenting the dynamic characteristics of the system.[59]

Preliminary Stiffness Calculation of Frame

A parasite for the motion transmission is that other parts start deforming that should ideally be perfectly stiff. The actuators' reaction force will also deform the frame it is attached to. A simple simulation of a frame can be seen in Figure 2.17a. The applied reaction force deforms the frame, leading to extra unwanted errors.

A similar situation for a linear actuator is with a PZT stack positioned is a frame on the mount, so the fibre can be moved with respect to the sleeve on the PCB, as shown in Figure 2.17b. A PZT stack that Single Quantum currently has is the P-888.91 of 36 mm long with a stroke of 32 μ m and a blocking

force of 3800 N.[65] As discussed in subsection 2.3.3, will the actuator lose around 90% of its stroke at cryogenic temperatures.

To have a first order of magnitude calculation of the error of the deformation, it will be assumed that the total length of the frame is 40 mm, each having a cross-sectional area of 1 x 1 cm. It is also assumed that the frame will also be made out of pure copper just like the mount, having a Young's modulus of 138.6 GPa at cryogenic temperatures.[66] The strain of the frame can be calculated with Equation 2.1.

$$\delta = \frac{PL}{EA} \tag{2.1}$$

Here is δ deflection in m, P is the load in N, L is the length in m, E the Young's Modulus in Pa, and A the total cross-sectional area in m². It is assumed that the actuator is actuated at 20 N. Filling in the equation gives a cryogenic deflection of 28.9 nm and a room temperature deflection of 36.4 nm, which means that around 0.1% of the stroke is lost at room temperature, and 0.9% of the stroke is lost at cryogenic temperatures. This is not that significant for the overall system in this design case of the frame. Its influence should be non the less evaluated when a more detailed frame design is known.

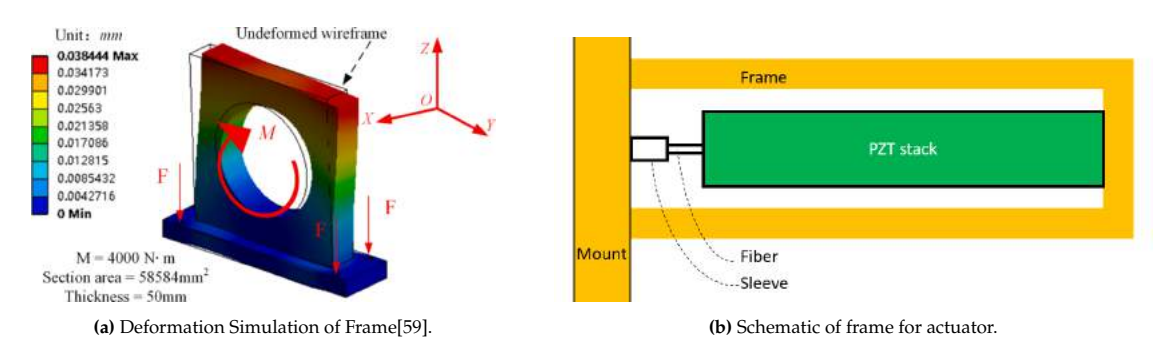


Figure 2.17: Approximation of elastic frame deformation.

2.3.5. Positing Feedback

Position feedback is just as important as driving with your eyes open. One needs to know the relative position first, before correcting the position of the fibre to its optimal position. The resolution and accuracy of the positioning system also need to be below the required positioning resolution of 10 nm.

There are several sources of errors in positioning sensors. These are nonlinearity, which can be taken into account after measuring them. Drift and stability depend on environmental conditions like the temperature or humidity. The bandwidth, which is determined at the -3 dB drop. Noise arising from thermal noise in the resistors, and current and voltage noise coming from the circuit transistors. Resolution limitation when the distance between two measured points is smaller than the uncertainty, one can mistake one point for the other. And lastly, there is the possibility that the reference sensor used to set the initial position has a calibration error. There is a worst-case scenario where all sensor errors are summed together. This is simplified since some errors are dependent on the position, but it makes it practical to combine all errors in the worst-case error.[67]

Sensor Type	Resolution [nm]
Resistive strain gauge	23
Piezoresistive strain sensor	0.49
Capacitive sensors	2.4
Electrothermal MEMS	10
Eddy current	1
LVDT	5
Interferometry	0.49
Encoder	6

Table 2.5: Position Sensors Characteristics[67].

Several sensor options achieve nanometer resolution, which are summarized in Table 2.5.

The first one is the *resistive strain gauge*. These sensors are meanders of a conducting foil of which the electrical resistance will change when strained. Gauges are low-cost and simple and often used in combination with piezoelectric actuators. They can either be integrated or directly bonded on the PZT. Its resolution is however not high enough

Second is *piezoresistive strain sensors*, made from a planar n-doped resistor. The design has a low strain limit of 0.1% with disadvantages such as a high temperature sensitivity, a 1% nonlinearity and poor long-term stability. It has however a very high position resolution and is easily integratable with MEMS devices, greatly reducing the costs.

Third are *capacitive sensors*, the most common close-distance positioning sensors with a relatively low cost, but a relatively high complexity. It works with two parallel plates of which its relative movement can be measured by the capacitance via an AC voltage. Plates of different sizes can move axial or lateral, making an optimal situation for the resolution with minimal noise.

Fourth is the thermoelectric MEMS, which also uses the same sensing principles as the capacitive sensor. The deflection is measured with the relative distance change between the teeth of two combs.

Fifth is the *eddy-current sensors*, which uses an alternating magnetic field to induce eddy currents in an electrical conductive target. The AC resistance of the excitation coil depends on the opposing field and therefore the distance. The largest benefit is that the sensor is insensitive to dust and pollution. It is however sensitive to the temperature of the conductive target, and it also generates heat in the target with the eddy currents.

Sixth is the *linear variable displacement transformers (LVDT)*, often used for large distance motion of a few cm that required a high accuracy. A permeable core moves inside a driving coil and two sensing coils. The amount of flux through the core is linearly proportional to the length of the core passing through each sensor coil. The advantages are its small resolution with a large range and a simple design.

Seventh is *laser interferometers*, achieving a sub-nanometer resolution over a range of multiple meters. It uses the path length difference of a split light beam to determine the distance via constructive and destructive interference. Design options for interferometry are the classical Michelson interferometer, the Heterodyne interferometer using 2 wavelengths, or the fibre interferometer. It is generally the most expensive displacement sensor, but also the with a very high resolution.

Eighth and last is the *linear encoder*, consisting of a read-head and a reference scale. Optical encoders achieve the highest accuracy, magnetic or inductive encoders are however cheaper and more tolerant of contamination. Optical systems are very sensitive to dust, requiring several parallel measurements to average out the errors. [67]

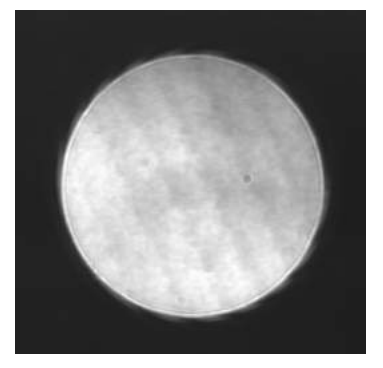
The system has limitations for magnetic and electrical fields as discussed in subsection 2.1.3. Several actuators use this as their actuation principle. Options that don't are resistive strain gauges, piezoresistive strain sensors, interferometry, and optical encoders. Looking at the criteria for the resolution and required stroke is interferometry the most logical option. Also, because an optical fibre is available, so it can be directly attached to the system, not adding the need of adding a sensor in the cryostat.

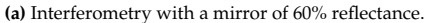
Companies such as attocube[68] and SmarAct[69] offer interferometry setups that can be used. Fizeau interferometer with a broadband laser would be the best option to measure the optical cavity size. The optical cavity size can be measured with its harmonics.[70] The interferometry setup works best when there is a high and a low reflectance surface. Figure 2.18a shows the fringes with a mirror with a reflectance of 60%, and Figure 2.18b shows the fringes with a mirror with a reflectance of 4%. There is a clear difference in fringe contrast. The end face of the optical glass fibre has a 4% reflectance and can be used as the low reflective surface. Combining this with a PCB with a gold mirror as a highly reflective surface will result in clear fringes. A camera is used to measure the intensity different between difference images, making it possible to calculate the optical cavity size.[70]

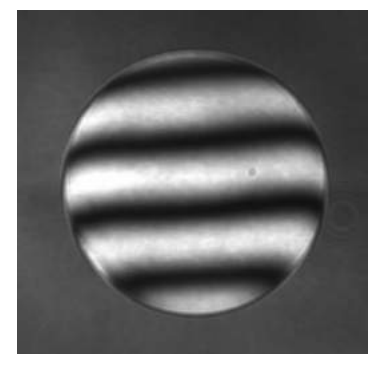
2.3.6. James Web Space Telescope Nanoactuator

A perfect textbook example of an operational nanoactuator which combines a lot of the aforementioned parts is the actuator used on the James Web Space Telescope (JWST). It uses 6 of these actuators per mirror to control the 6 degrees of freedom. A set of two of these actuators can be seen in Figure 2.19a. It has an astonishing positioning resolution of 10 nm over a stroke of 21 mm using only one actuator.[41] It does so with a coarse and a fine stage, both being attached to the eccentric bearing driving the flexure shown in Figure 2.19b with a motion reduction of 100:1.

The fine stage operates with a series of gears to reduce the transmission. The stepper motor is attached via a 60:1 gear head to the axle. The coarse stage is split off here, via a 3:1 spur gear and an





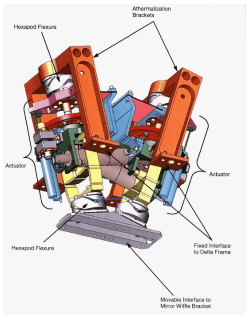


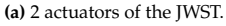
(b) Interferometry with a mirror of 4% reflectance.

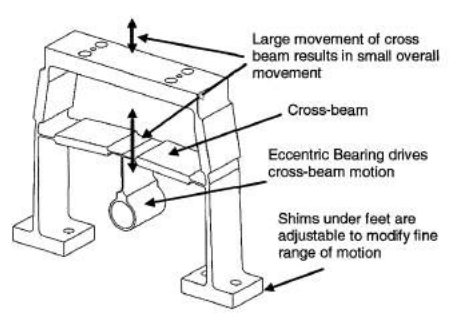
Figure 2.18: Interferometry fringes for surfaces with different reflectance[71].

8:1 gear which in turn drives an 8 mm ball screw with a 2 mm pitch. Once the coarse state is set, it decouples the driveshaft to the coarse stage and only continues to drive the fine stage. It does so with the coupling mechanism, which has a tumbler-type coupling with a 324-degree backlash, as shown in Figure 2.19c. Note that when the coupler is engaged that both the coarse and the fine stage are actuated.

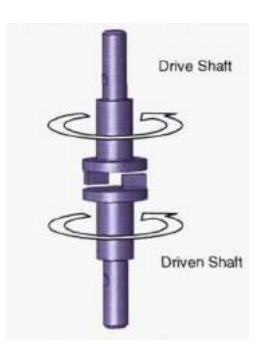
Inspiration can be drawn from the working principles from the fine stage of this actuator. It achieves the same positioning resolution as required for the relative fibre position, but the system is significantly bigger than would fit in the cryostat. The reliability of this actuator is also higher since maintenance is not possible on the JWST. It also operates at 40K instead of 3 K. Nonetheless, it proves the functionality of using one actuator with a relatively simple drive train and a flexure mechanism to achieve the nanometer positioning resolution.







(b) Flexure of the actuator.



(c) JWST coupler mechanism.

Figure 2.19: JWST Actuator Design[41].

2.3.7. Previous Experiments by Single Quantum

The project of active fibre placement isn't new to Single Quantum. Different experiments were performed in the past one to two years, which was the foundation for this continuation of the project.

Fixating the Ferrule

It was tried to fix the ferrule in place, to prevent it from moving at all. A clamp was put around the sleeve to stop it from moving. Some movement was limited, but not the desired result was achieved. STYCAST was added and removed from different places to experiment with the influence of glueing and not glueing different parts. The ferrule was glued into place, fixing it in place, but now at an impossible to control distance, with a small chance of it being close to the optimal position. The glue under the chip was removed to see what would happen. The shift was less, suggesting the chip moved slightly upwards. The experiments were repeated without spacers, but no ideal solution was found. This created the wish to actively control the fibre position since no passive solution was found.

Static Friction Force Experiments

A fundamental question is how much force is required to move the ferrule in the sleeve. Measurements were done at room temperature (RT) and cryogenic temperatures. It was not possible to measure the pulling force inside the cryostat, so liquid nitrogen (LN) was used as an alternative to still be able to take measurements at a temperature of 77 K. The pull-out force was measured for different iterations. This is shown in Figure 2.20. The pulling force usually doesn't go above the 8 N, with 3 outliers.

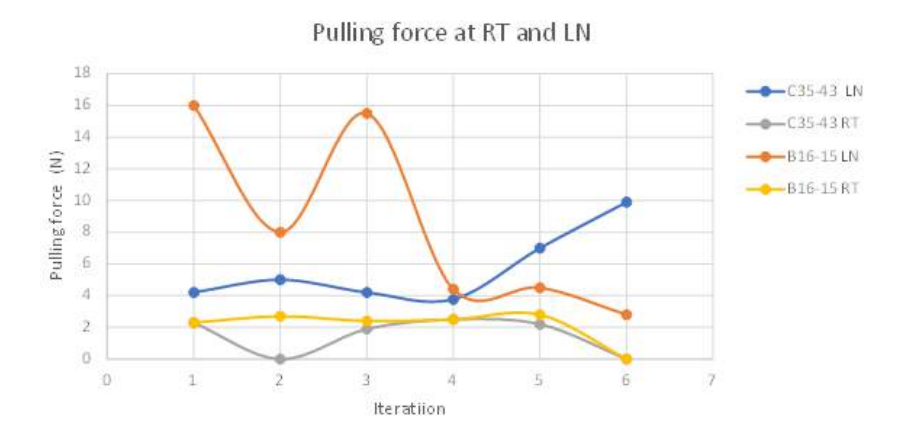
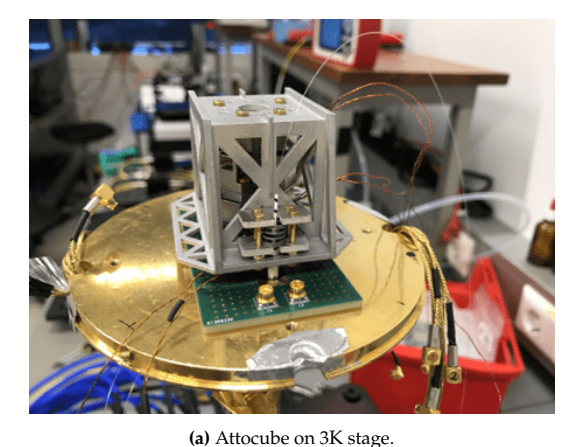


Figure 2.20: Pulling force at room temperature (RT) and at cryogenic temperature (LN).

There were five experiments performed, of which the two successful are shown in Figure 2.20. The sleeve broke at the other three attempts. The ferrule was pulled out with pliers at cryogenic temperatures. The theory is that the pull-out force increased when one is not pulling straight. This possibly caused the sleeves to break. The pullout force peaked at 30 and 26 N before breaking the sleeve. So, the actuator should ideally pull with a force of at least 20 N to have enough force to move the ferrule into a sleeve.

Piezoelectric stage

Experiments were done with a piezoelectric XYZ positioning stage. The Attocube stages ANPx101 and ANPz101 use an inertial piezoelectric actuator to achieve high accuracy over a large stroke.[72] The stage was positioned on the cold head, with the ferrule on the end effector as can be seen in Figure 2.21a. The Y stage was unfortunately not functional, making the original plan of not using a sleeve not possible anymore. However, the force of the Attocube was not high enough to move the ferrule in the sleeve, it was modified to lower the friction force. The extra slots in the sleeve can be seen in Figure 2.21b. In the end, it still had a hard time moving upwards, so most experiments were done by moving the ferrule downwards.





(b) PCB with modified sleeve.

Figure 2.21: Setup with Attocube.

During the experiments, it was shown that it is possible to move the ferrule in the sleeve, even at cryogenic temperatures! An initial set of tests were done at room temperature and a chip with a

gold mirror instead of a SNSPD. A laser shined on the mirror, reflecting the light. Power changes in the reflected light are caused by the interference with the incoming light, and the gap size. As can be seen in Figure 2.22a. Clear steps in the reflected power can be measured corresponding to steps of the Attocube. This is the proof of concept that lead to the continuation of the project. The main drawback of the Attocube is that it is too large and expensive to use in each system. So now a compacter, cheaper and preferably a more accurate system needs to be built.

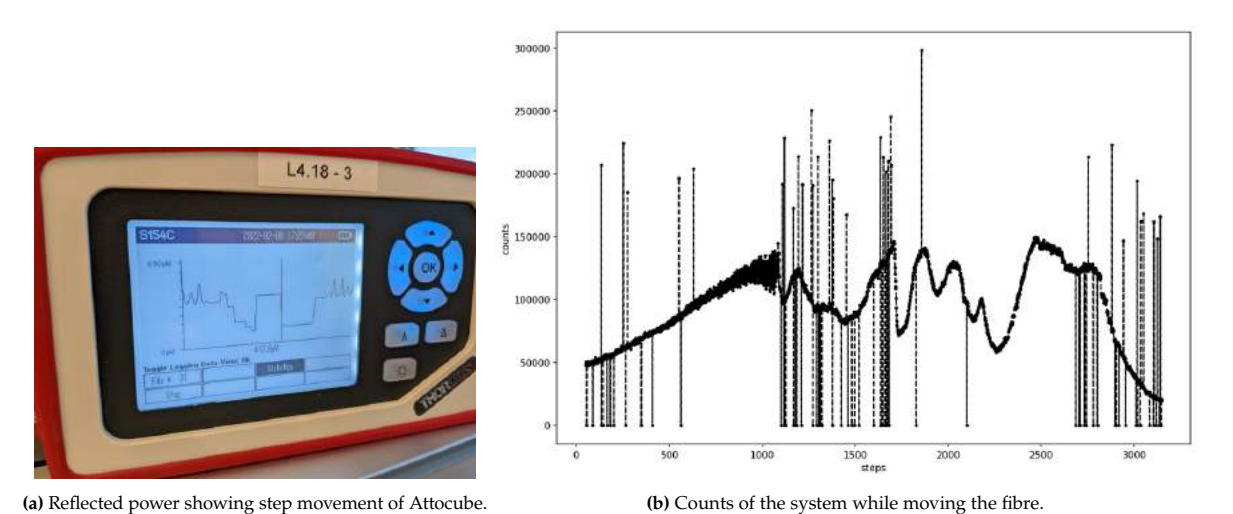


Figure 2.22: Readout with moving fibre.

A second set of experiments was done with a SNSPD at cryogenic temperatures. This represents an almost real situation of the detector. The counts of the detector were now directly measured, instead of the reflection of the light. This result can be seen in Figure 2.22b. The number of counts changes significantly when moving the actuator. It was difficult to conclude from these results. Some potential fringes are between the 1700 and 2200 steps, but no real conclusion could be drawn from this.

Elastic Flexure deformation Simulations

A simple Finite Element Method (FEM) simulation was done on the deformation of an amplification mechanism. The end effector was set to have a force of 30 N to overcome the friction. This already required a deflection of the piezoelectric actuator of 3 microns at cryogenic conditions. Note that just 10% of the actuators stroke remains at this temperature as discussed in subsection 2.3.3. For amplified piezoelectric actuators this is already its limit of stroke and/or force.[73][74] No more losses are acceptable to make the system barely work with an amplified piezoelectric actuator.

2.4. Conclusion on the State of the Art

What can be concluded from the state of the art? Three design options could solve the task at hand, of which one has the most potential. The first option is placing the nanowire on an out-of-plane MEMS actuator. The MEMS design is not realistic as mentioned in Figure 2.3.3. The second option is a PZT stack with a compliant mechanism and an interferometry sensor. The literature on the actuators seemed very promising, but the previous experiments of Single Quantum showed more issues than anticipated. This leaves the third and most promising option, which is a scaled-down version of the fine stage of the James Web Space Telescope Actuator[41], and the actuator presented by LaCroix et. al. (1990).[61] A stepper motor or another rotational actuator driving a reduction mechanism, with potentially a compliant mechanism and an interferometry sensor. Such a design will likely work the best in the situation.

2.5. Design Objective

Such a system will be able to have a high and reproducible SDE. An experimental test setup will be built to help in the design process in finding the most optimal design. First, the motor is selected and tested, followed by the design of the reduction mechanism, making it possible to do already simple

experiments. The setup will be kept up to date and will change for different experiments. It is likely that with the knowledge of this setup, an improved setup will be built, with a compacter higher performing design. An alternative scenario is that the initial setup will be good enough to do the experiments with.

In the end, it is also interesting to look at what the final design can accomplice besides positioning and optical fibre. Grotevent et. al (2022) showed a miniaturized Fourier-transform waveguide spectrometer in which they moved a mirror with a step size of 50 nm.[75] It can also be used in this setup to achieve even higher accuracy. Possible applications in different fields could also widen the objective of this research.

Testing of Crucial Components

The motor needs to be tested cryogenically. This is done inside of a cryostat made available by Single Quantum for the purpose of this active fibre positioning project. It is an older 8 channel system, and has a 4 channel mushroom mount. This mount is outdated and can be machined into and used during the project. Later in section 6.1, new optical fibres are added to the system. Wiring is also modified to be able to control the motor inside the cryostat. First, the testing process of the motor is described in section 3.1. Next in section 3.2 the testing procedure of the precision screw is described. An attempt to speed up the design iterations is described in section 3.3 and lastly the value input of an PhD is mentioned in section 3.4

3.1. Making a Cryogenic Stepper Motor

The key part of an actuation system is the motor. Cryogenic capable motors are however expensive, so there was a wish to make a cheap stepper motor work cryogenically. Most stepper motors have a temperature limit of a bit below the freezing point, but the assumption was that the motors just weren't tested at lower temperatures. It was a bit of a leap, but with some minor modification it turned out to be correct. This section will elaborate on the process of making a cheap stepper motor work at 3 K.

3.1.1. Hardware Selection

Common stepper motors are the standardized NEMA stepper motors, of which the related number gives the outer dimension of the motor frame in tenths of inches. The smallest NEMA stepper motor is the NEMA 8, with outer dimension 0.8x0.8 inch, so 20x20mm. This specific motor was selected purely due to it being the smallest stepper motor in this cheap standardized line. It has a maximum current per phase of 0.6 A and a rated voltage of 3.9 V. It torque is also higher than required, so that the motor torque is not a limiting factor in testing the design. The required torque calculation will be verified here.

The Arduino Nano was selected as the micro-controllers for the stepper motor. An Arduino Nano clone was bought to save some costs and the extra required driver was installed to get it working.[76]

Initially, the DRV8833 controller was selected, since the rated voltage was within the operating range of the driver. However, it was found that stepper motor need a higher voltage than their rated voltage, and a different driver was required[77]. The A4988 driver was eventually selected with a 12V power supply.[78] The driver's current limit needed to be set with a set screw, so it wouldn't go above the maximum current per phase of the stepper motor. This current limit can be set to the correct value by changing a set screw. A reference voltage can be measured between this set screw and the ground pin of the driver and this reference voltage needs to be set to a certain voltage, if the current is to be limited to a certain value. This reverence voltage V_{ref} can be calculated with Equation 3.1. Unfortunately, the resistance of sense resistor R_s wasn't. It was calculated by setting V_{ref} to some value and measuring the current through the coils. Now R_s is the only unknown in the equation and it can be calculated. Keep V_{ref} on the low side, so the current doesn't go above I_{max} . R_s is calculated to be 0.124 Ω . This set a maximum V_{ref} of 0.594 V. Taking a 5% safety margin, the reference voltage was set to be 0.564 V.

The values were verified by measuring the current through the motor coils. A current of 0.404 A was measured with the motor in full step mode. According to the data sheet of the A49888 drive should the

current run at 70.7% of it current limit I_{max} in full step mode.[79] Multiplying the maximum current per phase on 0.6 A by 70.7% and the 5% safety margin, nicely gives the measured current of 0.404 A.

$$V_{ref} = I_{max} \cdot 8 \cdot R_s \tag{3.1}$$

A 12 V power supply was used to power the stepper motor. A universal 12 V DC adapter was used, with jumper cables connected to the male DC output. The pins were bend to have some preload on it to have a continues force on the electrical contact to maintain the electrical connection.

Compatibility with Different Motor

The NEMA8 motor is large for the size of the 3K radiation shield and will likely be the limiting factor for adding more active fibre positioning systems in one cryostat. So to make it also possible to further develop the design with a smaller motor, there is the wish that the motor mount is also compatible with another motor. The company Faulhaber has many compact stepper motors, with the smallest having an outer diameter of 6mm.[80]

An important selection criteria for the motor is that it should be able to apply enough torque to be able to move the fibre. The required moment to move the screw is given by Equation 3.2.[81] Here M is the required moment to overcome the static friction in the screw, W is the axle load on the motor, r is the radius of pitch diameter of the precision screw that will be discussed in section 3.2, α is the tread angle, and ϕ_s is the friction angle given by Equation 3.3. Here N is the normal force, assumed to be equal to W with the small angle approximation, and F is the friction, given by Equation 3.4. Here N is the normal force and μ_s is the static friction coefficient of lubricated steel on steel given to be in the range of 0.5 to 0.8.[82] It can now be seen that the friction angle is just a function of the static friction coefficient.

$$M = Wrtan(\phi_s - \alpha) \tag{3.2}$$

$$\phi_s = \arctan^{-1}\left(\frac{F}{N}\right) \tag{3.3}$$

$$F = \mu_s N \tag{3.4}$$

Plugging in the values for the worst case scenario with a friction coefficient of 0.8, gives a friction angle of 39 degrees. The thread angle is 4.3 degrees, since for every revolution of 1/4"* π length, there is a lateral translation of 0.15mm. The axle load is 50N, and the radius is 1/8". Filling in these values in to Equation 3.2, gives a torque requirement of 109 mNm for the precision screw. The worm gear that will be discussed in section 4.1 has a gear ratio of 80:1 and an efficiency of 21%.[83]. This gives a required motor torque of 6.5 mNm for the motor. Repeating the calculations for the most optimal condition with a friction coefficient of 0.5, gives a required torque of 3.9 mNm. If grease is added, it lowers the friction coefficient to 0.16, reducing the required torque to 0.79 mNm. Adding lubricant can do a lot for the friction in the system. An overview of the required motor torques can be seen in Table 3.1.

As a comparison, the Nema 8 stepper motor has a (holding) torque of 1.8 Ncm, or 18 mNm and a constant torque of 15 mNm.[84] It should thus have no problem with moving the screw. This is a good confirmation that the NEMA 8 is not a limiting factor in making the system work. Once everything works, a smaller less powerful motor can be implemented.

Table 3.1: Overview of motor torques.

Situation	Torque
Worst case scenario ($\mu_s = 0.8$)	6.5 mNm
Optimal condition ($\mu_s = 0.5$)	3.9 mNm
Lubricated ($\mu_s = 0.16$)	0.79 mNm
Nema 8	18 mNm
AM1524	6 mNm

One of the motors that meets the required torque is the Series AM1524.[85] It has a torque of 6 mNm, which almost can handle the worst case situation. The next motor in this Faulhaber series is

over specified with 22 mNm and a diameter of 22 mm. So just not reaching the worst case scenario was deemed the best compromise. A motor spacer was made for this motor, which can be seen in Figure 4.9b. It can be added to the same frame as the motor spacer in Figure 4.8b.

Lubrication

The solution to make the parts work at cryogenic temperatures, is by removing the lubrication with an ultrasonic acetone bath. Removing the lubrication comes at the expense of the lifetime of the part, while also increasing the friction and the required motor torque. Preferable there would be a cryogenic lubricant suitable for the application. Two options are MoS2 or PTFE lubricants[86]. PTFE has a good thermal stability between 4K and 529K. The specific wear rate of PTFE composites at 4K is however roughly double of that at 77K and 20K, but still lower than at room temperature. The good thermal stability of the PTFE was the reason that a PTFE lubricant was bought.[87] It is rated up until 93K °C, which is in the working range of the LNG industry of 111K. This is a very large market compared to the ones working with lower temperatures. So a lot of products are rated at this temperatures, although still being operational at lower temperature.[86]

3.1.2. Wiring

The wiring diagram of the setup is relatively straight forward. A schematic can be seen in Figure 3.1. The inductors of the motor are wired up to the 4 output channels of the A4988 motor driver 1A, 1B, 2A, and 2B. The motor power supply is hooked up to VMOT and GND, with a 100 μ F capacitor in series. The VDD and GND are used to power the logic circuitry with the 5.5V logic power supply outputted by the microcontroller, which is here the Arduino nano. The STEP and DIR pins of the driver are the two input controls, which give the number of steps to turn, and in which direction. The RESET pin is a floating pin, and can be connected to the SLEEP pin to put it to HIGH, so it is turned off. When activated to LOW, all STEP inputs are ignored. The MS1-3 pins are used for micro-stepping and are ignored for now. The ENABLE pin is used unlike shown in the diagram to fully turn off the the stepper motor, to reduce the heat load in the cryostat. These pins are connected as follows. The DIR pin is connected to D2 pin on the Arduino, the STEP pin is connected to the D3 pin, and the ENABLE pin is connected to the D4 pin. Everything was connected with standard male to male jumper cables. The Arduino is connected with the computer via an USB to mini USB.

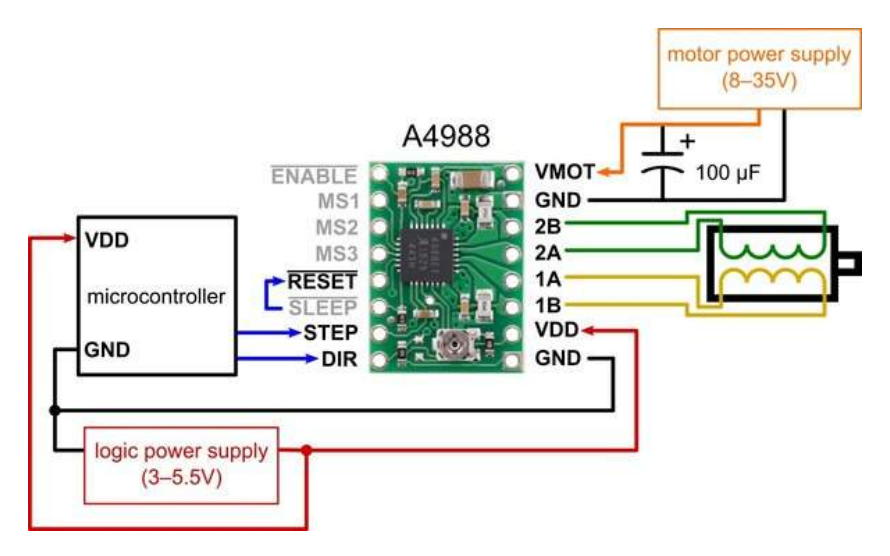


Figure 3.1: Wire Diagram.

3.1.3. Arduino Code

Arduino uses a variant of the C++ programming language. Everything is programmed in the Arduino IDE V2.0.4. which is then uploaded to the Arduino to run the code. The structure of the code used has two main parts. The is the void setup() and the void loop(). The latter runs indefinitely, while the first one just runs once. So that means that the pinmodes of the Arduino are initiated in the void setup(), and the actuator is controlled in the void loop(). It is also possible to initiate global variables if defined before

the void loop(). And example code can be found in section B.1 of Appendix B, which for rotates the motor 1 full circle in one direction, and then 2 in the other detection with a 1 second delay inbetween.

3.1.4. Modifying and Testing Process

A stepper motor is a contactless motor, except for the bearings. The lubrication of the bearing had to be removed to prevent it from freezing and blocking the motor. The stepper motor was taken apart and the bearings were cleaned in an acetone bath in a petri dish and stirred around for 5 to 10 minutes, so it can also clean behind the shielding of the bearings. There was quite some residue after letting the acetone evaporate, as seen in Figure 3.2. Doing it a second time already showed a significant reduction in the residue, and it was assumed that the bearing were clean (enough) to be cooled down. The lifetime of the stepper motor is likely to be reduced significantly by reducing the lubrication. But this shouldn't cause issues since the operational time is minimal.



Figure 3.2: Petri dish with residue.

A very simple way of finding out if the stepper would work is cooling down to 3 K, rotate the motor 180°, and warm up the system to see if the motor has moved. Wires were made to connect the motor to the output SMA ports of the cryostat and are shown in Figure 3.3. Just the core of the coax cable was used. Similar cables were made at the other end of the output to connect it to the the Arduino. A copper bracket for the stepper motor was made to have a place to mount the stepper motor onto, while also providing a path for the heat to flow. Also, the back of the stepper motor was connected with a strand of copper to function as a cold finger. The result is shown in Figure 3.4.

The example code from section B.1 was slightly modified to let the motor turn just 180° before entering an infinite while loop and can be seen in section B.2 of Appendix B. Tests at room temperature were done to confirm the functionality of the soft- and hardware. A list with action was made to prevent making mistakes while everything was inside the cryostat. The entire system was a black box after all. You blindly give your input, and you only see you output a few hours later when you can open up the cryostat again. The following action list was made.:

- 1. Attach copper wire at the back of the motor.
- 2. Disconnect the motor.
- 3. Put the marker at the top side of the axle.
- 4. Make a picture of the setup.
- 5. Put on the two heat shields and the vacuum cylinder.
- 6. Create a vacuum of of at least 4 E-4 Hpa.
- 7. Turn on the compressor.
- 8. Check for cryogenic temperature after a few hours.
- 9. Open the Arduino IDE.
- 10. Plug in the USB, attach the motor, and turn on the power supply (2x).
- 11. Upload the code.
- 12. Check if the voltage and the current.
- 13. Check if all print statements are there, and the code has run successfully.

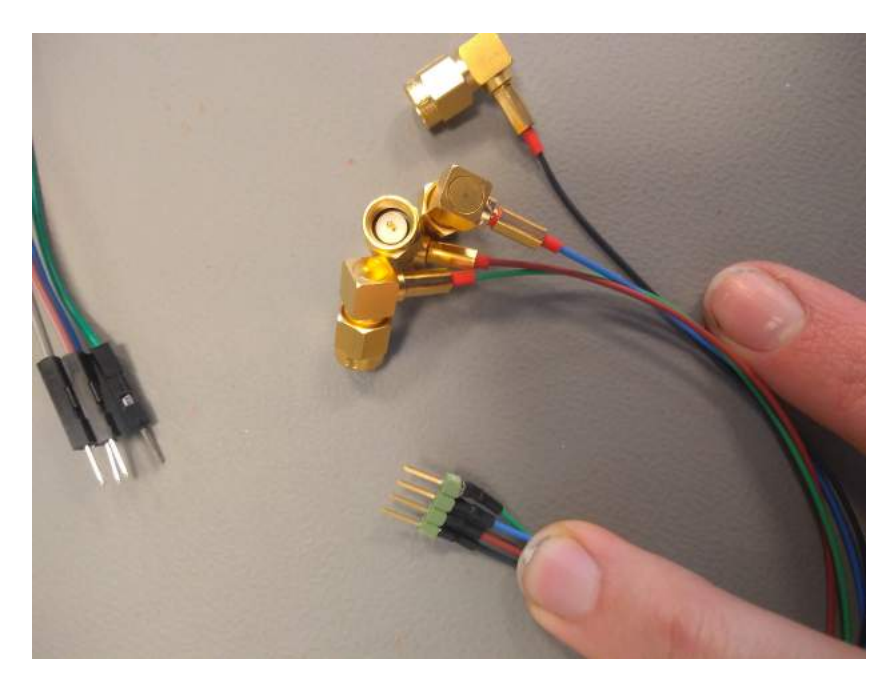


Figure 3.3: SMA motor cables.

- 14. Download the temperature data.
- 15. Turn off the compressor and let the system warm up.

The first cooldown results were disappointing since the stepper motor didn't move, only to find out the second power switch of the power supply wasn't turned on. The stepper motor did however still function as expected, so it was able to survive a cooldown. Everything was cooled down a second time and the checklist was repeated. Some extra measurements were now also taken. At 3.4 K the motor would draw just 0.09 A from the power supply instead of 0.254 A at room temperature. The current through the motor is unequal to what is drawn from the power supply and was 0.404 A, This shows that the current limiter of the A4988 driver still functioned accordingly. The resistance in the motor coils dropped from 7.7 Ω at room temperature to 0.6 Ω cryogenically. During the experiments, there was power supplied to the motor for around 50 s For the majority of the time the motor was stationary, and the power was used to increase its holding torque. Figure 3.5 shows a clear increase in temperature inside the cryostat, while supplying the roughly 1 W into the system. After warming up the system, there was partially good news. The motor had rotated, but just 120°. This unpredictable behaviour raised more questions than it answered. It was at least good news that it was able to move at cryogenic temperatures.

3.1.5. Position Feedback

The next step would be to gain insight in what was actually was going on inside of the cryostat with the motor. A simple way seemed to implement a rotational potentiometer and easily get a readout on it with the Arduino. A simple $100~k\Omega$ potentiometer was bought, under the same assumption that it could work once the lubrication was removed with acetone.[88] The position of the potentiometer can be read with the code from section B.3 in Appendix B and returned a position on the linear scale from 0 to 1023. It could rotate 270° , and it position was linear proportional to its output value.

A desired motor position was given as input. It was compared to the position of the potentiometer and the required number of steps was calculated to reach this position. There is a chance on an error in the number of steps or in the sensor position, so the code was looped until the position was reached. The program should thus break from its loop in this case, which is ideally after one loop. This code can be seen in section B.4 in Appendix B.

The setup can be seen in Figure 3.6. The potentiometer is positioned in the copper bracket on the right. It was temporarily fixed to the motor axle with heat shrink and 2 tie wraps. This worked good enough and was never replaced with the proper beam coupling that was ordered.[89] Pencil marks were

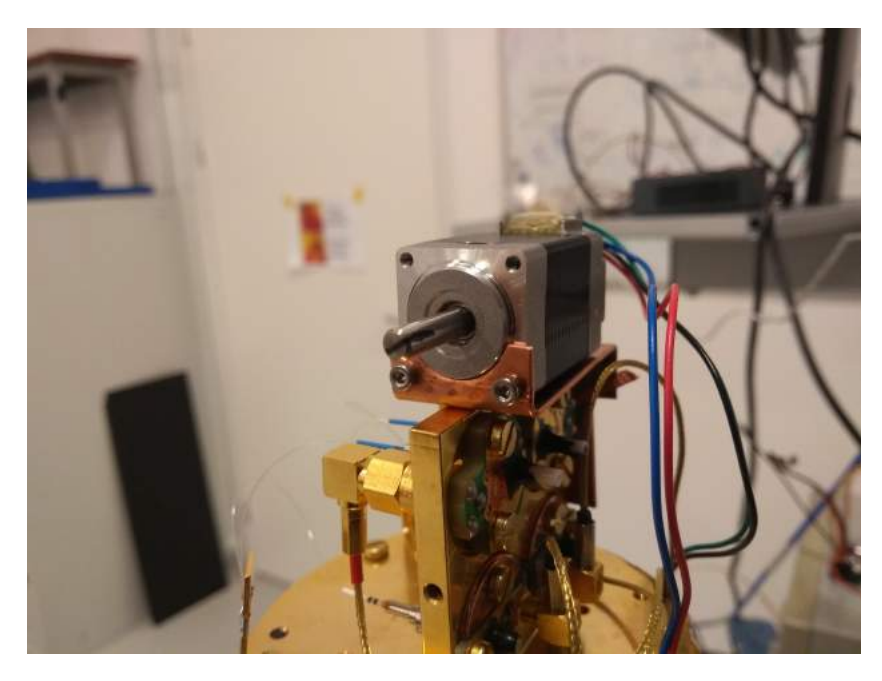


Figure 3.4: Stepper in cryostat.

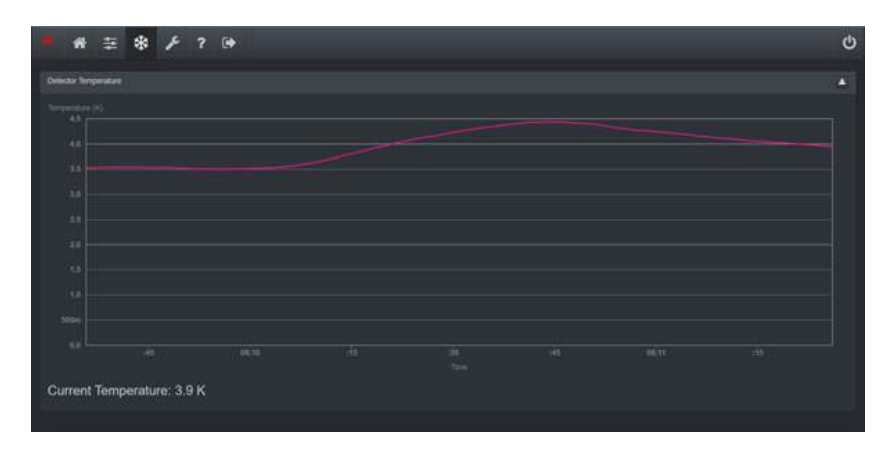


Figure 3.5: Temperature increase in the cryostat.

applied on the axle, heat shrink and the potentiometer to be able to notice slippage. The potentiometer wiring is also fed through the same type of cables to the SMA output of the cryostat. The other end is soldered onto the potentiometer. Several tie wraps were used to speed up the design iterations. Initially, a nice copper bracket was made for the motor as could be seen in Figure 3.4. This is however time consuming and tie wraps proofed to work quite well at 3 K.

Initial warm tests proved that everything worked accordingly, and the potentiometer was cleaned in an ultrasonic acetone bath to get rid of the lubrication to make sure it would work at 3 K. Afterwards, not the same accuracy was achieved, likely to do damages that occurred during the bath. A nominal readout of a potentiometer can be seen in Figure 3.7a. The output values are inbetween 41.2 and 41.7 $^{\circ}$ when stationary. The potentiometer that had the ultrasonic bath gave the readout shown in Figure 3.7b in yellow with output values inbetween 47 and 65 $^{\circ}$. A 36 fold increase in sensor error! The error was luckily predictable, and could largely be mitigated by taking the average sensor value over a certain time shown in green in Figure 3.7b. The average value of 100 sensor values was taken at every 1 second interval.

Everything worked now as it should and the system was cooled down with disappointing results. The motor and the potentiometer didn't move, so there was still no feedback on the stepper motor inside the cryostat. The experiment is repeated twice without results. After warming up the system, everything worked once again as it should. However, when rotating the axle by hand, a clear high

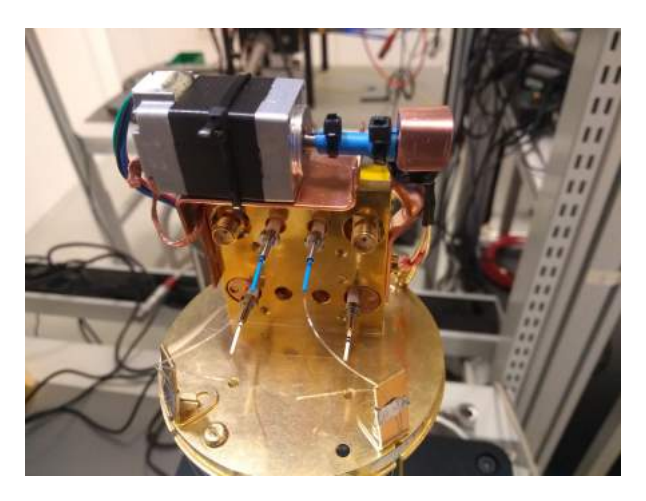


Figure 3.6: Potentiometer attached to the motor.



Figure 3.7: Potentiometer readouts.

resistance point can be felt. This is the position in which the motor was cooled down in. So the motor was taken apart and it was found that one bearing was 'broken'. It had a high friction compared to the other bearings. That lead to the idea that the bearings weren't completely clean yet.

3.1.6. Cleaning the Bearings

The bearings were shielded with a shield that was difficult to take of. In theory it appeared possible, but other employees in Single Quantum deemed it impossible to open them up. In fear of destroying the bearings, 3 sets of new bearings were ordered.[90] Later, also a set of the same bearings were ordered without the shielding to be able to properly clean the inside of the bearing.[91] In the meantime, there was success with taking the shielding off. The broken bearing from the previous test had a lot of white powder on the inside, as can be seen in Figure 3.8a. This looked like the same residue as when initially cleaning the bearings from Figure 3.2. This residue was cleaned off with acetone and it left the bearing shining like the other bearing as seen in Figure 3.8b. It also became fully functional again.

The clean bearings gave hope for the stepper motor now working properly. The motor was assembled and it was cooled down without the potentiometer. The motor was rotated 180 $^{\circ}$ and it finally worked accordingly! The experiment was repeated with rotating the motor 1170 $^{\circ}$, so three and a quarter turn, which it did perfectly. There was finally a working cryogenic motor.

The latter experiment also had a nice byproduct. That morning the cooling water got too warm and the compressor shut down because of it. This happened just before the experiment. Without the noise cold finger, the motor could be heard outside of the cryostat, even though it was in a vacuum. The sound is quite unique and similar to the sound it makes at room temperature. This suddenly made it possible to distinguish different behaviors of the motor by the sound it makes. When the compressor was on, the sound could still be heard when putting your ear closer to the vacuum shield, which previously went





(a) Bearing before cleaning.

(b) Bearing after cleaning.

Figure 3.8: Difference in cleaning bearings.

unnoticed.

3.1.7. Issues that Occurred

Not everything ran as smooth as initially hoped. There were a number of issues that occurred through the testing process.

- During the first 2 weeks of doing tests at room temperature, there was the issue of the motor vibrating and rotating around 160 degrees between starting and finishing the upload of the code to the Arduino. After that it would run fine. It would stop with vibrating before the first line of code was run, which made it difficult to track down the bug. It was eventually partially solved with using the ENABLE pin to turn off the motor when not actuating it. There was also the issue of the motor making a high pitched tone and pulling 6 V instead of the 12 V. It turned out that it didn't happen when the code that had previously ran was properly ended. So removing the USB from the Arduino while it was running, caused this behaviour for the next time it was running a piece of code.
- As mentioned in subsection 3.1.5, the noise in the potentiometer suddenly increased tremendously. This however only occurred for half of the time. The other half it would have worked just fine with little noise. Changing some parameters in the code or wiring would switch it from a broken state to a fixed one, but undoing the changes didn't reverse its state. So there was some correlation, but it couldn't be explained. In the end it didn't matter anymore, since it got stuck in it's broken state, with a large amount of noise. This was fixed with writing a piece of code that would take the running average.
- There was also a period of time that the readout of the potentiometer would just give a readout in the range of 300-1000. In the situation that it should have given a readout of lower than 300, it just returned 300. It still showed linear behaviour between 300 and 1000. The wires in the potentiometer didn't have a short circuit, and weren't broken either. This issue was never solved, and a new potentiometer was used. It was likely broken in the ultrasonic acetone bath. A similar potentiometer was used, but this had $10~\mathrm{k}\Omega$ instead of $100\mathrm{k}\Omega$. The power consumption was now a ten fold higher, but it was still neglectable.
- The ultrasonic bath increased the resistance in the potentiometer from $100k\Omega$ to $135k\Omega$, and from $10k\Omega$ to $13k\Omega$. This didn't matter, since the output was linear between zero and its maximum resistance.
- In the initial versions of the code, it would not take the correct number of steps before reaching its position. After each step the position was evaluated if it should take another step. It turned out that the motor is not that reliable when taking individual steps. They turned out to be on average 2.2 degrees instead of 1.8 degrees. So some steps were skipped. The solution was to calculate the total number of required steps and move to this position in one go, and evaluate afterwards. This drastically reduced the error.

Not only bad things happened. The polarized capacitor was by chance connected in the correct way, so it didn't explode, which is nice.

3.2. Making a Cryogenic Precision Screw

The next step is making the fine threaded precision screw work cryogenically. This would make it possible to transfer a rotational motion, to a very fine linear motion. The 1/4"-170 screw from THORLABS was selected, since it had the highest number of threads per inch while still making the thread and bushing out of the same kind of material.[92] The idea was that this would prevent problems while cooling down.

The fine threaded screw was attached to the motor to also test it at 3 K. A connection with a motor coupler to a 2 mm hex key was made to connect everything. A 2 mm hex key fits in the knob of the precision screw to easily actuate it. Increasing the diameter of part of the hex key with thick aluminum to 4 mm made it possible also attach it to the motor coupler. The only option to mount this inside of the cryostat was vertically. Little effort was put in to making a proper attachment, since this was just a temporary setup to test the precision screw. Most parts were fixed in place with tie wraps, which apparently hold out well at 3 K. A thin strip of copper was also attached to create a vertical sliding constraint, to the bushing can rotate and move freely vertically. The sliding element was also quickly made with tie wraps. The whole setup can be seen in Figure 3.9.



Figure 3.9: Setup with Precision screw.

The precision screw was put in an ultrasonic acetone bath with the bushing still on the thread. It was uncertain if they could be assembled again, so it was first tried still being attached. The screw partially survived the ultrasonic bath. The ball on the tip fell off during the bath. It was attached with epoxy, and can be reattached at some later moment. The 170 threads per inch, meant that 1 rotation resulted in a translation of roughly 150 µm. It was chosen that it would rotate 30 full revolutions to see if it would be able to move. The vertical distance was measure with a caliper to check if everything moved as programmed. The code used was a modified version of the previous code, and can be found in section B.5 in Appendix B. After the first cooldown it had rotated around 15 full rotation, instead of 30. It was cooled down a second time, but now the value 'delaystepper' was set to 1000 µs instead of 500 to reduce the rpm and hopefully increase the torque. It didn't change much, since after this cooldown it rotated around 20 full revolutions. This wasn't really a predictable result. The expectation was that that there were still some lubrication residues, so the bushing was taking off and the parts were cleaned another time in an ultrasonic acetone bath. It was assembled again, and it still rotated really smooth for a screw with no lubrication. The system was cooled down another 3 times before before there were good results. The first cooldown had to be aborted, since the vacuum was not low enough due a wire which slipped between the rubber seal and the vacuum shield. The second cooldown gave no results due to a mistake in the code. And the third cooldown showed that the expectation were correct, because this time is perfectly rotated the full 30 turns. There was however a misalignment of 90°. So either it overshoot a little, or undershoot it by 270°. It was unclear what caused this error, which didn't occur before at temperature tests.

3.2.1. Production Tolerances

The production tolerances of the precision screw become very relevant. Especially when potentially using the precision screw as a final stage. The product page mentions that "the adjusters and bushings are manufactured to tighter tolerances than the ASME/ANSI Class 3 UTS standard". This is the highest precision there is in this rating, before entering negative production margins.[93] The exact production tolerances are however not given. The company Thorlabs was mailed asking about the production margins and the maximum linear positioning resolution. The mail and the reply can be seen section C.1 and section C.2 in Appendix C.

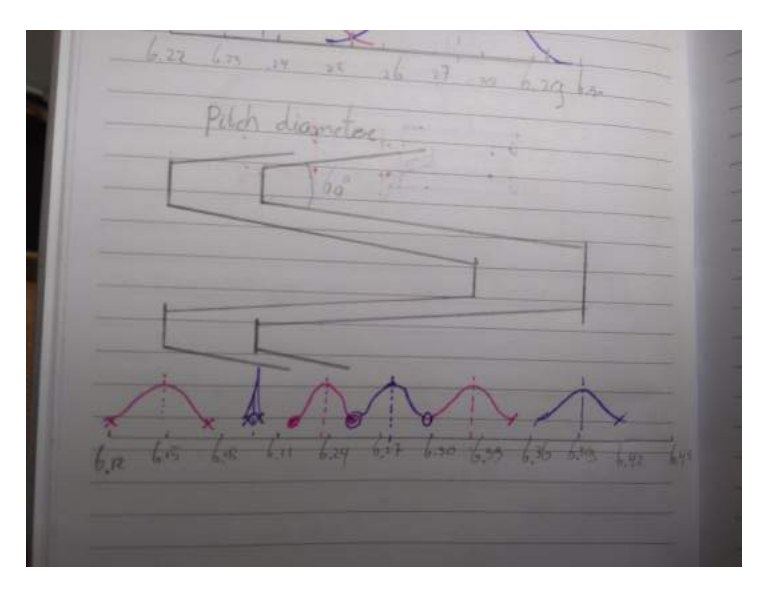


Figure 3.10: Production Margins Thorlabs.

The production margins of the precision screw are shown graphically in Figure 3.10. All the production margins are expressed in the diameter ranges of the major diameter, minor diameter, and the pitch diameter. There is likely a bell curve inbetween the values given by Thorlabs. Their precision screw adhere to the ansi AQL 1.5 quality level, meaning that there shouldn't be more than 1.5% defective items in the whole order quantity, putting it somewhere between σ 2 and σ 3. The figure shows an estimation of this statistical relationship.

Interesting to note from this data, is that the lower limit of the internal pitch diameter and the maximum of the external thread pitch diameter is equal. Likely because if they would overlap, there would be a negative margin left, rendering the precision screw nonfunctional.

The production margin is in the range of 3 to 4 microns. This is significant more than the preferred positioning accuracy of 10 nm. These production margins are for the diameter of the thread, not the axle precision of the screw in general. The assumption is that they are correlated, but not 1:1.

It is very difficult to get an accurate value for the axle accuracy of the screw. Although not being a correct way to calculate it, relating the error in the diameter via the 'horizontal' and axle component of the thread could give a guesstimate. The length of the thread for one revolution is $\pi*1/4"=19.8$ mm, for each axle translation of 0.15mm. This means that the proportions of distance traveled horizontally and axle is 1:132. If it is also true to also correlate the error in diameter to the axle error, that would mean that the axle error of the screw is somewhere in the range of 23-30 nm.

Although that the surface roughness is unknown, it is likely that it is higher than the error or 30 nm. But there is also a lot of surface area. The bushing is 13mm long, meaning that over a length of 1.72 m, there is contact between the internal and external thread! This should even out some uncertainties of the surface roughness, since the two surfaces will likely mostly touch on the highest points on the surface. What it would mean exactly for the axle accuracy is hard to tell.

3.2.2. Issues that occurred

A second precision screw was also bought from Newport with 254 threads per inch and a 280 nm sensitivity.[94] It was taken apart and also given an ultrasonic acetone bath. The screw had quite some rotational resistance before the bath. There was some hope it would be better afterwards, but the resistance in the screw remained very high. It could also be a combination with issues of potentially misaligning the thread when putting the bushing back on, since the problem was worse than before the ultrasonic bath. The screw was eventually discarded because of this issue.

3.3. Speeding up Design Iterations

The cryogenic testing process is time consuming due to the long iteration time. The cooldown process roughly takes 4 hours, and the warming of the system another 4 hours. Doing some changes on the system, cooling it down, doing the test and letting it warm up again often drags on to the next working day. It is therefore interesting to properly plan the day and be done with the system at the end of the day, so overnight it can either warm up or cool down for the next morning.

In the past, Single Quantum experimented with putting a resistor in the cryostat to heat up the system faster. A meeting was set up with a colleague to discuss his previous work on this. It was a straightforward simple design, with just a $50~\Omega$ resistor screwed on the cold head, with some power running through it. So two SMP connectors were soldered on a similar Thick Film Resistor as shown in Figure 3.11 and was screwed on the coldhead with a screw.[95]

The heater didn't work as expected. The extra wiring caused the temperature to increase to above 3.5K. And the heating power seemed to be minimal compared to how much enthalpy needed to added to the system. Not soon after the idea of this heater was discarded.

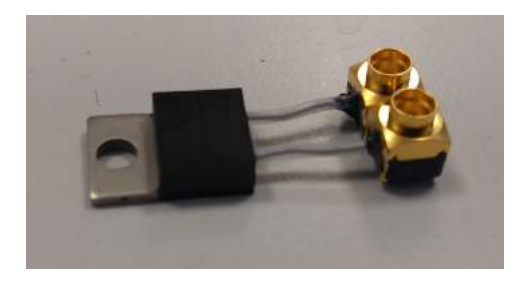


Figure 3.11: Resistor that was placed in the system.

3.4. Expert Meeting

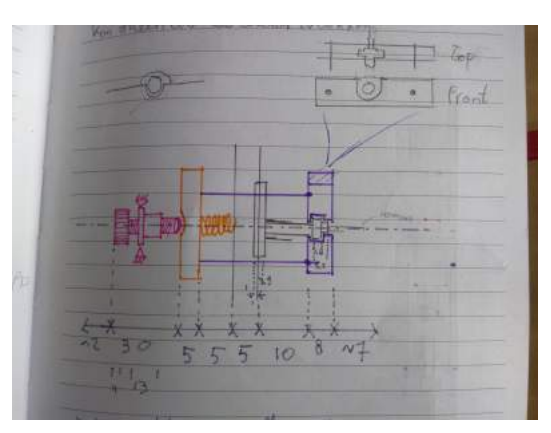
At this point in the project, there was a rough idea for 2 designs. One with a bevel gear, worm gear and a flexure mechanism, and the other with a bevel gear, precision screw and flexure mechanism. However, no one in the company had an expertise on precision mechanisms. It was preferred to have a discussion with an expert to verify the design before continuing with a more detailed design. Five different experts of the TU Delft were contacted together with an external company, but none had the time or could freely be spoken with because of not having an NDA. Also the PHD A. Amoozandeh Nobaveh was contacted, who fortunately did have the time to discuss the design. He has an expertise in compliant mechanisms and wrote multiple papers on the topic.

There were two key takeaways from the meeting. First, he suggested to reduce the the number reduction mechanisms from three to two. The current idea involved a gear, with a rotational motion as its input and output, a precision screw with a rotational input and a linear output, and a compliant lever with a linear input and a linear output. He pressed that three different mechanism are too much. Ideally, it should be just one that is not realistic. So the option of just 2 reduction mechanisms is now further researched. The position resolution can still be achieved with a worm gear and the precision screw. The second key takeaway is the tip to stick to just rigid mechanics or a full compliant mechanism. Otherwise the systems has both of the issues of a compliant and rigid mechanism. The rigid mechanisms have problems like friction and backlash, while compliant mechanisms have elastic deformation and a relative complex design.

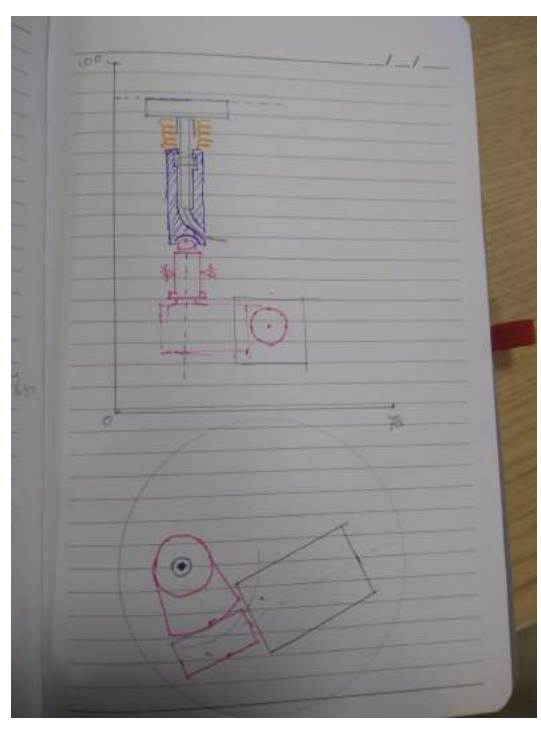
Design Process

As a starting point of this design, there was the wish that all the forces would be put on one workline. This will prevent bending moments, but will require a compact design. Next to that, the idea of using the precision screw to directly drive the fibre was pushed forward, after the discussion with Ali described in section 3.4.

The inner dimensions of the 3 K cold shield are 78 mm diameter and a height of 100 mm. Within this dimension there should fit: the radius of curvature of the fibre, the ferrule, the PCB, the mount, precision screw, and the main wheel of the worm gear. Multiple designs were made to see how everything would fit inside of the assembly. One of the initial ideas can be found in Figure 4.1a. The purple part is the mount holding the fibre, the gray part is the mount and the detector, the orange part is a preloaded block that transfers the motion of the precision screw. It does so without transferring a torsional reaction force of the precision screw due to it being a point contact. This is connected with two wire flexures to the fibre mount. It is thus preloaded in a fixed position, and can be moved backward with the precision screw. The wire flexures transfer only one Degree Of Freedom (DOF). The other DOF's of the ferrule are already constrained by the sleeve.



(a) First sketch of the assembly.



(b) Second sketch of the assembly.

Figure 4.1: The first Designs

The dimensions of the assembly are too large to fit inside the shield. When sawing off the remainder of the precision screw it would barely fit. The total fibre length is 25 mm, the mount is 5, the block and the spring will likely each take 5 and the precision screw another 30 mm. This leaves just 15 mm, including the rotational space of the incoming glass fibre. These have a minimum rotational diameter of around 25 mm. The limiting diameter is a little bit lower, before the losses in the fibre start to increase.

Single Quantum performed transmission experiments for mandrels with different diameters. Mandrels are used to wrap optical fibres around to reduce the dark counts consisting of higher wavelengths. For a wavelength of 1550 nm it was shown that a mandrel diameter lower than 23 mm shows a significant reduction in transmission with an increase in loops in the mandrel. The diameter is preferably 27 mm, since it showed little to no loss in the fibre.

To create more room for the entire system and the radius of curvature, it was redesigned and put vertically in the cold shield. This redesign can be seen in Figure 4.1b. Everything here is drawn to scale. The design featured all parts of the actuation system. Note that the preload is here in the opposite direction. The fibre is now constantly being pressed out instead of inwards. Also the orange block from Figure 4.1a could be removed from the design thereby simplifying it. Also no wire flexures were needed anymore.

The height is around 80 mm. The width could vary, depending on if the worm gear would be a sector gear or not. In theory it could easily be a sector gear, but it is for now preferably kept circular for R&D purposes.

The current status of the design had some changes. The number of springs is reduced to one, and fitted around the sleeve. A small part is added to prevent loading the tail of the SNSPD coming out of the sleeve and redirect the compressive force of the spring. Also, the indent on the bottom of the fibre holder is removed, so it is just a flat surface. The idea is that the precision screw is now not able to create a horizontal force on the surface of the fibre mount. This force would also induce a moment on the sleeve. Perhaps the surface can be even polished to minimize the horizontal force. There might be however a small horizontal misalignment creating a moment, but it is assumed that this is small enough to be neglected.

Other design options were also considered, like fixing the fibre in place and moving the PCB, creating a push pull motion with the precision screw, changing the position of the bushing and worm gear, all in horizontal and vertical orientations. These ideas had a number of complications, and were deemed inferior or were further developed to the design idea in Figure 4.1b. The elements of this design will now be worked out in further detail.

4.1. Worm Gear Selection

The 80:1 worm gear from Maedler was initially used in the design to get a rough idea of the dimensions of all the parts.[62] Other producers of worm gears were looked into. The priority of the worm gear was a combination of a high reduction ratio, and how compact it was. The module here is an important parameter, which is the ratio of the number of teeth to the outer diameter of the worm wheel. This particular gear had a reduction ratio of 80:1, with an outer diameter of 26 mm, setting the modulus at around 0.3.

A real comparison was never made between different gears, since not once had specifications in the same range. The reduction ratio got close to 80, but it was always smaller. Besides that, all had a modulus of at least 0.5, therefore requiring more space, for a worse performance of 60:1.[96] So the Maedler worm gear was eventually ordered to be used in the design.

The worm wheel had an inner diameter of 6 mm, which would need to fit around the 1/4", or 6.35 mm diameter precision screw. This hole was widened to 6.4 mm at the IWS (Inloop Werkplaat Studenten) at the TU Delft. The IWS unfortunately only had metric sizes and their reamers would be 6.5 mm.

The worm has a 2mm hole, so it can be attached to the axle. The worm wheel had just a dent that needed to be drilled and trapped. A set screw will be used to lock it in place. Eventually a M3 3mm setscrew was bought, and the hole was drilled and tapped accordingly.

The hole in the worm runs through, and it meant for a pin running through the holes. Initially it was thought that this was a tapped hole, but unfortunately it isn't. It is hardened steel, and Single Quantum (SQ) doesn't have the tools to tap this hole. The next best alternative is to glue it in place. Therefore, Loctite was bought on the advice of a colleague. Initially the wrong one was bought. Loctite 638 for

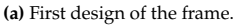
4.2. Frame 35

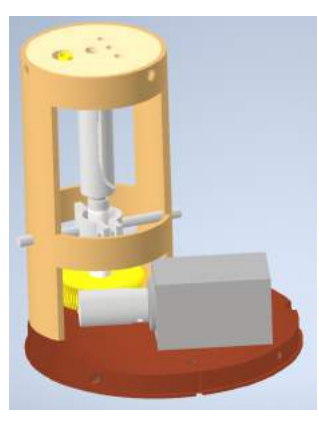
cylindrical attachments was bought, and the worm was glued in place on the axle of the motor, with the help of a 4 mm to 6 mm spacer.[97] This now means that one of the bearing of the motor can not be replaced anymore without breaking this glued bond. It is possible to remove it with heat, but it could potentially destroy the permanent magnet of the stepper motor.

4.2. Frame

A frame is needed in the design to fixate the rest of the parts to. The first idea was to make an open frame with L stiffeners. A first design idea of this can be seen in Figure 4.2a. The PCB would be mounted on the bottom side of the top plate, with the rest of the actuation system below it. Literature like Design principles for precision mechanisms suggests using sheets to resist shear, bearing in mind that the sheets are not loaded in bending.[98] The main loading force is however tension instead of shear, so the design was opted for better tensile performance. The load path would run between the bushing and the detector through the frame. This initial design made it tricky to place the frame on the mount and not have a conflict with the motor, and attaching the bushing to the frame. So it was changed to a cylindrical mount seen in Figure 4.2b.







(b) Second Design of the Frame.



(c) Third Design of the Frame.

Figure 4.2: Changes in the frame design.

The supplier Facturee was recommended to produce the frame. At cryogenic temperatures, is copper is a very suitable thermal conductor, and is thus the obvious material choice.[4] Oxygen copper is currently used for cryostat parts, so this type of copper is also used now.

The diameter of the frame is preferably as small as possible to have the minimal thermal mass and a compactor assembly. The minimal diameter is given by the PCB mount, discussed in section 4.3, which is 42 mm. Three different wall thicknesses were offered. So a preliminary estimation of the frame deformation was done to see which thickness was required, and is shown in Table 4.1. The outer diameter is here 42 mm and the wall thickness is 1.5, 2.0 and 3.0 mm respectively. The length of the frame which will be tensile loaded, is around 40 mm long. The modulus of elasticity is 70 GPa.[99] Equation 2.1 is used here to calculated the deformation for a force of 50 N. 20 N is needed to move the fibre, and a preload doubles that value. Including some margin, gives a value of 50 N to design for.

The frame elongations are all in the nano meter range, so the frame is stiff enough to prevent significant deformations. Note that these calculations were done for a tube with 50% of the material removed as cut outs to be able to assemble the parts. Eventually a wall thickness of 1.5 mm we selected to minimize the mass. The difference in elongation was deemed insignificant.

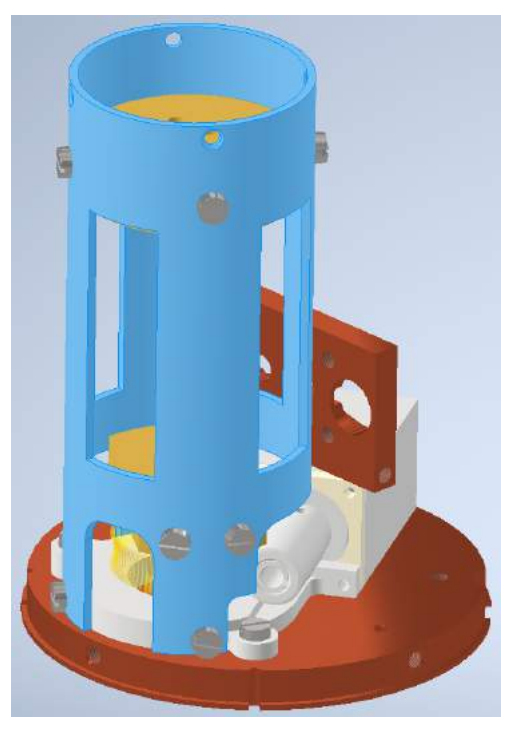
Table 4.1: Elongation for different tubes dimension for copper.

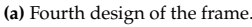
Tube size	Elongation
42x1.5 mm	161 nm
42x2.0 mm	121 nm
42x3.0 mm	80.7 nm

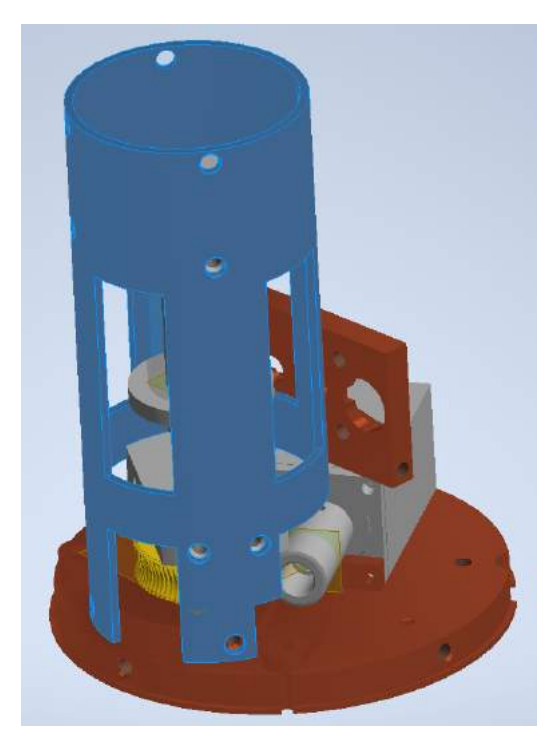
4.3. PCB Mount 36

The frame was redesigned halfway through June 2023. It now had attachment holes for the bottom plate. The height of the holes for the bushing clamp were lowered, making it possible to place the flange of the bushing on it for a consistent position. The open frame that will be loaded in tension now has four 'columns' instead of two, since it was found that the frame was not stiff enough in the horizontal direction. But while still having an open frame, it is possible to inspect the inside to check if everything functions as it should. Initially, one vertical member was 60 degrees wide, but it was reduced to 50 degrees to be able to fit a finger through so the assembly becomes easier. The top part remains the same, but now with an extension of the tube. If the design changes at some point, there is some extra material to work with if needed. The design of the frame can be seen in Figure 4.2c. The frame is still symmetric, so it will deform uniformly. Since one of the lower parts of the frame broke, fillets were added to have some extra material in this corner. Holes were also added to the top for potentially attaching the wire flexure for this different design option. This design is discussed in subsection 4.9.1.

The frame had to be rotated and moved slightly to account for the thickness of the head of the screws. This caused a conflict between the frame and the attachment on the bottom mount. The two screws at the bottom were replaced with one, and a third vertical member was added to properly constrain the frame to the bottom mount. A small cutout was also required to make the design work. This new design can be seen in Figure 4.3a.







(b) Fifth design of the frame.

Figure 4.3: More changes in the frame design.

At a later point the fillets at the bottom were removed, since it breaking off was likely only a problem for the 3D printed part. The holes were also widened to 3.5 mm instead of 3 mm, to allow for production errors. The height of the PCB mount was also lowered. This creates more space on top for potentially putting flexures. This does mean that the precision screw needs to be sawed in two, since the full length doesn't fit anymore. The 'unused' length of precision screw is now removed to create more space. The final version of the frame design can be seen in Figure 4.3b. The technical drawing of the part can be found in Appendix G.

4.3. PCB Mount

The PCB needs to be mounted on a horizontal plate that will be facing downward. First it was a square to fit its frame, but was redesigned to be circular. It was preferred to make the mount compatible with the two types of PCB's that are currently used by Single Quantum. Their 'mushroom' PCB and their

4.4. Fibre Mount 37

'domino' PCB. The later being redesigned and improved version based on the mushroom PCB which is new becoming more obsolete. It was non the less preferred to make the mount compatible with both designs to not limit it's options. The important part is here to keep the sleeve in the same place for the two PCB's.

There were several relative orientation options for the PCB, but one was more logical with no inconvenient intersecting of holes in the mount. Figure 4.4a shows the orientation of the PCB's. The holes and cutouts that were made ensure a good fit for the parts. A number dimensions were largely based on the existing mount of Single Quantum. After the first 3D print of the part, it was found that the hole for the sleeve needs to be larger, since the volume of the stycast wasn't taking it to account. And it needs to be evaluated if there needs to be a way to disconnect the SMP connectors with pliers, like usually is done. This prevents it being loaded on its soldering points, instead of the frame of the SMP itself. There is the chance of it breaking when loaded to often on the soldering points. Hugo mentioned that the loading for the PCB is good enough, so this part of the design can stay the same.

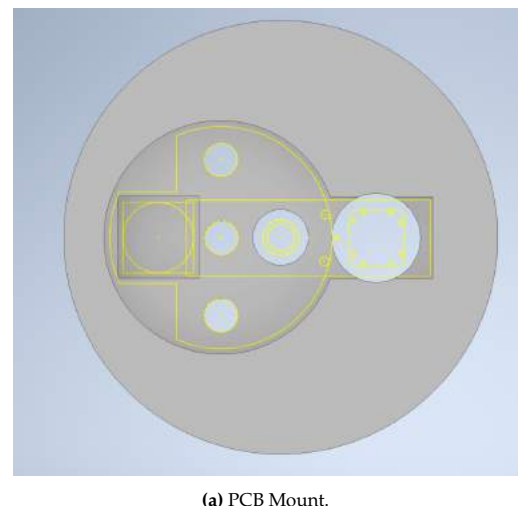
On the sides there were 4 holes added to be able to attach it to the frame. These holes are the same M3 holes as for the heat shield in the mount, to keep the screws needed nice and consistent. The thickness of the part is the sum of the regular thickness for the frame, so 5 mm, and the height of the domino PCB. This means that the top surface of the PCB is at the same height as surface of the PCB mount. This makes it possible to potentially put a bracket over it to keep it lock it in place.

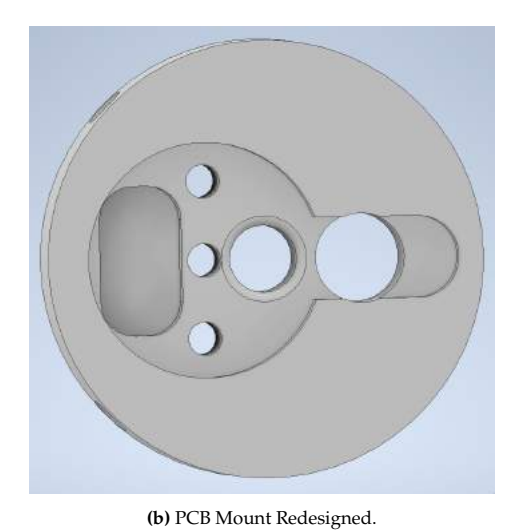
The thread depth is given by Equation 4.1, where T is the depth that needs to be drilled, T_a is the desired thread depth, T_b is the tip margin of the tap, and P is the pitch being 0.5 mm for M3 tread. T_b is unknown, and is assumed to be equal to be 1 mm.[100] This set the drill depth to be 7 mm.

$$T = T_a + T_b + 2P \tag{4.1}$$

The PCB mount has a minor redesign to be better able to produce it while milling. The sharp corners are impossible to mill, so that's is why the new design looks like Figure 4.4b. The technical drawing of the part can be found in Appendix G. The corner are rounded up to their maximum radius of 3 mm. A fillet was also added to the hole of the sleeve, so that there is room for the stycast. Otherwise the PCB wouldn't lay flat on the mount. The thickness is also increased to create a raised edge for the PCB-plate discussed in section 4.8. This will nicely keep it in its place, without it touching the sleeve.

Minor mistakes were removed from this part when making the technical drawings, like the three holes not having thread, and giving the right two curvatures with a diameter 6 mm instead of 7.3 mm making it easier to produce with a 6 mm diameter mill.





(b) I CD Would Redesigne

Figure 4.4: CAD models of two mounts

4.4. Fibre Mount

The first idea of the fibre mount can be seen in the top right corner of Figure 4.1a. The function is to transfer the force for the motion in to the fibre. The amount of constrains added needs to be kept in

4.4. Fibre Mount

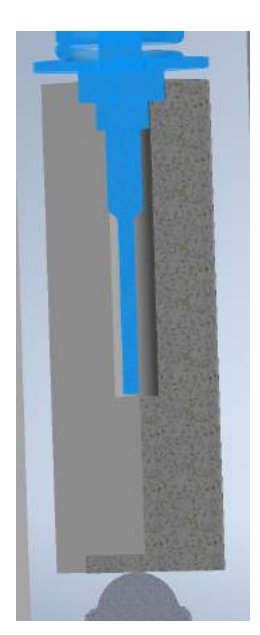
mind to not overconstrain it, and should only transfer a compressive force on the fibre. No lateral forced or moments should be induced on the fibre and sleeve.

The initial idea was to slide the fibre in to a matching slot, but it would induce backlash if it wasn't tight enough. So this idea changed to spring pushing the fibre in to the mount to get rid of this backlash, while also preloading the precision screw at the same time. The number of springs went down from 2 to 1, when it was realized that it could be put around the sleeve instead of parallel to it. The force of the spring and the fibre holder would act on the largest metal brim of the fibre, and on nothing else. This would keep the mount and the fibre constantly pressed against its mount.

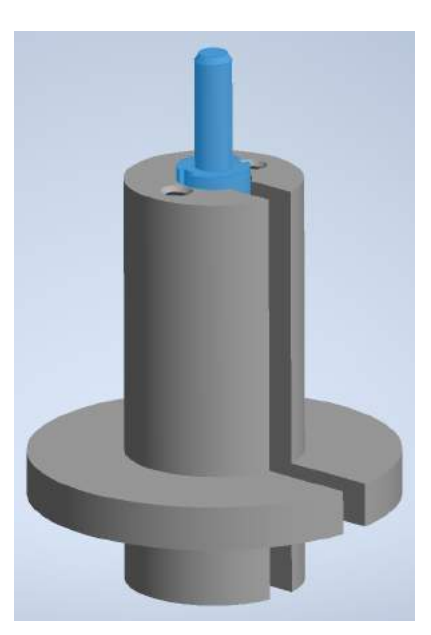
The inside of the fibre mount was just a cutout with the contours of the fibre, as shown in Figure 4.5a. There was a margin around it to prevent contact of other parts besides the largest brim. A small channel was added for the fibre to run through and be able to properly assemble it. This channel has a turning diameter of 27 mm as discussed in the introduction of chapter 4. This summed up the first design that was 3D printed. It was found that the radial spacing around the brim can be lower, and that the fibre doesn't follow the channel as expected, since the path of least resistance is in a different plane than expected. So this channel will be put in a different orientation to prevent this from happening.



(a) First Design Fibre Mount.



(b) Second Design Fibre Mount.



(c) Third Design Fibre Mount.

Figure 4.5: Development of the Fibre Mount.

Eventually, a different spring was selected with a larger inner diameter than the fibre, so the top part of the fibre mount was removed, and a separate plate was added to transfer the load of the spring. The part was simplified to be easily producible. The hole for the fibre now has one diameter, with still a brim to transfer the loads to the fibre. The slot is widened to 2.2 mm, so it can be milled with a 2 mm mill. It is also made rectangular, so milling it becomes more easy. The curvature of the fibre is still the same when it will rest on the corner. The result can be seen in Figure 4.5b.

A final change was needed, since a different spring was selected for one last time. This diameter was significant larger than the fibre, with an inner diameter of 16.4mm. The new idea was to physically attach the fibre to this part, and let the fibre press against the added flange. The fibre is attached to the part by clamping it with two M2 screws. This design can be seen in Figure 4.5c. The technical drawing of the part can be found in Appendix G. An added benefit of this design is that it becomes easier to keep the fibre clean during the assembly process. While doing the test described in chapter 5, it was found to be tricky to press the fibre down in the sleeve with a spring around it and needing to put this part over it. This needs to happen while not letting the fibre end touch anything, since it needs to be thoroughly cleaned before assembly.

4.5. Precision Screw Mount

There needs to be a clamp that creates firm connection between the bushing of the precision screw and the frame. There are many different clamp types to clamp a cylindrical object as seen in Figure 4.6a. The initial idea was to copy a design of a 'pipe clamp', as seen in Figure 4.2b. After some time passed, there was the idea to roughly copy the clamp used by the Thorlabs precision stages, that also clamp down on this bushing. This lead to the design shown in Figure 4.6b. Two of these would be put around the bushing, and will clamp down on it due to the 2 bolts running though it. The diameter is 10 micron smaller than the outer diameter of the bushing to have some clamping force on it.[101] Later it turned out that this was outside of the production tolerances. There is also a small gap of 0,2 mm between these two clamps to ensure proper clamping. The outer radius is the same as the inner radius of the frame. The blind holes to attach it to the frame have the same dimensions as the ones used in the PCB mount.

At a later point a counterbore was added, since the head of the bolt would otherwise conflict with the motor mount. The thickness was increased from 5 to 7 mm to make this possible. The hole diameter was increased from 3mm to 3.2 mm, to allow for some production margins. The technical drawing of the part can be found in Appendix G.

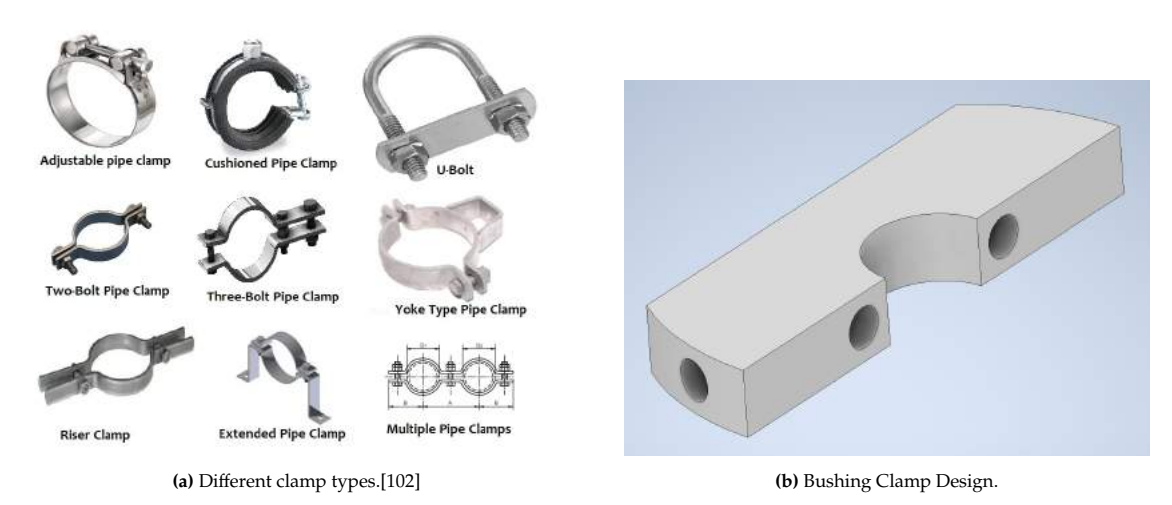


Figure 4.6: Bushing clamp options and design.

4.6. Motor Mount

This parts forms the connection between the frame and the mount, but also be the attachment point for the motor. It will be a similar plate as the PCB mount, but now having an attachment for the motor instead of PCB's. Not a decision could be made on what production process will be used for this part, so it also remained uncertain if the part should be produced for sheet metal of a milled part. The first version of the design can be seen in Figure 4.7. The motor would fit perfectly on the mount, and attach it to the frame.

This part was eventually split up in two separate parts to make it easier to manufacture. There is the frame mount seen in Figure 4.8a, and the spacer to around the circular brim of the motor as seen in Figure 4.8b. To attach the frame to this parts, the same threaded holes are used here as before. The holes for the motor are not threaded, so it can properly 'pull in' the stepper motor when tightening the bolts. At this point there is not an attachment point to the mount of the cryostat. That will be added at a later stage. A similar motor spacer is designed for the alternative and more compact motor discussed in subsection 3.1.1 and can be seen in Figure 4.9b.

When assembling this part, it was found that the worm would intersect the part, so it was locally lowered in height. The attachment points for the cryostat mount were also added. These holes align with two existing threaded holes in the mount. Also fillets were added, such that everything can be milled with a 4 mm diameter mill. This updated design can be seen in Figure 4.9a

The thickness of the screw heads were not taken into account before, so when adding these the assembly didn't fit anymore in the radiation shield. The holes for the cryostat mount needed to be repositioned. The frame now fits with just 0.75 mm margin. Preferably there would have been a bigger

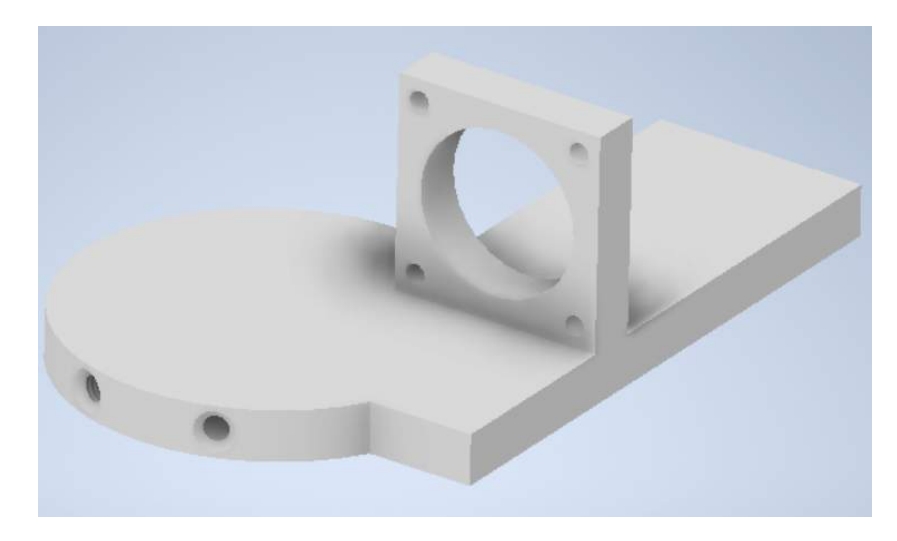
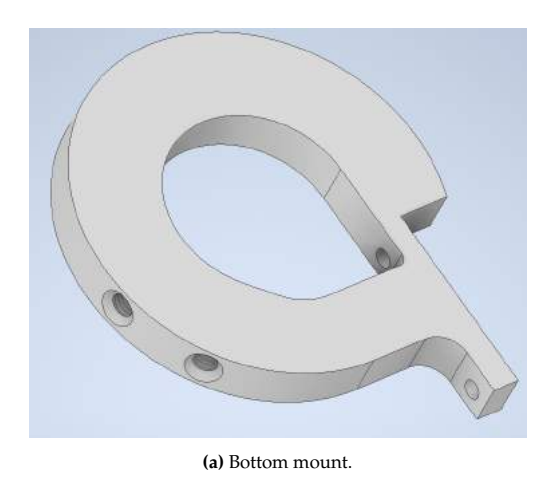
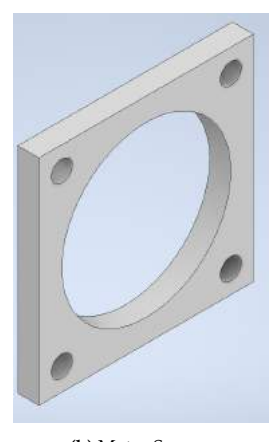


Figure 4.7: First Design Bottom.





(b) Motor Spacer.

Figure 4.8: Motor Frame Mount.

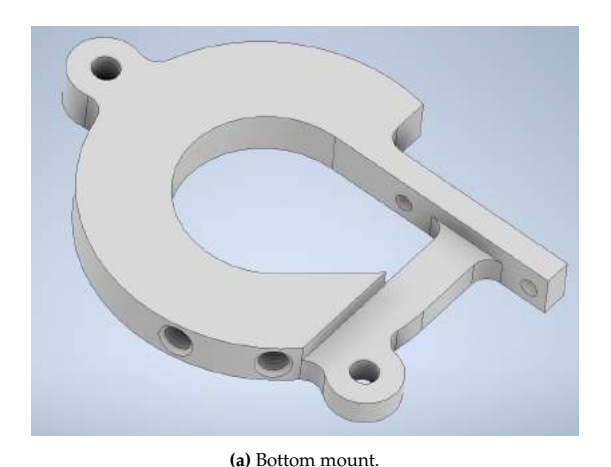
margin, meaning that a smaller diameter tube would have been selected. This would mean that the design would not be compatible with a mushroom PCB anymore due to the lack of space.

The frame had to rotate slightly to fit. In this new orientation, the screws are not conflicting with the cold shield. However, the frame now conflicted with the hole on the mount, so it was reduced to only one screw, but a third attachment point on the side was added to keep it properly constrained.

At the latest point in the design when everything was checked, the very useful tip was given to place a 3D print of the motor mount on the 3K mount in the cryostat, which was an older version of the 3K mount and had a lot of different versions and poor documentation. The CAD model that the motor mount was designed for was indeed outdated and the holes were in a different place. The part was quickly redesigned as can be seen in Figure 4.10. Another minor change that can be seen in that the thickness was increased from 5 to 6 mm, so that there is now just enough space for the head of the screw. The parts that attaches to the motor was kept at a thickness of 5 mm to not conflict with the worm. The technical drawing of the part can be found in Appendix G.

4.7. Spring Selection

A spring is used to preload the precision screw and fibre. This gets rid of the backlash in the precision screw. There are three spring types that can be selected. There are regular compression springs, disk springs as mentioned by Ali in subsection 4.11.1, and multi-wave springs. The latter is compacter and more complex version of a regular compression spring, and it looks like it is less common in the industry. The disk spring seems to be very beneficial, since they can be stacked and their equivalent





(b) Motor Spacer for AM1524.

Figure 4.9: Motor Frame Mount redesign.



Figure 4.10: Bottom mount.

spring stiffness $k_{eq-series}$ follows Equation 4.2 when stacked in series, where k_{disk} is the spring stiffness of an individual disk, and n is the number of disks stacked. In this way, the total spring stiffness can be tuned by adding or removing disks. It is also possible to stack them in parallel. For this situation, $k_{eq-parallel}$ follows Equation 4.3. Or one can combine them in series and parallel to get the desired equivalent stiffness, as shown in Figure 4.11.

$$k_{eq-series} = \frac{k_{disk}}{n} \tag{4.2}$$

$$k_{eq-parallel} = n \cdot k_{disk} \tag{4.3}$$

However, disk springs need a minimum force applied on them, which is around 100 N for the dimensions for this design. This is simply too high for the application, making disk springs not a feasible option.[104] The inner diameter of multiwave springs seems to be relatively large, being large than the diameter of 4.94 mm of the metal brim on the fibre. Preferably, the spring would press down directly on the fibre, since otherwise an extra part could be needed to transfer the load from the spring on to the fibre. The preferred choice is therefore a regular technical spring, since it can directly press down on the fibre thereby simplifying the design.

It is important that the spring will also function properly at cryogenic temperatures. The spring constant k in N/m should more or less remain the same. The equation for the spring constant is given by Equation 4.4, where the shear modulus G is given in GPa, d the wire diameter, D the mean diameter, and n the number of active coils with the dimensions shown graphically in Figure 4.12.[105]

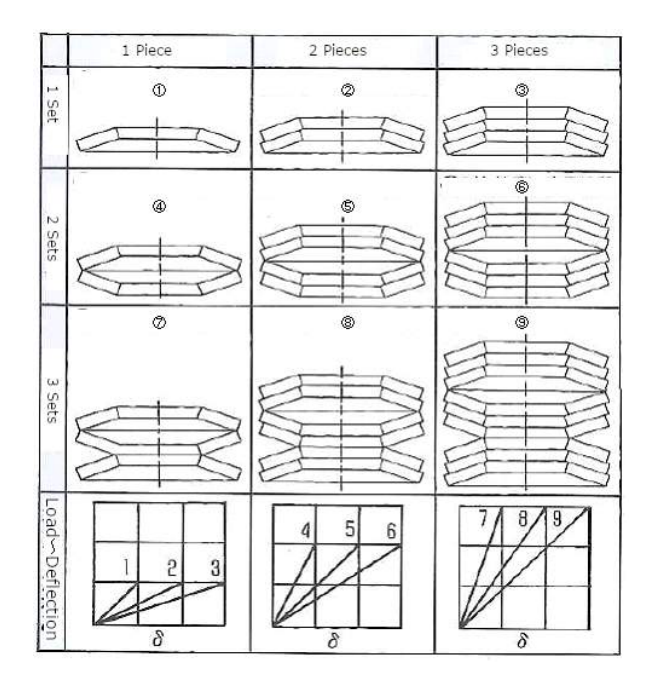


Figure 4.11: Disk springs in series and parallel combinations.[103]



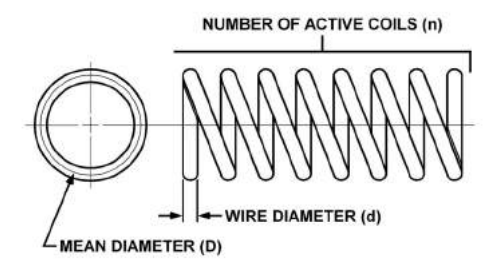


Figure 4.12: Spring geometry.[105]

The only non geometrical factor is the shear modulus, which could change with temperature. No data could be found regarding this. An attempt was made to link the shear modulus G to the young's modulus E and the poison ratio v via Equation 4.5. The relation of E and v versus the temperature can be seen in Figure 4.13. It unfortunately doesn't continue to 0 K, but it does gives some insight. The young's modulus slowly goes up with a decrease in temperature, and the poisson's ratio slowly goes down. This means that the shear modulus and thus the spring stiffness will likely go up with a decrease in temperature. The geometry in Equation 4.5 will also change due to thermal shrinkage, but this effect is here neglected.

There was no real confirmation at this point that a spring would or wouldn't work at 3 K. My supervisor at SQ was reassuring that it would likely work. Part and products are rarely tested at 3 K. Not being able to claim that it works, is different than it actually not working. At this point, the spring selection was continued, without confirmation about the spring behaviour and functionality at 3K.

A source was found that claimed that stainless steel is commonly used material in the industry for technical springs in a cryogenic environment, besides copper alloys and titanium. When choosing a material, several aspects need to be considered like thermal expansion coefficients, and mechanical properties like modulus of elasticity and yield strength at cryogenic temperatures. The cryogenic

temperature means that the material will likely operate Ductile to Brittle Transition Temperature (DBTT), making them far more brittle at cryogenic temperatures. It is also possible that a material loses its ability to deform plastically.[106].

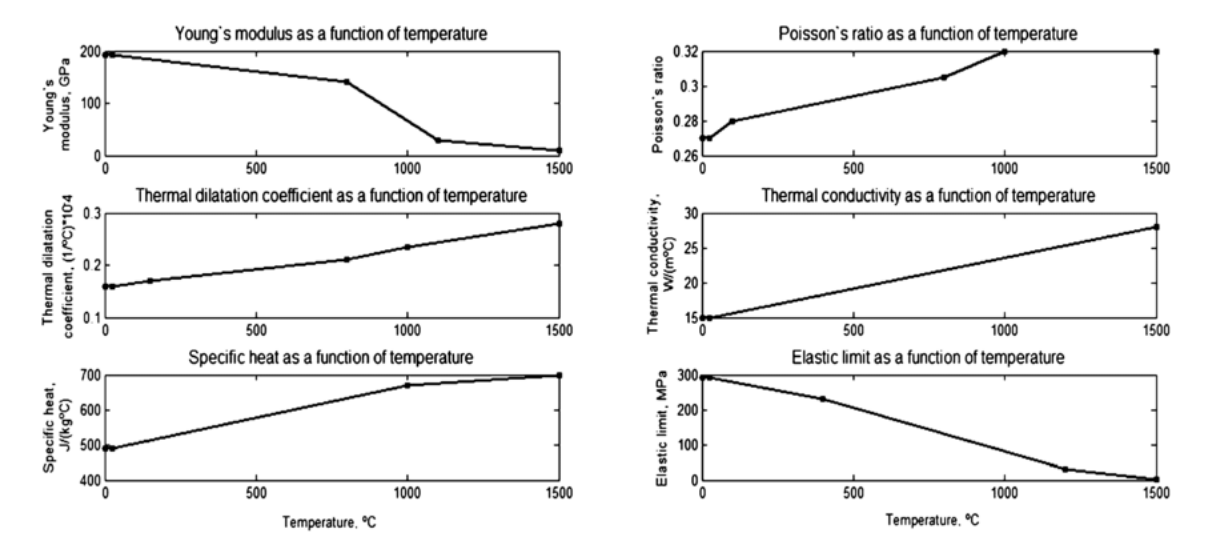


Figure 4.13: Temperature dependent materials properties of AISI 304 Stainless Steel.[107]

$$G_{shear} = \frac{E_{Young}}{2(1+v)} \tag{4.5}$$

4.7.1. Wrong Assumption

So far the supplier Amatec was used to find a suitable spring in their offer. In a call with Amatec, it was discovered that their springs have a lower limit of -200 degrees Celsius. "Despite rising tensile strength low temperatures have an unfavorable effect on the material, as the toughness decreases and brittle fractures can occur." An overview of the materials they offer was sent by mail and can be seen in Table 4.2. The mail contact can be seen in section C.3. The initial assumption that the spring properties would not change significantly was wrong. The springs would likely break at temperatures of 3K according to Amatec.

Spring material	Lowest working temperature in ° C
Patented drawn spring steel wire according to EN 10270-1	-60
Oil tempered valve spring wire according to EN 10270-2	-60
X10CrNi 18.8 (1.4310)	-200
X7CrNiAl 17.7 (1.4568)	-200
X5CrNiMo 17-12-2 (1.4401)	-200
CuSn6	-200
CuZn36	-200
CuBe2	-200
CuNi18Zn20	-200
Inconel X750	-100
Nimonic90	-100

Table 4.2: Lowest working temperatures of Amatec Springs.

This required a new approach to finally find a functional spring. Searching for space grade springs didn't yield the expected results, since the temperature onboard spacecraft is often far above 3K , although already being cryogenic temperatures.[109]. A suitable material needed to be found first. Type 302 Stainless Steel looks suitable at first glance, but no data was here provided that temperatures lower than 77 K.[110] Type 304 Stainless Steel was found not much later to be the better candidate.[111] Its

elongation was still 35% at 4 K, compared to 55% at 300 K, still showing significant flexibility. Because of this reduction, it shouldn't be put under its maximum room temperature deflection, since it is less flexible at cryogenic temperatures.

The crystal structure of the metal plays an important role. A BCC structure has a dramatic decrease in elongation with a decrease in temperature as can be seen in Figure 4.14. FCC structures show a much better response, and are therefore the preferred crystal structure. 304 stainless steel also has a FCC crystal structure.[112]

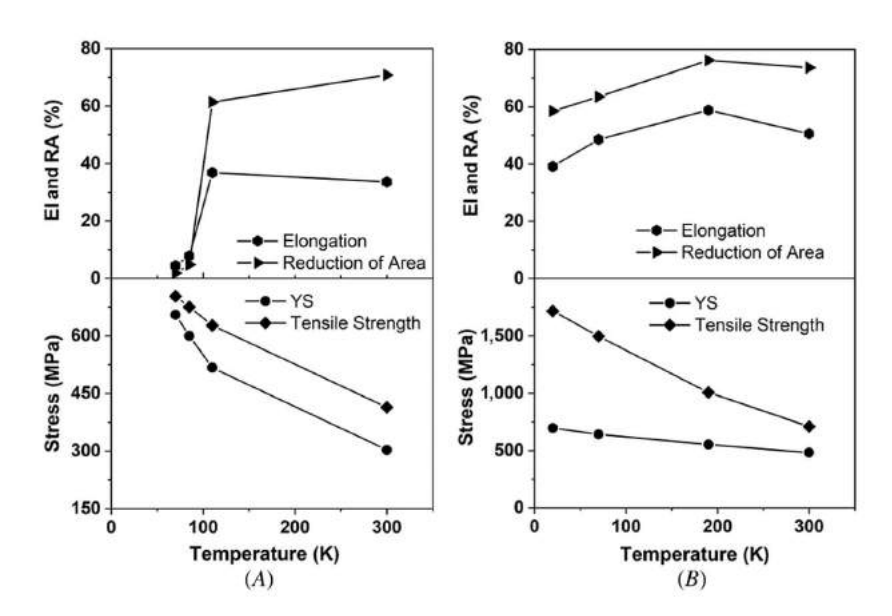


Figure 4.14: Variation in Yield Strength (YS), Tensile Strength, Elongation and Reduction of area for BCC structures (A) and FCC structures (B).[111]

After some searching it was found that Misumi offered springs made out of stainless steel 304, or under a different name '1.4301 Stainless Steel (X5CrNi18-10)'.[113] To stay away from the maximum deflection and load of a spring, since that could cause problems at cryogenic temperatures. All the springs had a larger diameter and a significant larger length. The spring would now go around the fibre, and press on a flange on this part. The fibre is now physically attached to the fibre attachment, to transfer the load of the spring. The compressed length of the spring should be in the the range of 25 mm, with a force of around 30 N. The C264 nicely met these requirements. Its specifications can be seen in Table 4.3. With a free height of 35 mm and a spring constant of around 3 N/mm, gives the exact specifications required. Different springs were possible, but were often too long to properly fit in the system, or had a low stiffness, requiring a lot of deflection to generate enough force. This high deflection is undesired at cryogenic temperatures, since the maximum elongation drops as shown in Figure 4.14.[112]

The C264 spring wasn't used in the 3D printed model initially, so a placeholder spring was used instead. The technical spring was taken from a 123inkt ball pen and used in the 3D printed model to show its functionality. It had to be shortened to have a blocking height low enough that would fit in the system. It was put on a scale, and with a 3 mm deflection and a force of 150g was measured indicating a stiffness of 50 g/mm or 0.5 N/mm. The inner diameter was 3.5 mm, which fits nicely around the 3.2 mm sleeve. With some trial and error, it was found that the 'cut' end of the fibre needed to be on the PCB side and not on the fibre, since otherwise it wouldn't push straight and it would jam. The force of the spring was barely enough to push the fibre out of the sleeve, so the spring was plastically deformed to have a higher initial length and a higher force at its compressed length. This improved the performance of the spring, but it still struggled to push the fibre out of the sleeve when it was compressed longer than several hours. This spring was nonetheless successfully used in the first two experiment described in chapter 5.

4.8. PCB Plate 45

Material	Stainless Steel (EN 1.4301 Equiv.)WPB
End Face State	Grounded
Height H2 in Allowable Load(mm)	16.34
Coil Outer Diameter OD(mm)	20
Spring Constant K(N/mm)	2.991
Reference load P1(N)	33.34
Wire diameter d(mm)	1.8
Total coils Nt	7
RoHS	10
Allowable Load(Range Specification)(N)	50.01 to 73.00
Allowable Load P2(N)	55.8
Free Height Hf(mm)	35
Coil Internal Diameter ID(mm)	16.4
Load Height H1(mm)	23.9
Coil Center Diameter D(Ø)	18.2
Solid Height Hs(mm)	12.6

Table 4.3: Product specification and dimensions of C264 spring.

4.8. PCB Plate

The spring will press down on the PCB, but it shouldn't press down on the lip of the SNSPD that sticks out of the sleeve. A small plate is added to diverge the load path around this. The first idea of this is shown in Figure 4.15a. It follows the contours of the PCB, and can be put in place with the same screw as the PCB is mounted with. Further, it has a groove in which the spring will rest, to keep it also nicely centered. This design can however still push against the ferrule, which is not preferred due to overconstraining it.

The second redesign of the PCB plate can be seen in Figure 4.15b. A different spring was selected, which had a larger diameter. This would overlap with the screw, so the screw was embedded in the part and it would have the same height as the surrounding surface. This increased the thickness of the part requiring an iteration for the spring selection, which required a different spring. Only one spring would fit, but that was good enough.

A third redesign was required, since a different spring was selected. The slot was now closed on the top, to give this spring with a smaller diameter more stability. The thickness of the part was also slightly reduced, since otherwise no spring would fit, and it would reach its blocking height before the ferrule would be close enough to the SNSPD. This design can be seen in Figure 4.16a.

The fourth and final redesign was needed to suit the new spring. This had a significant bigger diameter. The idea of the part remained the same. The height of the slot at the bottom was increased in height, so there would be enough space and it wouldn't damage the bonding wires. This final design can be seen in Figure 4.16b. The technical drawing of the part can be found in Appendix G.

4.9. Other Explored Design Directions

There were a few different design ideas that were explored. The two main ideas are made to prevent the sleeve from being over constrained.

4.9.1. Wire Flexure Design

The design is not overconstrained, as long as everything is perfectly aligned. But if the precision screw is not exactly in line, some moment will be applied on the sleeve thereby overconstraining it. It is expected that this is very minimal, but it could cause a problem. Ali mentioned that it is better to first continue with the design, since it could be unnecessary added complexity for a problem that doesn't exist. The full details of the conversation can be found in subsection 4.11.1.

But if problems are encountered, it would be better to have the possibility to easily change the design to get rid of the unwanted moment on the sleeve. The solution would be to mount the PCB on a wire flexure, to make sure other degrees of freedom of the PCB and the sleeve are free, except for the force of the fibre pressing down on it.

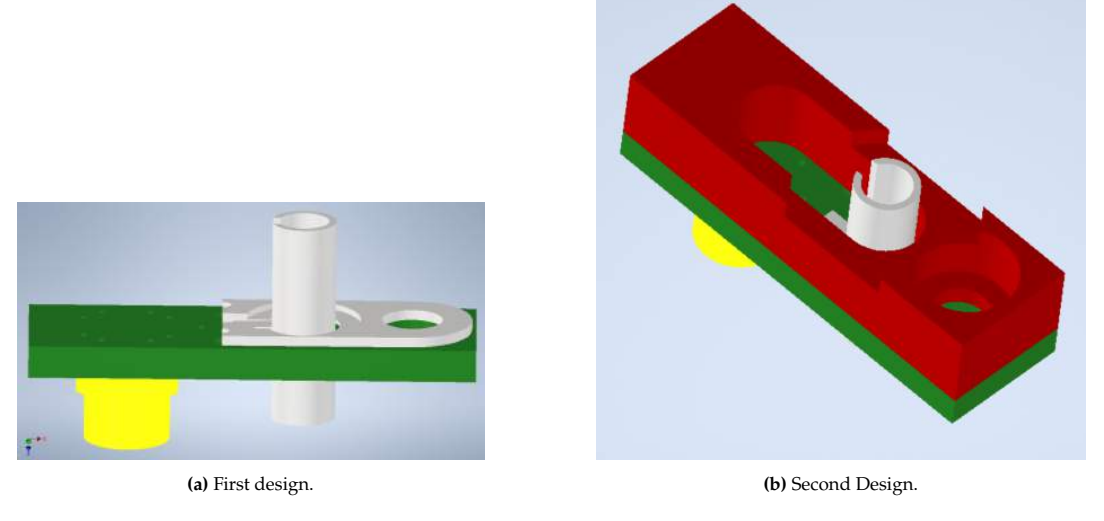


Figure 4.15: PCB plate, placed on top of the PCB.

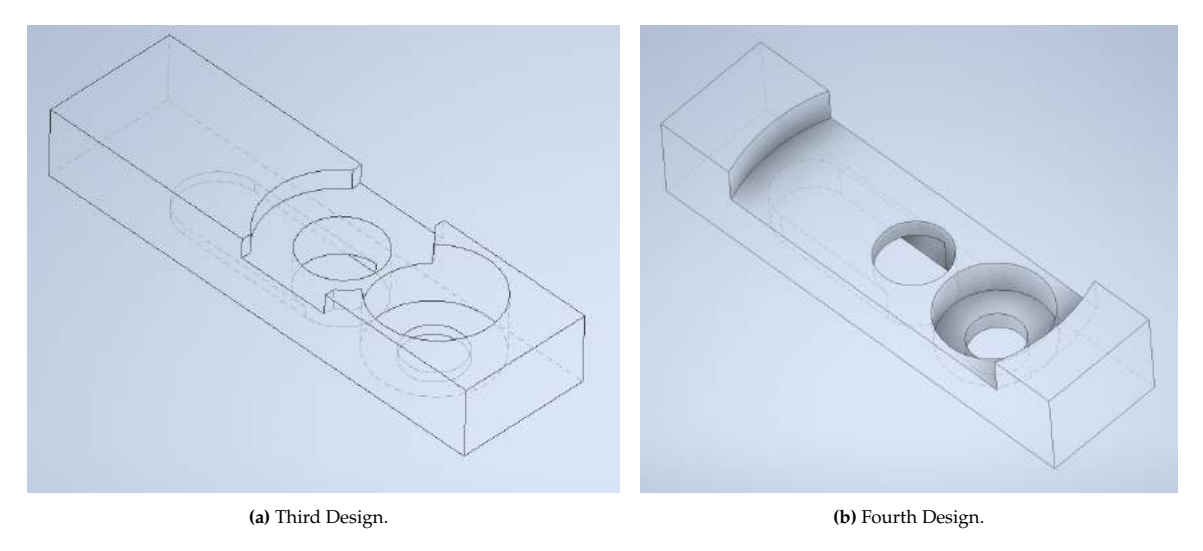


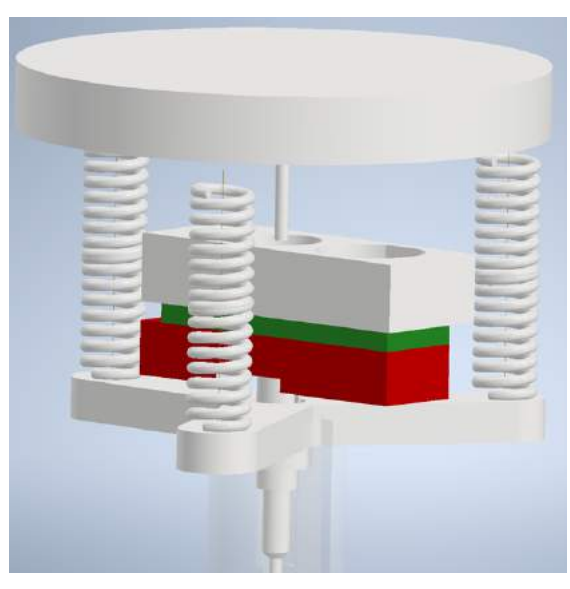
Figure 4.16: PCB plate, placed on top of the PCB.

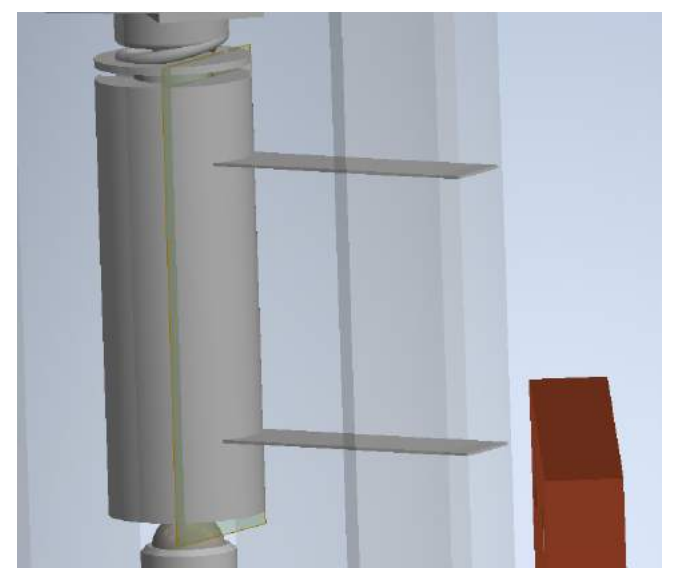
In this design, there was the idea of putting a large spring around the PCB, to not transfer the preload through the wire flexure. Unfortunately, there were no off the shelf springs with a diameter large enough to fit around the PCB, with a compressed length of 5 mm. So this spring was replaced by 3 identical springs around the PCB with equal spacing. The load of these springs would be transferred by a platform with 3 arms. This idea can be seen in Figure 4.17a.

The part the fixed end of the wire flexure is attached to, can be assembled on the top of the frame. Using the maximum available space a flexure of 8 mm can be added. This can be longer by reducing the length of the precision screw, but this length is used for now.

The wire flexure should be strong enough to prevent buckling, which is likely to be its critical condition. To calculate the thickness of the wire flexure, the Euler buckling equation is used, shown in Equation 4.6. Here F is the allowable load, n is the factor for the end conditions, E is the Young's modulus, L is the length and I is the moment of inertia which is $\pi d^4/64$ for a flexure with diameter d. For a force of 20 N, a flexure length of 8 mm, a free end and thus setting n to 0.25[114], and a young's modulus of around 207 GPa for spring steel[115], gives a minimal diameter of 0.475 mm to prevent buckling. With the diameter, the stiffness of the flexure can be calculated. The stiffness k of a cantilever beam is shown in Equation 4.7[116], giving a stiffness of 3.04 N/m or 3 N/mm.

$$F = \frac{n\pi^2 EI}{L^2} \tag{4.6}$$





(a) Design with the PCB on a flexure.

(b) Leaf Flexure

Figure 4.17: Alternative Designs.

$$k = \frac{3EI}{L^3} \tag{4.7}$$

If a part of the precision screw was sawed off, there is extra length for the flexure. Roughly 10 mm of the thread can be removed. Doing the calculations again for a flexure with a length of 18 mm, gives a minimal required thickness of 0.713 mm, and an out of plane stiffness of 1.35 N/mm.

To end this section, the system will be first build without this flexure. If there are issues with the sleeve being overconstraint by unwanted bending moments, the system can be relatively easily be rebuild to this design, since it has been already made compatible with the flexure design. For now, the flexure design won't be worked out further.

It would also be possible to use the buckling of the flexure as a safety mechanism, so that not too much force is applied on the SNSPD, since it can buckle when the force is too high. Later it was reassured, that the spacers of the SNSPD can handle quite some force, and that it is not easily broken by pressing the fibre down hard on it.[16]

4.9.2. Leaf Flexure Design

There was the idea of putting leaf springs on the fibre mount. This would make sure the fibre only transfer one DOF to PCB, and that no bending moments were acting on the sleeve. If it would be combined with the PCB on a wire flexure, it would be certain that nothing would be overconstrained, since the PCB would be constrained in just 1 DOF, and the fibre would be constrained in the other 5 DOF. The leaf flexure would be added as shown in Figure 4.17b

Some parasitic motion would be added, which follows Equation 4.8.[98] Here Δy is the parasitic motion, Δx is the movement of the flexure, and L is the length of thee flexure. The flexure can have a length of 14.5 mm, and a motion of 0.1 mm is assumed, which is significant larger than the reality. This would result in a parasitic motion of 0.4 μ m. This is small compared to other errors, like production margins discussed in Appendix D, so it is assumed that parasitic motion is not an issue.

$$\Delta y = -0.6 \frac{\Delta x^2}{L} \tag{4.8}$$

4.9.3. Backlash mechanism

The frame will contract during the cooldown process. This will introduce additional force on the fibre. It is not sure how significant this problem is. It could be prevented by introducing some backlash in the system, that acts as a buffer for the thermal shrinkage. The fibre could be positioned in its optimal

position at room temperature and by decoupling the actuator. The shrinkage of the system is absorbed by the backlash in the decoupling mechanism. Also drift could be prevented by decoupling the actuator and the fibre. The drawback of this backlash mechanism is that it introduces extra complexity into the system, and that it is uncertain if the problem exists and/or is significant enough to act upon.

4.10. Assembling the Parts

The design was assembled multiple times throughout the design for different versions and situations. This section discusses that was learned for each time a new version of the design was assembled.

4.10.1. Assembly First Iteration

It was tricky to put the parts together for the first time. It was found that assembling the parts inside the frame while it is upside down is the safest way, since the fibre mount will otherwise fall from its position. Part of the sleeve broke during the first try of assembling it.

The parts fitted together quite well nonetheless. The assembly can be seen in Figure 4.18. What was learned from this is that it is more logical to place the clamp on the bushing on the lower side, so it is always in the same location. In the digital assembly, it was placed in the center.

In general, the 3D print also gave a better idea of the physical size of all the parts.





(a) Upright.

(b) Upside down.

Figure 4.18: First physical assembly.

With the parts as they are currently, they fit inside a circle with a diameter of 75.45 mm which is close to the inner diameter of 78 mm of the 3 K cold shield. The setup will thus not fit in a smaller radiation shield that SQ has.

4.10.2. Assembly Second Iteration

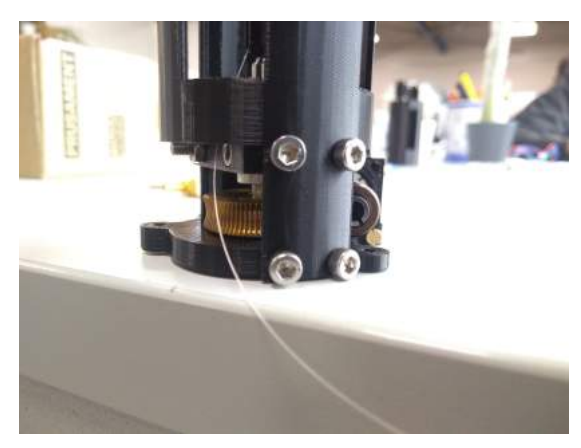
The frame is now higher to fit the entire precision screw, and it can now stand upright. The motor, the motor mount and the gears are now added into the 3D print, which can be seen in Figure 4.19. There were issues with a part of the 3D print breaking and with the assembly order of the parts. The motor should be added last, because otherwise the gears won't fit nicely into each other. However, one of the screws for the motor assembly will be unreachable if done in this order. So, it needs to be first assembled before it can be screwed to the cold head. But, the gear could conflict with the position of screw that

would attach it to the mount. There is however the possibility that it will fit. Later it is shown that it is possible to add the bottom mount with the motor and worm attached to the rest of the frame.

The thickness of the motor spacer is increased by half a millimeter to create some clearance between the worm and the head of the screw that will attach the motor mount to the cryostat, since otherwise there wouldn't be any margins left for assembling it.

This assembly is already getting close to a fully functioning system. If the worm wheel and the worm were attached to their axle with a set screw and a pin respectively, it would already function at room temperature.





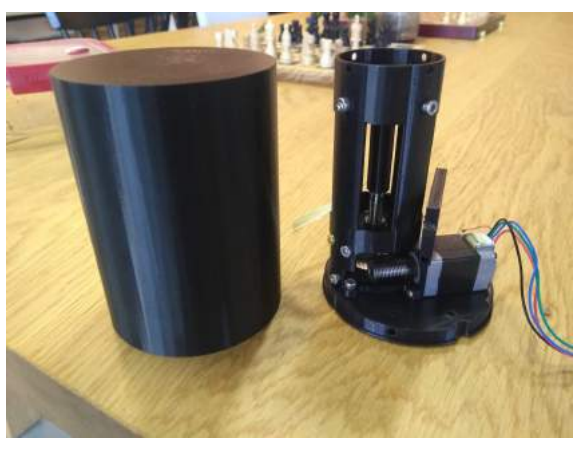
(a) Front view.

(b) Back view.

Figure 4.19: Second physical assembly.

4.10.3. Assembly Third Iteration

In this iteration the PCB mount changed and the bottom mount changed and was mounted on a 3D printed 3K mount Also a cold shield was printed to see if it would fit inside of it. The spacer for the spring on top of the PCB was also added. The result can be seen in Figure 4.20a. The screws were also partially replaced with copper screws, since the screw head is flatter, and otherwise it wouldn't fit inside of the cryostat.







(b) Final Design Assembly.

Figure 4.20

4.10.4. Assembly Fourth Iteration

To do the warm test described in section 5.3, the fibre had to be cleaned and kept clean during the assembly. It was a straight forward assembly, up to the point that the spring needed to go around the ferrule. This needs to happen at a point that is hard to reach with your fingers. There is a risk of

4.11. External Input 50

contaminating the ferrule end and needing it to clean again. The setup in Figure 4.20a was used in this experiment, but with a different PCB and fibre.

4.10.5. Assembly Final Design

The assembly of the final design was harder, due to the stronger spring. It was difficult to keep straight when assembling the parts. The sleeve was likely loaded in unconventional ways during the assembly because of this, but it didn't break during the process. The rest of the assembly was the same as previously. The result can be seen in Figure 4.20b. It was noted that there is now more friction in the precision screw because of the higher spring force.

Some parts are now printed with red PLA. This is because the order for new black PLA was delayed and red PLA was the next best alternative. It is a nice benefit that this final print is now in the corporate style of SQ.

4.11. External Input

There were a few occasions that someone shared their thoughts on the project during the design process, giving some useful tips. Three relevant discussions are described in this section.

4.11.1. Second Meeting with Ali

At this point in time, a month has passed since the meeting with PhD student Ali discussed in section 3.4. There was another meeting to discuss the current status of the design, and some potential issues it faced.

The spring needs to fit in a compact space. Ali suggested that the spring could also be placed elsewhere, and that it pulls on the fibre via a cable. He also mentioned that disk springs are also an interesting type of spring that could be used, since they have a high load capacity for a small deflection. These were not considered, since their existence wasn't known. Disk springs were added to the spring selection discussed in section 4.7.

The tolerances of the precision screw play an important role in achieving the required accuracy. He mentioned that tolerances are often discussed in terms of them acting in series and parallel, and how they affect the position of the end effector. It would be interesting to also do this analysis for the design. To check if the design would meet the specifications, Ali also suggested to do an experiment with a laser to see how it would behave at room temperature.

Also the frame was discussed. He noticed that the two vertical elements acted a little bit like flexures. It would be better to make it out of four vertical elements, to prevent motion in all direction. This will be changed in the following version of the design.

Lastly, there was the potential issue of overconstraining the fibre. If the fibre mount was not fully correctly aligned, it would create a moment on the sleeve. He suggested two potential solutions. The point force of the precision screw could also act on the fibre as a 'point force', therefore not being able to transfer a moment on the fibre. The compressive force would act around the fibre, on a very small ring on the fibre, closely resembling a point contact, although not being one. It would drastically reduce the moment if there was one to occur. The second option involved putting horizontal flexures on the fibre mount, making sure it was always centered and leaving only axial translation as it only degree of freedom. The latter options seemed the most feasible, since there is also enough space to add these flexures. Nonetheless, Ali suggested to first go ahead without these solution, and first see if the problem would even occur, or would be serious enough.

4.11.2. Brief Meeting with Ronan

In a quick meeting with someone with SQ, the thermal conductivity was discussed. The detector should have a good thermal connection with the mount, to be able to properly cool it down. The current idea was to make the frame out of aluminum, and the rest out of copper. Copper is a better thermal conductor than aluminum at cryogenic temperatures. That's why there are a lot of copper parts in the cryostat of SQ. If the frame would be made out of aluminum, there could be a thermal gradient between the cold mount, and the somewhat warmer end of the PCB mount.

To solve this, his initial suggestion was to flip the design upside down to place the PCB closer to the mount. The other option he suggested was to run copper wires between the mount and the PCB mount to create a thermal bridge. He also nuanced the problem by saying that the problem didn't even needed to exist. He suggested me to talk to Niels, and potentially make a quick Comsol simulation to check if

and how severe the thermal gradient would be.

4.11.3. Brief Meeting with Niels

After the feedback from Ronan, Niels was consulted about the thermal gradient issue. If the frame would be made out of aluminum, Niels could also see an issue that it would not cooldown to the same temperature as the cryostat mount. But a low temperature is not that significant for this test, so some temperature gradient is not that bad. Niels mentions that in cryostat design, they use braided copper to create a thermal bridge between different parts. In this way, the PCB mount will likely reach a cooler temperature. A place for a bracket will be added to the PCB mount, so a breaded copper wire can be clamped on here.

The top of the PCB mount has two remaining holes for the attachment of a mushroom PCB. There is a high change that a domino PCB will be used, so these tapped holes are unused. It appeared that these holes have almost the same spacing as an old version of a 'strain relieve' clamp that SQ used to clamp wires on the cold head. With a small modification, this can be used to clamp a braided copper wire on the PCB mount.

4.12. Design Process Discussion and Evaluation

The design process was a long and tedious process. Instead of building a setup for around 3 months, it took double the amount of time. Creating a functional model wasn't the issue, but designing one which would work at 3 K was. The quality of this first design is however higher than anticipated.

The first tests were done with the 3D printed model in July. This could have been done earlier. The setup was roughly done one month earlier, and by prioritizing the minor modifications of the worm gear it could have been another month earlier. Doing this experiment earlier could have confirmed the functionality of the design much earlier. Not much would have changed probably, since the results presented in section 5.3 didn't influence the design. It already worked as expected.

Making 3D prints of the parts really helped push the design forward. Figure 4.21 nicely shows the development of the individual parts and the iterative design process. The design of the parts are interlocking on each other. If one part changes, other parts needed to change as well. This was especially true for the frame, which had the most redesigned of all parts. It is interesting to note that the general shape and idea of each part roughly stayed the same. This could suggest that it was already functional enough earlier on in the design.



Figure 4.21: Design iterations.

In the end there were still a few minor mistakes in the design. The PCB plate was fitted for the

diameter for the spring, but this was done for the centre diameter instead of the outer diameter. This needs to be corrected later by hand to make it fit.

Only at the last week of the design have the ISO standard tolerances for the production been taken in to account. There are presented in Appendix D. Because of this, many holes needed to be widened to make sure it would be possible to bolt everything together. It was however forgotten there should also be some allowed production error between the solid interfaces of the parts. So the PCB mount and the frame have a perfect fit. So it could be that the outer diameter of the PCB mount needs to be sanded down to be able to fit inside the frame. The same holds of the clamp and the bottom mount. These are however on the open side of the frame, making it easier to deform radially and fit around the parts. The last mistake is that the PCB mount would make a short circuit via the soldering connection of the PCB. Some material was removed to fix this.

System Testing at Room Temperature

At this point, the design of the parts has progressed far enough to be able to test the entire system. The separate tests were performed to test the functionality of the setup. The first test was done to prove the basic functionality of the system. The second test had a stronger spring and the third warm test was done with the copper model. The code used during these experiments was also improved during this testing process. But first, the measuring setup used is described.

5.1. About the Setup

The SNSPD is designed to absorb as much light as possible at a wavelength of 1550 nm. This absorption is different for different wavelength of light and for different cavity sizes. Most of the light that is not absorbed is reflected backwards to the source. This reflected light can tell a lot about the fibre position. A broadband laser is used to analyze the reflected spectrum over a wide range of wavelengths. The reflected spectrum should have a minimum at 1550 nm when the fibre is in its optimal position. The shape of the spectrum can tell a lot about the fibre position. These plots are cross sections of the plot from Figure 2.9a.

This reflected spectrum can tell a lot about the fibre position. For a large cavity size, it can be seen that there is a higher frequency for the efficiency over the spectrum. For a cavity size of 1/4th the wavelength, there should be just a valley at 1550 nm. There is thus a higher frequency in the reflected spectrum for a large fibre distance. This can also be seen in Figure 2.9a for a fixed fibre distance. The amount of fringes of the reflected spectrum can tell a lot about the fibre distance. This method is used in a first experiment to show the basic functionality of the first 3D printed PLA model. This model already works in theory, but hasn't been tested for its accuracy.

Being too close, so a cavity size of zero gives a spectrum shown in Figure 5.3c which is more a plateau. When it is optimal, there is thus a clear minimum as can be seen in Figure 5.3b and when the fibre is too far away there is a clear sinusoid as in Figure 5.3a. The Y axis shows the reflected intensity of light in nW over a spectrum of 1200 nm to 1700 nm.

The schematic of the setup used can be seen in Figure 5.1. A broadband laser emits light with a wavelength ranging from 600 to 1700 nm. The setup is designed in twofold. Once for the lower wavelength from 600 to 1000 nm, and one from 1100 to 1700 nm. The beam splitters used in the U-Bench are optimized for 600 nm to 1000 nm and 1100-1700 nm, and using twice the same setup for two different wavelength ranges keeps the efficiency higher. The PCB used is for 1550 nm, so the part for the higher wavelengths is used, and the part for the lower wavelengths is blocked.

The light emitted by the laser first passes through filters to reduce the intensity of the beam and make it safer to work with. A laser safety training was followed within SQ nonetheless. After the filters it is split with a beam splitter which reflects the light below a certain wavelength, and transmits the light above a certain certain wave length. This was so far a free space optical setup. The light is direct towards the U-Bench via an optical fibre. Here the light passes through straight initially and continues to the PCB. Here part of the light is absorbed, transmitted, and reflected. The reflected light enters the U-Bench again, but is now deflected towards the Spectrum Analyzer. The one used here is the AQ6370D Telecom Optical Spectrum Analyzer of Yokogawa. This analyses the spectrum by sweeping over it, and

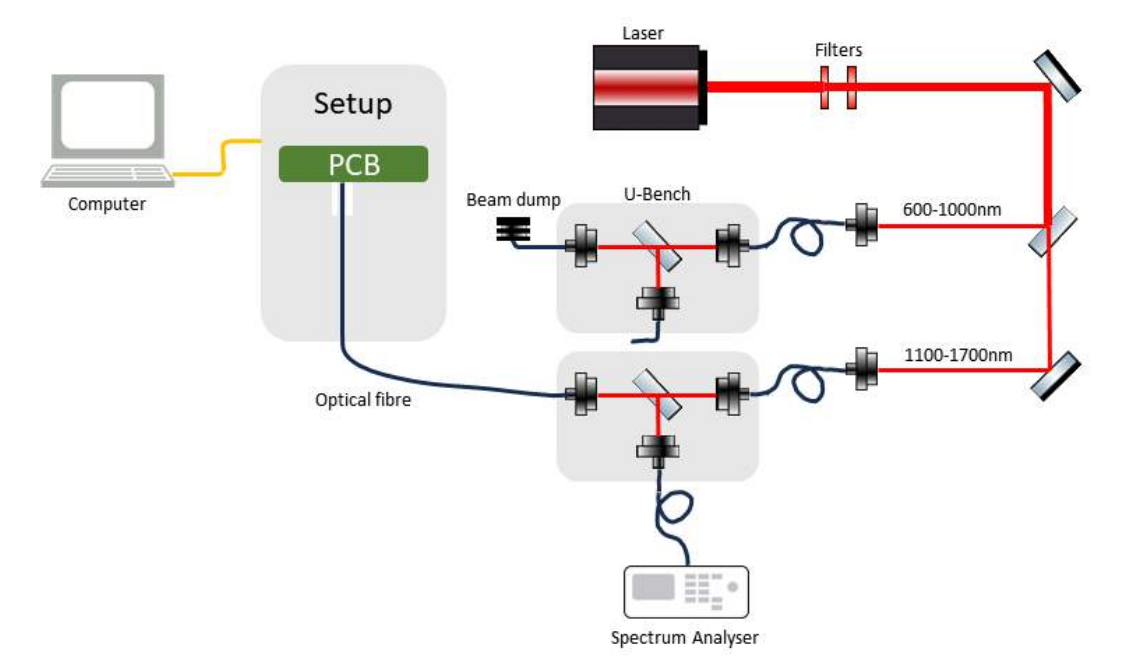


Figure 5.1: Schematic of Optical Setup Used.[117]

returning the light intensity in nW. The computer will control the fibre distance, and the effect can be read on the spectrum analyzer.

The optical setup can be calibrated before usage. The total power of the unobstructed spectrum is measured by using a PCB with a mirror so all the light is reflected. Figure 5.3 shows this maximum power over the spectrum with the yellow line. The noise in the system is also measured by using a beam dump. The spectrum is also saved and can be seen with the green line at the bottom of graphs in Figure 5.3. This noise needs to be subtracted from the total power and also the reflected spectrum of the setup.

The reflected spectrum can be fitted to a model to estimate the exact fibre distance. This is however a difficult process which is prone to errors. The experienced person with this within SQ strongly recommended using detector counts and the reflected power at 1550 nm instead. He couldn't help anymore, since he left SQ to start his PhD.

5.2. Determining the Fibre Position

It is nice to have a good overview on how many steps the motor needs to take for a certain fibre movement. There are 200 steps per revolution, and the worm gear has a reduction ratio of 80:1, so one step is 1:16,000 of a revolution. One revolution is $149.4 \mu m$, so one step is, in theory, 9.3375 nm.

A quick overview relating for the number of steps and the fibre position is given in Table 5.1. It goes up to half a mm. This is unreasonably large, but gives a good idea of the scale.

The reflected spectrum also provide information about the fibre position. This was already previously discussed in the introduction, but will be repeated here due to it's relevance for the experiments.

The detector should have maximum absorption at a wavelength of 1550 nm when the fibre is in its optimal position. This also means that there is a minimum in reflected power. When projecting a broadband laser on the detector and analyzing the reflected light, there should be a minimum visible at 1550 nm since more light should be reflected at different wavelengths. A simulation of the optimal position is shown in Figure 5.2a. This shows the relative absorption, transmission and reflection over the wavelength range of 1200 nm to 1700 nm. There is an absorption peak at 1550nm and the reflection shown by the red line shows a minimum. This reflected power is something that can be measured, and changes for different fibre positions. When the fibre is too close the reflected spectra is more a plateau with a higher reflected power as can be seen in Figure 5.2b. When the fibre is too far away, a sinusoidal can be observed where a higher frequency corresponds to a larger distance between the fibre and the detector. A simulation with a cavity size of 10 micron is shown in Figure 5.2c which shows that the

Fibre translation	Motor Steps	Angular rotation
9,3 nm	1	1.8 °
46.7 nm	5	9.0 °
102.7 nm	11	19.8 °
504.7 nm	54	90.0 °
999.1 μm	107	193 °
4.996 µm	535	2.7 revolutions
10 μm	1071	5.4 revolutions
50 μm	5355	26.7 revolutions
100 μm	10,710	53.5 revolutions
500 μm	53,548	267 revolutions

Table 5.1: Relation Motor steps and Fibre translation.

maximum absorption is no longer at 1550 nm. The shape of the reflected power can tell a lot about the fibre position and if and how the fibre is moving. This represents the primary method for obtaining feedback on the fibre's position during system testing.

5.3. First Warm System Test

For the test was the detector C1513-45 used, together with the fibre 3123951-66 with an transmission of 95%. The fibre was pressed down on the detector at the start and moved back by 10,000 steps, in 2 steps of 2000 steps, and one step of 6000 steps. This resulted in the spectrum shown in Figure 5.3a. The Y axis shows the reflected intensity of light in nW over a spectrum of 1200 nm to 1700 nm.

The fibre was now roughly 100 µm from the SNSPD. Harmen, the SQ employee who built the setup, mentioned that the fibre was indeed far away. This position was the starting point. The fibre was now moved closer again, with increments of 2000 steps. When the spectrum on the spectrometer started to show a lower frequency in the reflected spectrum, the number of steps were slowly decreased to 500 steps, 100 steps and 20 steps with Harmen providing guidance on how close the fibre was, and how many steps to take. The reflectance when the fibre got close is shown in Figure 5.3b. At a certain point the spectrum didn't change anymore when moving the motor. As expected is seemed that the fibre was pressing on the spacer and couldn't move any closer to the detector. This spectrum is shown in Figure 5.3c. Harmen mentioned that he was positively surprised by how well the fibre could be positioned and how nicely the graphs resembled the optimal spectrum and the 'too close' spectra he has seen before.

There was an attempt to move the fibre backwards, but this didn't go well. It just stayed in its position. It was first moved backwards with 50 steps, and after that with 1000 steps, but it didn't change. The 123inkt spring wasn't strong enough to push the fibre backwards. After giving the system a few taps by hand, the spectrum changed to Figure 5.3d, indicating the the fibre had moved backwards. A handful of things need to be taking in to account when looking at these results:

An issue with the motor occurred when starting the experiment. It first started vibrating with a slow movement when uploading the code. After that the code ran without problems. This bug has occurred before, but was thought to have been solved. It rotated roughly 200 steps before initiating the code. Because of this, the motor was turned by hand, when the input needed to be 500 steps or lower to mitigate this error.

Another side note of this setup is that the reflectance is measured. The inverse of the graph is the absorption. This however neglects the transmittance of the SNSPD. This is however minimal to the absorption, and can be neglected because of it.[16]

During the experiment there was a discrepancy between what the fibre should have moved, and the movement that Harmen deducted from the change in the graph. There was an order of magnitude difference. When the fibre was move in theory by 1 μ m, Harmen mentioned that the movement was in the nm range.[16]

When the motor was far away, the resistance of the worm increased significantly and it also started squeaking. This is because of the system's design flaw. The worm wheel also moved down together with the fibre, creating its own misalignment with the worm. During the experiments the deflection

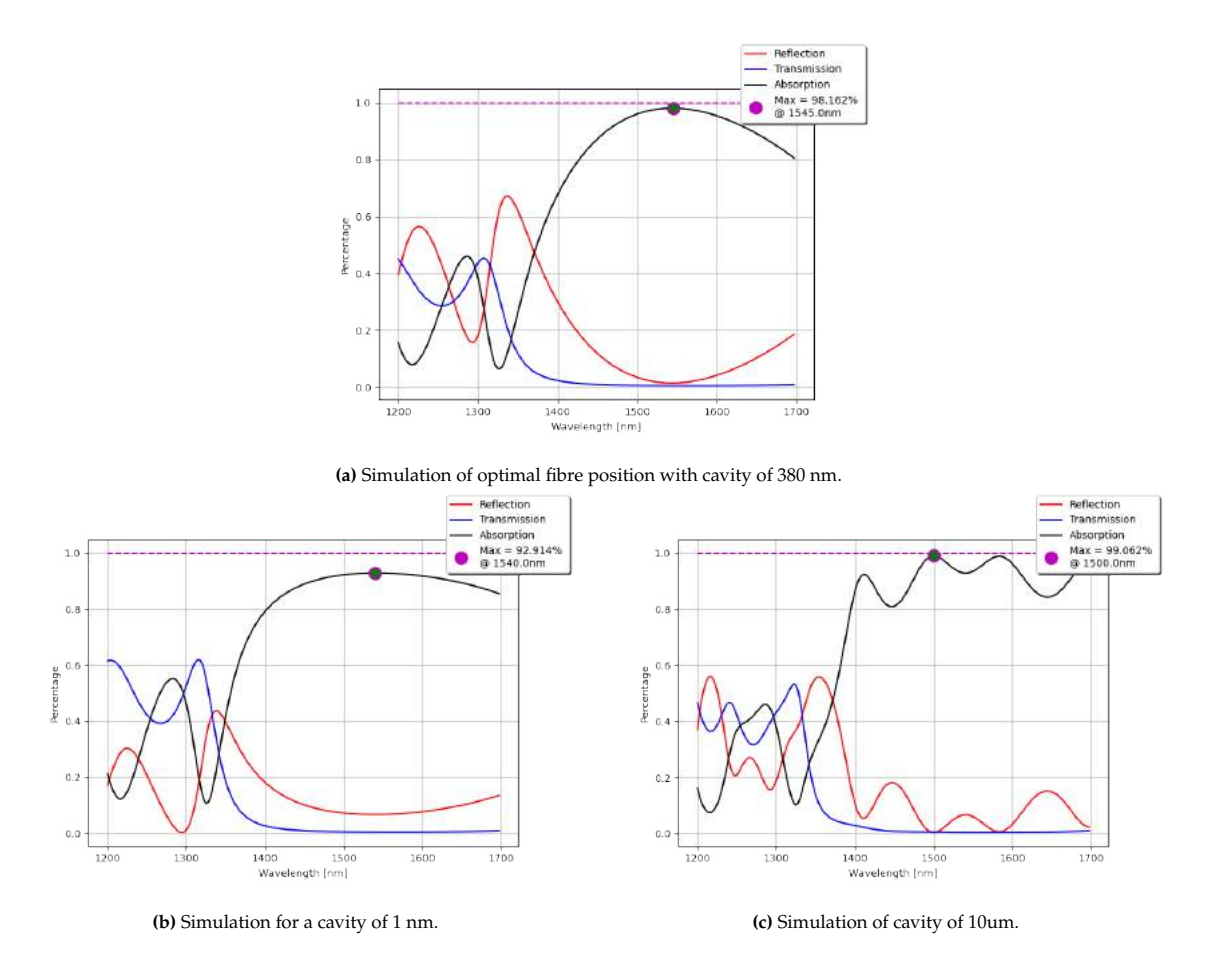


Figure 5.2: Absorption (Black), transmission (blue) and reflection (red) over a wavelength of 1200-1700 nm.

was way larger than usual. It was expected to say in the range of 1 μm, not 100 μm.

Nonetheless, the quick and dirty results of this first experiment were promising. It proved the basic functionality of moving the fibre with small steps. The motion was smooth and it didn't jam and the spectrum showed that the fibre was straight in front of the SNSPD. A next step could be to better quantify this experiment, and export the data for a constant change in fibre position.

5.4. Improved Motor Actuation

The motor issues described in subsection 3.1.7 that were thought to be solved, reoccurred during the experiment described in section 5.3. The unwanted movement occurred when uploading new code to the Arduino. A workaround was found to limit the influence of this. If it were to occur when doing cryogenic tests, a day or more could be lost to this issue. Therefore, a new code was written to work around this issue.

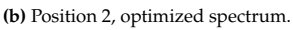
With python, it is possible to send inputs to an Arduino with pySerial. The code used can be seen in section B.6. The code used on the Arduino can be seen in section B.7. The python scripts asks the user for an input on how much the fibre should move. The script converts it to a byte array with a number of steps and a direction, which is sent to the Arduino. The Arduino code scans for incoming byte arrays, and executes them. This code was based on an existing code at SQ.[118]

It was noted that the motor jerked a little when putting power back on the motor, indicating that it was somewhere inbetween steps. The code was written such that it would turn off when it reached its final position. It seemed like this was too quick, and that the inertia would cause it to overshoot a little. Adding a delay of 100 ms got rid of vibration, indicating that the keeping the holding torque for a short while kept the motor on the correct step instead of overshooting it.











(c) Position 3, too close

(d) Position 4, far away.

Figure 5.3: Reflectance of broadband spectrum of fibre in different positions of first test. Reflected power in nW on the Y-axis for wavelengths 1200 nm-1700 nm on the X-axis.

5.5. Second Warm System Test

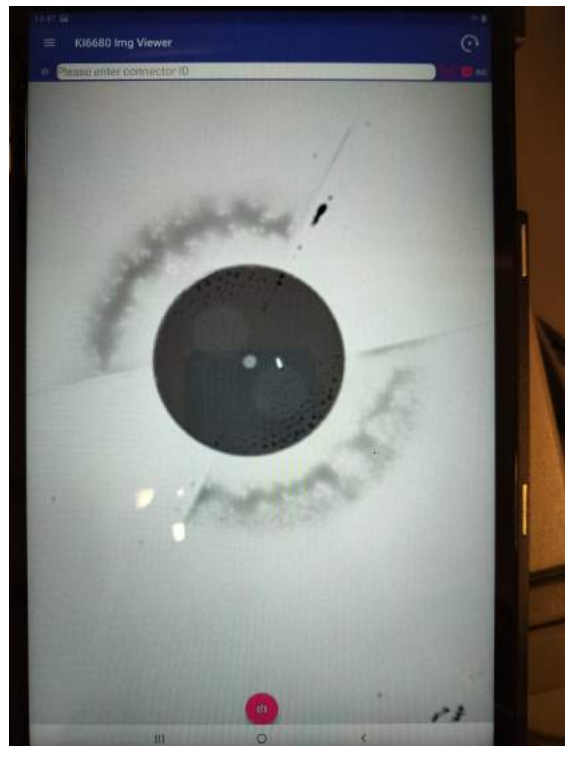
The goal of this second warm test is to see how predictable the motion is. The fibre is first placed on the spacers and moved backwards from this point. It is also moved inwards again to see how repeatable the motion is.

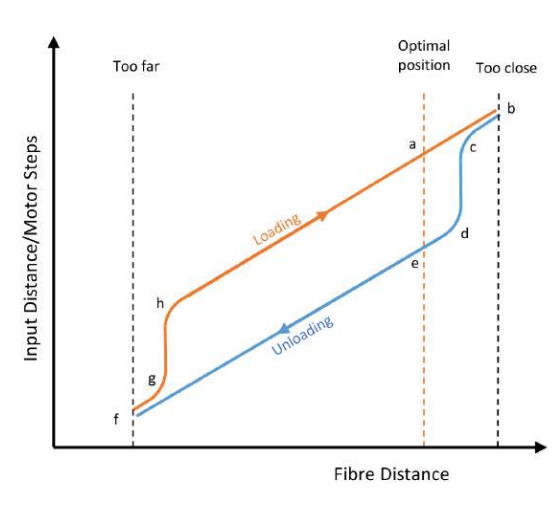
This second experiment used a different detector than before. The experiment described in section 5.3 used a detector with chromium spacers. The drawback of chromium spacers is that it leaves debris on the fibre and the spacer. When preparing and cleaning the system for this test, it was found that the fibre had gotten dirty from the last experiment. Figure 5.4a nicely shows the mark left by the spacers on the fibre end face. These markings do however confirm that the fibre and SNSPD are centered in the sleeve. The fibre endface is cleaned with a special kind of paper to get rid of the debris. Adding a bit of alcohol will help when it doesn't come off completely.

To keep the fibre cleaner, the new PCB has gold spacers. They are from the C1461 batch (this one is the C1461-17) and have a thin spacer of 300 nm. Current PCB's are produced with a 550 nm spacer, as it was found to be the optimum. The thinner spacer allows the fibre to actually get too close, so it can be demonstrated that the fibre can be positioned at the optimum of 1550 nm, which is at around 400 nm. Later in the experiment it is shown that the optimum wavelength when touching the spacer is indeed lower than 1550 nm.

As a start, the total reflection and total absorption were measured. This is done with a gold mirror and light traps. This creates the yellow and green graphs in Figure 5.5. The noise needs to be always subtracted from the total power and measured spectrum to be able to properly compare the spectra. As can be seen the power of the total reflected spectrum is not constant. So knowing this data, it would also make it possible to normalize the data.

The second test is initiated by moving the fibre closer to the detector until it touched the spacers. This





(a) Dirty Fibre Endface.

(b) Hysteresis Plot Estimation.

Figure 5.4

is done according to the readout of the optical spectrum analyzer. It is moved closer with increments of 2 μ m, 500 nm and later 100 nm when the fibre got close until the spectrum didn't change anymore which confirmed that the fibre was on the spacer. This formed the starting point of the experiment and the spectrum can be seen in Figure 5.5a. NB: when a distance is mentioned, it is the theoretical distance that the fibre should move according to the motor input. Due to hysteresis it is uncertain if the fibre actually moved this distance.

From the starting point the fibre was moved backwards by 300 nm, too observe the reaction when moving a small distance away from the detector from this starting point. Minor changes could be seen in the spectrum. This second spectrum can be seen in Figure 5.5b. The fibre was moved backwards another 300 nm, but nothing changed. The loss of tension in the system was likely the reason for the first movement. From here it was moved 4 times another 300 nm, 3 times 500 nm and 4 times 2000 nm. There were still no changes, and it still showed the spectrum in Figure 5.5b. The total distance that it should have moved is now 11300 nm, but didn't move at all. This suggests that there is hysteresis in the system. The movement at the first 300 nm could be explained by a deformed spacer pushing the fibre backwards once the stress was removed from the system. A visual representation of how the fibre moves according to the input given is shown in Figure 5.4b. This will be discussed in more detail later in section 5.8. The small movement of 300 nm can be seen here as going from b to c. The 11300 nm nm input without change in spectra is the vertical parts from c to d.

Only when giving it a motor input of a total 25,000 nm backwards, the spectrum started to shift. This could be the cause of a combination of hysteresis, backlash in the system. It was continued to move backwards. The total distance is now 37300 nm and spectrum was saved and can be seen in Figure 5.5c. The moved distance is about equal to the thickness of a human hair. A higher frequency can be seen in the pink graph when comparing it to its previous position. When looking at the hysteresis plot, this position is point f.

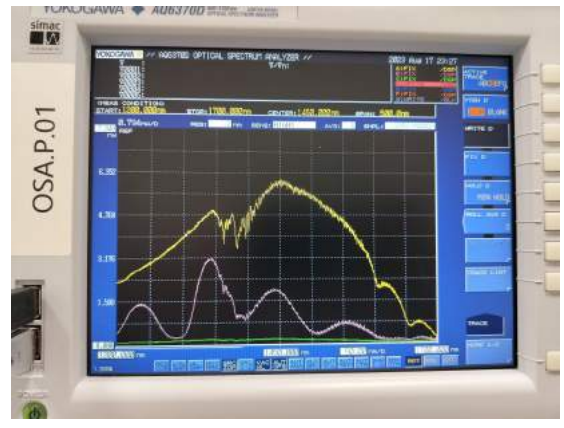
The fibre is moved inwards, by giving an input of 36,000 nm closer to the detector. At this point it was already getting really close, with now just 3300 nm remaining until the starting point of the experiment was reached. This spectrum was also locked on the screen of the spectrum analyzer, to see how it would change from this point and to check if it was possible to get back to this point after the fibre touched the





(a) Position 1, too close.

(b) Position 2, still too close.



(c) Position 3, too far away.

Figure 5.5: Reflectance of broadband spectrum of fibre in different positions of second room temperature test. Reflected power in nW on the Y-axis for wavelengths 1200 nm-1700 nm on the X-axis. Yellow is total reflection, green is background noise, pink is measured signal.

spacers. It was moved another 2700 nm closer. This brings it at just 600 nm from the starting position of the experiment. Lastly, it is moved the remaining 600 nm. The fibre is now once again on the spacer. Here is moved along th hysteresis curve to point b. The last 1000 nm the spectrum didn't change a lot anymore and it converged at this point the same way to the spacer as it did before when this experiment was started. This shows a great consistency with a movement over a larger distance!

Now, the fibre was moved backwards again by 3300 nm away from the detector to check if the same spectrum would be reached when giving it the same input, but now backwards. This is thus trying to moving from point b to point a on the hysteresis graph. Unfortunate, the fibre and the spectrum barely moved. It once again changed a little in the first few 100 nm and it remained constant after that. Only after moving another 24,000 nm backwards was the same spectrum reached. This once again shows a delay in the same order of magnitude as previously, here it being 24,000 nm. The vertical part from point c to d is thus roughly 24,000 nm input.

This experiment showed a great consistency when moving inwards. The movement likely follows a hysteresis curve, as shown in Figure 5.4b. The upper line, the loading path, seems to be consistent, with a reproducibility in the range of a few 100 nm. The unloading path however showed quite some variation, with a long vertical part before it starts to move.

5.5.1. Distance vs Reflectance Plot

A good way to get an idea of the consistency of the fibre distance is by plotting the assumed fibre distance versus its absorption. This is described in this subsection.

A marker is set at 1550 nm on the spectrum analyzer, so the exact power of the light at that wavelength can be written down. This way a plot can be made, and compared to the theoretical data. The resulting

plot can be seen in Figure 5.6a. First the fibre was placed in its optimal position and moved backwards afterwards. It shows that there is no movement for the initial 38,000 nm or 4,070 motor steps input. This is once again likely the hysteresis in the setup. When the fibre was continued to move backwards, the reflected power followed a sinusoidal periodic motion as seen in the graph with a period of roughly 900 nm. A closeup can be seen in Figure 5.6b. The first few period appeared clear, but it became more noisy after 47,000 nm. Also while taking the measurements, there was more drift in the values and the power at a certain position wouldn't converge as fast as before. This indicated that there is some drift in the system.

This plot was made by writing down a lot of values. It would be good to automate the making of this plot by extracting the data from the spectrometer directly onto the laptop and continuously plotting the data.

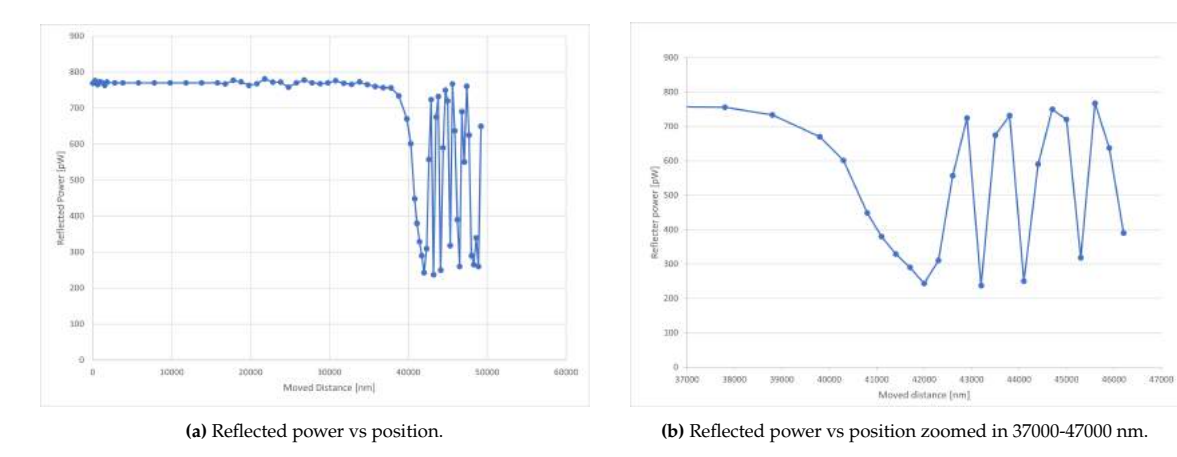


Figure 5.6: Reflected power vs position.

The plot shows a periodical movement. It must be noted that there is also a chance of aliasing. So the real frequency can be a factor higher.

The list of the motor inputs for making the plots in Figure 5.6 can be seen in section E.1 in Appendix E.

5.6. Improved Motor Actuation 2

After the test discussed in section 5.5, the code was once again improved and the current position of the fibre could now be directly compared to a previous saved position. And that this reference position can also be changed during the experiment. The new code shown in section B.8 of Appendix B. Notes can also be added during the experiment. These are also added to the log that is kept in the background. And every action now has a time-tag, to easily also link them to other data outputted by the spectrum analyzer or pictures taken. A short cut for a 200 nm step was also added. And the code was cleaned up a bit by combining some repetitive code.

5.7. Third Warm System Test

This warm test was done with the copper system. It showed it to be an improvement from the PLA model. An experiment has been repeated twice, which followed the contours of its hysteresis curve. It is roughly the same experiment as described in section 5.5 but with a different starting point on the hysteresis graph.

5.7.1. Assembling the Copper System

The mount has been made flat, cleaned and reinstalled in the cryostat. An indium foil is added between the cold head and the mount for better thermal conductivity. This soft material has a high thermal conductivity, so it helps with keeping the temperature inside of the cryostat as low as possible.

The copper parts arrived still very greasy from the manufacturer. All the parts can be seen in Figure 5.7a. It was first cleaned with dish washing soap. Later the critical surfaces for thermal conductivity were cleaned in the lab with alcohol. These are the surfaces between the frame and the PCB mount, and the frame and the bottom mount because this forms the thermal bridge between the





(a) Copper parts

(b) Copper Assembly

Figure 5.7: The Copper System.

PCB and the cold head. The fibre mount was cleaned in the ultrasonic bath, since the slot was difficult to clean.

There were two mistakes in the design. The PCB spacer was made for the centre diameter of the spring, not the outer diameter as it should have. However, a flaw became a feature. The spring can be deformed slightly to make it fit, and the spring force holds itself in place. Now it won't move around during assembly and operation. Another mistake was the absence of a production margin between the PCB holder and the frame. because of this it didn't fit, so the PCB holder was sanded down carefully until it snugly fitted inside the frame. The rest already fitted nicely and was assembled the same way as the PLA model was. It was noted that the parts were stiffer compared to the PLA model, since it was more difficult to put the motor and the worm in place because of the slightly concave worm wheel surface.

After cleaning it was assembled and the result can be seen in Figure 5.7b

5.7.2. First Test Copper Model

First, the control of the reflected spectrum was first demonstrated to the lead engineer to show the functionality of the design. Initially, it was moved inwards. It was a bit too far, and it was moved backwards by 3230 nm and the spectrum shown in Figure 5.8a was reached. This spectrum was locked on the screen. The position in the code was reset and this formed the reference position. It was moved further backwards by 6 microns and moved inwards again by 6 microns. It didn't reach the reference position position until it was moved an extra 2500 nm inwards. This is likely caused by the hysteresis in the system. There is however some movement in the first 200-300 nm, but this is minimal. This spectrum can be seen in Figure 5.8b. From here it was moved further inwards and the spectrum showed that it got too close. The reflected spectrum then starts to flatten out above a wavelength of 1450 nm.

From here it was moved backwards again. Once again it moved in the first 200-300 nm, and it seemed to stay in the same position until a total input distance of 2700 nm of moving backwards. This suggests that the hysteresis is somewhere is this range. This is significantly stiffer than the PLA model which had a delay of an input distance of around 30,000 nm

It got interesting when it got close to the reference position set in this experiment. When the reference spectrum was reached the fibre was just 80 nm off. This spectrum can be seen in Figure 5.8c. This showed a great consistency and predictability of the system.

A few conclusions can be drawn from this experiment. The hysteresis is around 2500 nm, and there is minor movement in the first 200-300 nm when it is actuated in the other direction. This happens in when starting to move backwards again, but also when starting to move inwards again. The most important conclusion is that the path along the hysteresis curve has a reproducibility of around 80 nm.







(b) Position 2, back on the reference position with 2500 nm extra input. (point a)



(c) Position 3, back on reference spectrum and 80 nm of the reference position. (point e)

Figure 5.8: Reflectance of broadband spectrum of fibre in different positions of third room temperature test, test 1. Reflected power in nW on the Y-axis for wavelengths 1200 nm-1700 nm on the X-axis. Yellow is total reflection, green is background noise, pink and blue is measured signal.

5.7.3. Second Test Copper Model

Next, the test was repeated, but now with better documentation. Previously it was a demonstration for the lead engineer. Now a more elaborate experiment was done with the goal of estimating the hysteresis plot and its predictability, but the movement from the previous experiment was roughly kept the same. So moving inwards to to the detector and beyond the optimal reference position, move backwards to and beyond the reference position and move inwards again back to the reference position.

The fibre was first moved backwards by 8 microns and next moved inwards again until it matched the plot set at the reference position of the experiment of test 1. This backward motion of 8 microns and moving from here inwards to the detector made sure the system was on the right side of the hysteresis curve when at the optimal position. This is thus point *a* on the hysteresis graph. The spectrum can be seen in Figure 5.9a. It doesn't exactly match, but it is important that it does match around the wavelength 1550 nm. From here it was moved an extra 500 nm inwards. This gave the spectrum shown in Figure 5.9b. This nicely shows the spectrum when the fibre is too close. After giving an input of 2500 nm backwards the fibre and the spectrum started to move again. With another 500 nm extra input it was exactly on the reference position once again. This can be seen in Figure 5.9c, and is very similar to Figure 5.9a. This is a beautiful confirmation that there is hysteresis/backlash of around 2500 nm, or 270 motor steps before is is engaged to move in the other direction. Once it is engaged, it requires the same number of motor steps to move it backwards as it initially did forwards. Here it was 500 nm.

The fibre was continued to move backwards until it was 6000 nm away from the reference position position and gave the spectrum shown in Figure 5.10a. This spectrum is a nice example of when the fibre is too far away. It has a higher frequency, which confirms the larger distance. From this position





(a) Position 1, start on the reference position.

(b) Position 2, too close.



(c) Position 3, back on the reference position.

Figure 5.9: Reflectance of broadband spectrum of fibre in different positions of third warm test, test 2a. Reflected power in nW on the Y-axis for wavelengths 1200 nm-1700 nm on the X-axis. Yellow is total reflection, green is background noise, pink and blue is measured signal.

it was moved inwards again. Now it required an input of 2000 nm before the fibre and the spectrum started to move again. It was continued to move inwards and the reference position spectrum was reached at 177nm beyond the reference position, or 19 motor steps extra. This spectrum is shown in Figure 5.10b. Also this experiment showed a great consistency when it comes to moving backwards a few microns and inwards again towards the optimal position. This and the previous experiment will make it possible to make an estimate of the hysteresis plot of the system.

Something to note is that it always moves a bit in the first 200-300 nm when changing direction, and then nothing until a total movement of 2000-2700 nm. The initial movement is likely because of the loss of tension in the system, or the elastically deformed spacer pushing the fibre backwards. The same behaviour was documented in the PLA model. After that there is likely a combination of elastic deformation and backlash causing the hysteresis before it starts to move again. What has been documented is a 'delay' of 2500 nm and 2700 nm and changing the direction to moving backwards, and a delay of 2000 nm and 2500 nm when moving inwards. This sets the average at around 2500 nm.

Two other things were noted. The motor receives a noisy random input when python is not open and other tasks are preformed on the laptop. Also when the system was picked up or the table was struck with something, there was also a shift in the spectrum. Shocks and vibrations thus have influence on the fibre position and cause small movements in the range of 100 nm. The vibrations of the cold head could thus have some influence on the fibre position when it is placed in the cryostat.

There is a margin of error during this experiment. During this experiment it was estimated when the spectrum was the closest. Steps of 30 nm were taken when matching the spectra to the reference position. This step size still showed small but visible movement in the spectrometer. The spectra can be directly compared to see which one is closest to the reference position, but inbetween it was not possible





(a) Position 4, too far.

(b) Position 5, back on the reference position.

Figure 5.10: Reflectance of broadband spectrum of fibre in different positions of third warm test, test 2b. Reflected power in nW on the Y-axis for wavelengths 1200 nm-1700 nm on the X-axis. Yellow is total reflection, green is background noise, pink and blue is measured signal.

to determine it from the spectrometer by looking at the screen. So there is likely an error margin of around +-30 nm because of this.

The amount of hysteresis was more difficult to estimate. At each step of 100 nm it was difficult to really say when it was engaged once again. It is safe to say that there is a margin of error of +-100 nm on the amount of hysteresis.

5.8. Hysteresis and Backlash

The behaviour of the system can be explained by a hysteresis plot. With the data acquired during the last tests described in section 5.7, an approximation of the hysteresis plot can be made.

It is assumed that there is a backlash of 2500 nm since this is roughly the average of the four measurements. It is thus also assumed that the backlash for moving backwards and moving forwards is the same. When starting to move the fibre in the other direction, there is some movement during the initial 200 nm or 20 motor steps input. After that the spectrum remains constant until the system is engaged again. This is taken in to account when plotting it. The estimation of the hysteresis plot can be seen in Figure 5.11

Here the fibre position is placed on the x-axis and the input of the number of motor steps is placed on the y-axis. Point a is defined as the optimal position under the 'loading' case, which is moving inwards. This was also the starting point of the experiment described in subsection 5.7.3. From a there was continuous movement when it was moved further towards point b. If the loading direction was changed, the fibre initially moved a little which is shown by the initial straight parts of the unload curve towards c and lasted for around 200 nm input distance. From c to d there is no change in fibre distance to the detector. After 2500 nm input distance, so from b to d, the system is engaged again and it starts to move. If the vertical part between c and d is neglected, the number of motor steps required to move from a to b, is the same as b to c. This was confirmed in the experiments described in section 5.7. When moving backward the fibre passes through the optimal position. After this it was continued to move backwards continuously towards point f, which is here defined as an arbitrary point in the far distance. In the last experiment this was 6 micron. When changing the loading direction again it shows the same behaviour as before. f to g is around 200 nm input distance. The vertical part from g to h is around 2500 nm, and afterward it has a continuous motion towards b.

The experiment in subsection 5.7.2 was started at e and made a full circle around the hysteresis curve back to e. Here there was a small loss of motion and an extra 80 nm input distance was required to end up at the same spectrum. The experiment in subsection 5.7.3 was started at point a and also made a full circle. Here, an extra input distance of 170 nm was needed to end up at the same spectrum.

There are two elements of the movement that were measured of which the exact cause is uncertain. There is the movement of 200 nm when starting to change the direction of motion, and the total lack of movement in the remaining initial 2500 nm input distance when moving in the other direction.

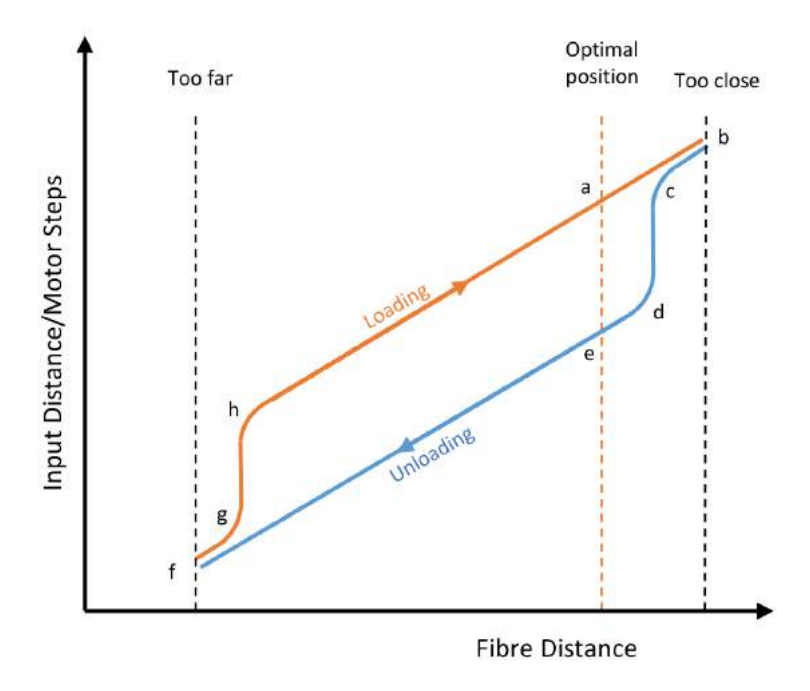


Figure 5.11: Hysteresis Plot Estimation.

The first part could have two explanations. When going from b to c it could be the case that the spacer is elastically deformed and it pushes the fibre backwards a bit when it is unloaded. This doesn't really explain why there is the same movement when moving from f to g. Another possible explanation in movement in the precision screw. Either due to the loss of tension in the precision screw when moving in the other direction, or due to some wobbling when rotating the screw in the opposite direction. The latter could also explain some scratches in the polished back surface of the fibre mount, but it could also be because of the difficult assembly process. It is thus hard to verify where this initial movement of 200 nm comes from.

The loss of motion for the remaining initial 2500 nm roughly behaves like backlash. It seems that it first needs to engage in the other direction before it starts moving. This is however unlikely since the precision screw is preloaded, and the worm gear alone doesn't explain this amount of backlash. This is equivalent to around 270 motor steps, so more than a full rotation of the stepper motor and thus more than a tooth difference in the worm wheel. Backlash in the worm wheel is thus a physically impossible explanation for 2500 nm 'backlash'. It must be noted that the backlash in the worm wheel still could be a part of it, but it is not the full explanation. The next sensible explanation is the elastic deformation in the parts. The pulling force of the ferrule in the sleeve is at room temperature around 2N to 3N as can be seen in Figure 2.20. This was for pulling it out straight. Pulling under a small angle increased the required force significantly. So it is likely higher than the 2-3N due to some misalignment in the system.

The spring pre-tensions the precision screw with 30N. To push the fibre inwards the precision screw needs to push with this force and the friction force combined to be able to push it inwards. And to move it backwards the force needs to be lower than the spring force minus the friction force. The difference in force between moving inwards and outwards is twice the friction force. But as calculated in section 4.2, there is not a lot of deformation in the frame under this load. The current design gives a total deflection of 161nm at room temperature when using Equation 2.1. This is just for the open section of the frame. The mount for the bushing and PCB are not taken in to account and are difficult to calculate. So it is higher than the calculated value. But the amount of elastic deformation doesn't change a lot if the friction force is as low as 2 N at these room temperature tests. So elastic deformation doesn't explain the shape of the hysteresis curve either.

Here it is thus hard to verify for the loss of motion and why the hysteresis curve is exactly shaped like Figure 5.11. A few sources like backlash between the worm wheel and worm and elastic deformation were discussed, but not one can clearly explain it.

System Testing at 3K

The copper system is almost ready for the first cooldown. The same experiments performed in chapter 5 are now reproduced, but at 3 K. First the correct optical fibres need to be added to the system and an attempt is made to digitize the plots from the spectrometer. Next 2 cryogenic tests are performed after solving a minor issue of the system not working.

6.1. Optical Fibre Selection

In the cryostat there is room for 4 mushrooms PCBs. There are connectors which make it also possible to attach a domino PCB. It is also possible to scale up to a mount for 8 PCB's. 10 fibres will be built into the system. It is chosen to use 6 polarisation maintaining fibres, and 4 non-polarisation-maintaining fibres. The PM fibres are needed for measuring the reflected spectrum with the spectrum analyzer, and the non-PM fibres are usually used in customer systems to reach the highest efficiencies. The fibres were all tested on their transmission. This is the fibre efficiency. An overview of the fibres can be seen in Table 6.1. Note that the fibre efficiency is just above 100% for some fibres. This is because of reflections within the setup.

The initial idea was to run different experiments in parallel with 3 detectors as shown in section A.1. The plan changed to putting just one PCB in the cryostat.

Channel	Fibre type	Fibre Serial #	Fibre Eff [%]	Mark	Color
1	3024951	08	101	I	Blue
2	3024951	23	100	II	Blue
3	3024951	21	103	III	Blue
4	3024951	37	99	IIII	Blue
Backup centre	3024951	10	102	IIIII	Blue
Backup edge	3024951	41	102	IIIIII	Blue
5	2576871	040	98	I	White
6	2576871	097	99	II	White
7	2576871	188	99	III	White
8	2576871	157	99	IIII	White

Table 6.1: Fibre data.

6.2. Plotting Absorption

Taking pictures of the screen of the Spectrum analyzer is sub-optimal and the optimal position is determined by eye. There is software which can connect the computer to the spectrum analyzer and automatically extract and plot the data. An example of such a plot can be seen in Figure 6.1. This can help with quickly saving the data from the experiment and comparing them later. There is a large drawback of using this code. So far a spectrum is locked on the screen, and from there it can be compared

to the current spectrum and how it changes. This is however not possible when the code is running. When saving a spectrum to the computer all the saved spectra are cleared, and only an individual plot is produced making it difficult to see small changes in the spectrum. There is also the issue that this code should run in parallel with the code controlling the motor, and the computer is only able to run 1 code at the same time. So two computers need to be controlled to make this work. Using the live screen on the spectrum analyzer is thus the preferred option thus far for the most accurate positioning and live motion tracking. The code could potentially be rewritten to make it work accordingly, but other things have a higher priority during this final phase of the thesis.

The spectrum analyzer also has the option to save the reflected spectrum on different traces and export these to an USB. It is however a tedious process due to the poor user interface of the spectrum analyzer. Doing a save for each position that needs to be documented was deemed to be not worth it in terms of the extra time required to save the data and plot it afterwards, compared to taking a picture of the screen of the spectrum analyzer. A faster way that was thought of too late, is to save a spectrum on different traces, and export all relevant spectra in one go. This data could have been plotted with the help of a python script.

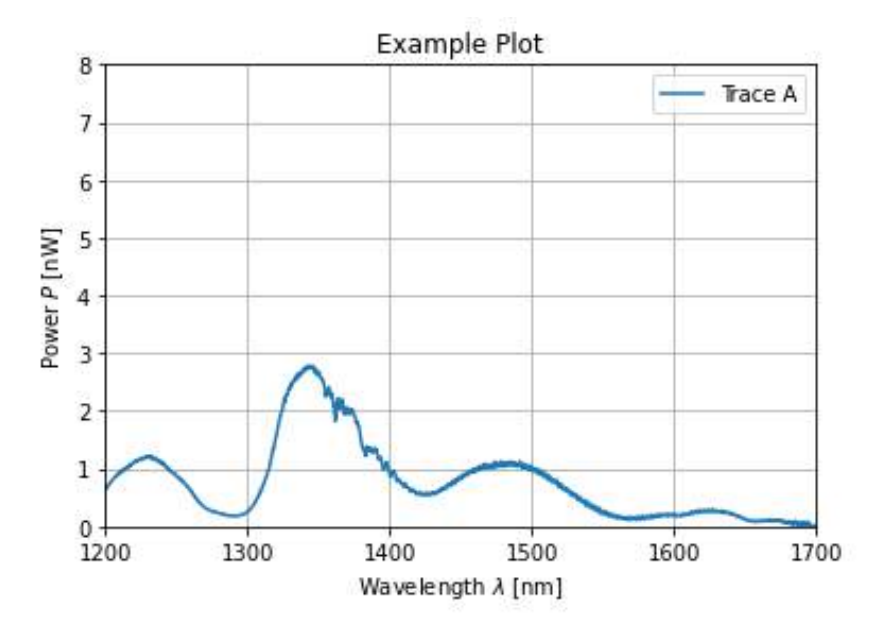


Figure 6.1: Spectrum Plots.

6.3. Cryogenic Issues

The system is cooled down for the first time and the spectrum analyzer shows that the fibre has got closer to the PCB. This is usually the case when cooling down.[16] The temperature is unknown due to a problem with the temperature diode. It gives a constant 1.4K output, which is the case when there is a connection issue with it. A fischer cable was replaced, but it didn't solve the issue. The connection inside of the cryostat will be checked when it is warm again.

The motor is attached and an input was given. The spectrum didn't change indicating that it didn't move. Also the sound coming from the cryostat is the sound of the stepper motor skipping steps instead of moving. It was moved 16 microns backwards, but it didn't change. From this point the fibre was given the input to move 42 micron inwards, but it didn't change the reflected spectrum.

To get it moving there was the idea to increase the current in the coils, thereby increasing the magnetic field and torque of the motor. The magnetic field of the motor is given by Equation 6.1, where B is the magnetic field strength in Tesla, μ_0 is the permeability of free space, N is the number of turn of the solenoid, I is the current through the solenoid and L is the length of the solenoid.

$$B = \frac{\mu_0 NI}{L} \tag{6.1}$$

Increasing the current would push the current above the current limit of 0.6A of the motor. The assumption is that it wouldn't burn through the motor's coils since it is cryogenic and needs to heat up more than 300K to be able to burn the wire.

The current through the motor is now 0.404A, which is below the 1A continuous current limit of the A4988 driver. Peaks of up to 2A are allowed.[78] Recalculating Equation 3.1 for I_{max} equal to 1A and 2A gives a V_{ref} of 0.943V and 1.885V respectively. It first has been set to 0.947V. This already solved the issue and the motor was able to move. A note was written down to turn the reference voltage back down, so the motor won't break when using it again at room temperature.

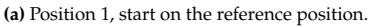
6.4. First Cold System Test

Initially, an input of 19 micron backward was given after the cooldown. Here it reached the optimal position, so point *e* in the hysteresis curve of Figure 5.11. It was put in the same optimal position before the cooldown. This indicated that the relative fibre position decreased by 19 microns when cooling down, but also that there was a lot of force on the SNSPD.

6.4.1. First Positioning Experiment

The start of this experiment is thus point *e*. The experiment in subsection 5.7.2 will be reproduced, but now cryogenically. The optimization of the absorption can be seen in the difference in the graph in Figure 6.2a after the cooldown and after repositioning the fibre. Two different graphs can be seen here. There is a marker at the wavelength of 1550 nm. The reflected power at 1550 nm first was 384 pW after the cooldown. After repositioning the fibre to its optimal position, it was lowered to 156 pW. The total power at 1550 nm is around 4370 pW. The transmission through the detector is neglected here as it in the theory significantly smaller than the absorption. The reflected power is reduced from 8.8% to 3.6%. The maximum possible absorption of the detector is thus increased from 91.21% to 96.43%. This is an increase of 5.22%!





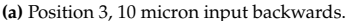


(b) Position 2, 6 micron input backwards.

Figure 6.2: Reflectance of broadband spectrum of fibre in different positions of first cryogenic test, test 1. Reflected power in nW on the Y-axis for wavelengths 1200 nm-1700 nm on the X-axis. Pink is after the cooldown, blue is optimal spectrum, orange is measured signal.

Next, the fibre is moved backward 6 microns. Just like in the experiment that was repeated. Not a lot of changes can be seen in the spectrum in Figure 6.2b. The fibre was moved backwards another 4 microns until the spectrum changed. This can be seen in Figure 6.3a. From here the fibre was moved inwards again. Only an extra 500 nm input was needed to reach the same spectrum as the starting point with the spectra plotted in Figure 6.3b. This is thus point *a* in the hysteresis curve. The fibre was moved an extra 500 nm to get it too close to the detector, and the spectrum can be seen in Figure 6.3c. Finally, the fibre was moved backwards to the starting point. However, the fibre didn't move smoothly backwards. An input of 4200 nm backwards was given, but the fibre didn't move at all. With an extra input of 2000 nm backwards, the fibre suddenly moved a lot. So from point *b* to *d* was longer than usual, and *d* to *f* was more or less horizontal. This showed a stick slip response. The final spectrum can be seen in Figure 6.3d.







(c) Position 5, too close



(b) Position 4, on the optimal spectrum again.



(d) Position 6, too far

Figure 6.3: Reflectance of broadband spectrum of fibre in different positions of first cryogenic test, test 2. Reflected power in nW on the Y-axis for wavelengths 1200 nm-1700 nm on the X-axis. Blue is optimal spectrum, orange is measured signal.

What can be concluded from this first cryogenic system test is that the spring struggles with moving the fibre backwards. There is a clear stick slip-response going on with no movement for a long time, and abrupt larger movements. It was also remarkable that the distance between point e and a on the hysteresis curve was just 500 nm. At room temperature this was around 2500 nm. It is nice that this loss of motion is much smaller, but it is unknown how repeatable this 500 nm is. The unpredictable behaviour of the spring is not helping. What was also noted that a new fibre position isn't fully stable. There is a small amount of creep going on. After 20-30 minutes the reflected spectrum isn't entirely the same anymore and resembles the displacement of around 50 nm.

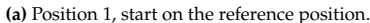
6.4.2. Second Positioning Experiment

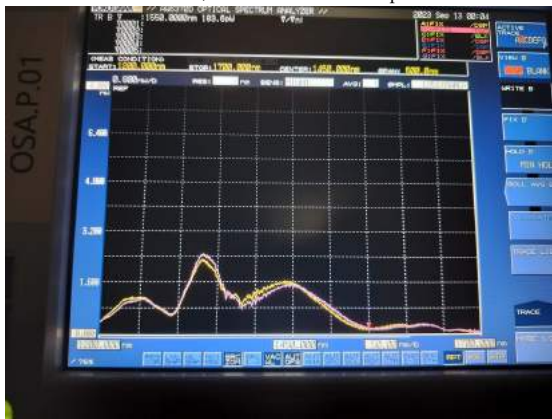
Next, the experiment in subsection $5.\overline{7}.3$ is reproduced at cryogenic temperatures. The starting position is point a. This spectrum can be seen in Figure 6.4a and is locked on the screen. The rest of the spectra can directly be compared to this spectrum. The fibre was moved 1000 nm inwards closer to the detector and gave the spectrum shown in Figure 6.4b. The absorption at 1550 nm clearly went down. From here the fibre was moved backwards again in the direction of point e. The spring struggled to move the fibre backwards just like in subsection 6.4.1. Only after an input of 4500 nm backwards, it started to move a little. Moving the fibre backwards another 200 nm (accidentally in the wrong direction,) it suddenly moved the fibre over a larger distance back to the optimal position. It is likely just luck that the fibre stopped at this position. This matching spectrum can be seen in Figure 6.4c.

From this position the fibre once again didn't move when trying to move it backwards, until a total input distance of 5650 nm backward from the reference position was given. From here the fibre suddenly moved a lot to the spectrum shown in Figure 6.4d. This is point f in the hysteresis curve.

When starting to move the fibre in again, the best results so far were documented. At some point the spectrum was closing in on the reference position. It was a bit unexpected, since in theory it was still







(c) Position 3, 10 micron input backwards.



(b) Position 2, 6 micron input backwards



(d) Position 4, on the optimal spectrum again.

Figure 6.4: Reflectance of broadband spectrum of fibre in different positions of first cryogenic test, test 3. Reflected power in nW on the Y-axis for wavelengths 1200 nm-1700 nm on the X-axis. Orange is optimal spectrum, pink is measured signal.

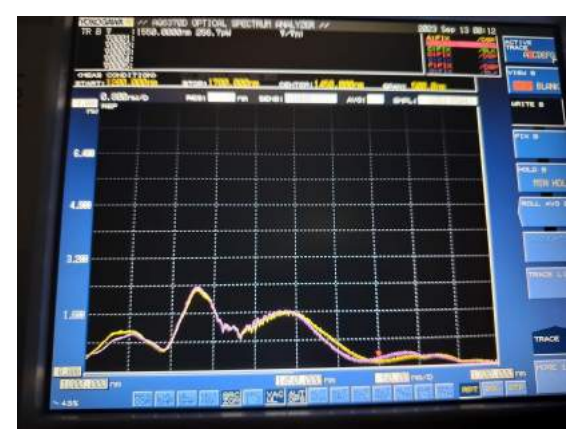
1440 nm away. But is matched really good was shown in Figure 6.5a. From there it was moved inwards further to see if it would converge again and show the behaviour when it would get too close. It initially did, but when close to the reference position it converged exactly to the reference position! This was 100 nm further than the reference position and thus 1540 nm closer to the detector compared to the previous spectrum. This is exactly 1 wavelength closer.

This experiment showed 2 significant things. There is just a motion loss of 100 nm when converging to point a on the hysteresis curve. This is roughly the same as was measured before at room temperature. At this point it could be concluded that there is a consistent motion loss of around 100 nm. Since the error is more or less consistent, it can be compensated for. Secondly, it shows that it is possible to move from one fringe to the next with the system. These are one wavelength apart and shows great accuracy.

The minimum around 1550 in Figure 6.5a is not exactly in line with the minimum of the reference position. It is just slightly off. Initially, there was a better match when the spectrum analyzer completed its first sweep after having moved the fibre. When it completed its second sweep, there was a small shift in the spectrum as can be seen in the figure. This thus shows that some movement is possible in the period after the motor is actuated.

The motor wasn't actuated for 30 minutes after it reached the matching spectrum from Figure 6.5b. But after 30 minutes have passed, there was once again a small drift visible, and the spectrum shown in Figure 6.5c is reached. The good news is that the reflected power at 1550 stayed the same. But it does show that the position the fibre is put in when actuating, is not the exact position it will stay in after some time

One explanation could be that the error is induced by the slow buildup in error in an amplifier in the spectrum analyzer. Every 10 minutes it resets itself to calibrate it error and start over. It could be the case that this error is visible. But it is unlikely since 30 minutes have passed, and the spectrum stayed more or less the same. This thus is likely caused by mechanical creep.





(a) Position 5, Optimal position, but it can do better.

(b) Position 6, Exactly on the optimal position.



(c) Position 7, Creep can be visible.

Figure 6.5: Reflectance of broadband spectrum of fibre in different positions of first cryogenic test, test 3. Reflected power in nW on the Y-axis for wavelengths 1200 nm-1700 nm on the X-axis. Orange is optimal spectrum, pink is measured signal.

6.4.3. Third Positioning Experiment, Efficiency Test

The detector used had an efficiency of 78% measured. The goal was to re-measure the efficiency and see if it was actually improved. This is the end goal of this thesis.

For an unknown reason the detector was not working. It was however superconducting due to it having a low critical current. When increasing the bias current, it didn't show the transition from the superconducting state to a normally conducting state. There were also no counts, not even dark counts. There could be two issues at hand according to more knowledgeable people at SQ. The detector is shorted, or the bypassing of the cryoamp is the problem. But for the latter small voltage spikes should have been visible with the oscilloscope, but only noise was seen.

Different fibre positions were tried, but it didn't make a difference. The next best thing was to warm up the system and locate the issue. A new detector from the same batch has been found to replace it. It is the C1461-11 with a previously measured efficiency of 78%.

6.5. Second Cold System Test

6.5.1. Solving Issues

The system was warmed up and the detector has a resistance of $2.35\,\Omega$ when measured from the output port of the cryostat. This confirms that there is something wrong with the detector, since it should have a resistance of above $1\,\mathrm{M}\Omega$. Detectors which fall slightly short of this value are by default discarded since statistically it is a broken detector. This one is thus definitely broken. Someone mentioned that the bonding wires could be broken. Therefore, it was put under a microscope to check. It showed a heavily damaged detector, as can be seen in Figure 6.6. A fracture of the detectors tail at the slot of the sleeve. This means that it is definitely broken. Also a lot of damage can be seen on the detector. A circular crack can be seen around the spacers. The fibre sometimes leaves a mark like this, but not this extreme. This

is likely caused by the high force of the fibre during the cooldown.



Figure 6.6: Damaged Detector under Microscope.

The new detector C1461-11 was put in the system. The resistance was measured, and it was way too low at $0.4~\Omega$. It should have been in the $M\Omega$ range. It was taken out and measured again, and it had a resistance of $7.9~M\Omega$. The cause was that there is a short circuit with the soldering point on the copper frame. Therefore, some material is removed from the PCB mount to make room for the soldering point of the coax connection.

There were a few other quick fixes. During the last cooldown there was condensation when warming up, which indicates a leakage. The rubber seal was cleaned to hopefully solve the leakage. The temperature diode is now working. It was connected incorrectly. Black should be connected to red, and red should be connected to black. It was connected to the driver and gave the correct room temperature readout. Lastly the fibre should have a specific orientation with respect to the PCB and SNSPD. The line between the indents in the fibre brim should be perpendicular to the long side of the PCB.

6.5.2. Influencing Photon counts

The system is cooled down. Before cooling down, the fibre was put in its optimal position and moved backwards 50 microns from that point to prevent crushing the detector. It needed to move inwards 24,5 microns to reach the same spectrum. So the relative distance between the fibre and the PCB shrunk with 25,5 microns during the cooldown.

The current temperature in the cryostat is 3.9 K. This is quite warm and became an issue with the efficiency tests. The efficiency follows a sigmoid function with an increase of the bias current. The higher the bias current, the more sensitive the detector is. But the detector fell out of superconductivity before the plateau of the sigmoid function was reached.

This made it impossible to do a full efficiency test, since this would measure the height of the plateau. The result from the efficiency measurement can be seen in Figure 6.7a. The X-axis shows the bias current and the Y-axis shows the efficiency in green and the darkcounts in black. No clear sigmoid function can be seen for the efficiency. When the system is colder the plot should have looked something like Figure 6.7b which was tested before. Although the fact that the system was too warm, it was still possible to measure the live counts. The counts were compared for different fibre positions to see if the same fringes can be seen as in Figure 5.6.

The number of detector counts was between the range of 110,000 count and 130,000 counts. If the fibre position was more optimal, the fibre count would be closer to 130,000 counts. The temperature inside of the cryostat also played an important factor. The temperature and counts would always go up after actuating the motor. An example can be seen in Figure 6.8. Here the motor was actuated a lot and a clear temperature increase from 3.9 K to 4.3 K can be seen. During fine movements the temperature would increase to just 4.1 K. The increase in temperature would increase the dark counts. So an increase in counts could either be because of the temperature increase, or the more efficient position.

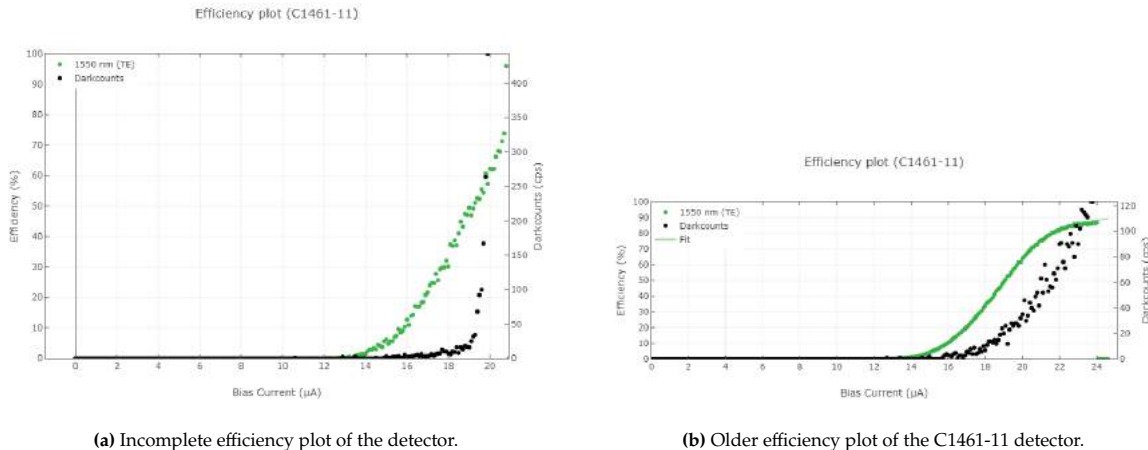


Figure 6.7



Figure 6.8: Temperature Increase after Motor Actuation.

Some trends were observed over a movement of 5 micrometer. It was sometimes closer to 130,000 count and in some ranges closer to 110,000 counts. Giving it some time to properly cool allowed the number of counts to properly converge. When the position was close to the optimal position it was around 120,000 counts and clearly higher compared to when it was moved 500 nm closer. From that point it went to 105,000 counts when letting it converge. Temperature definitely played a large part in the number of counts, but some correlation was observed between the number of counts and the fibre position. How strong this correlation is, is difficult to say with this experiment.

6.6. Reducing the Temperature

According to the CTO, the wires of the motor conduct a lot of heat. This is likely the reason that it is relatively warm. He suggested to replace these cables with coax cables by soldering an SMP connector on it. A second option could be to add a resistor in the cables, since this also makes it less thermal conductive. This would be a good next improvement.

 $\overline{}$

Discussion

The warm tests with the PLA model showed a reproducible motion that followed the hysteresis curve previously discussed. The copper model showed roughly the same behaviour but with just a fraction of the initial loss of motion. A clear sinusoidal can be observed in the reflected power when moving the fibre over a longer distance, indicating fringes. During the cold test it was shown that the fibre got too close during the cooldown and that cavity size could be optimized. A motion range of 50 microns was demonstrated. Thereby increasing the maximum possible absorption from 91.2% to 96.4%. A repeatable motion was demonstrated with a positioning resolution in the range of 10nm to 30 nm with a loss of motion of 100nm when unloading and loading the system. The detector counts can be influenced also with the fibre distance.

The specifications demonstrated are close to the required specifications previously defined in subsection 2.3.2. These specifications make it possible to position the fibre reliably on its optimal position thereby increasing the maximum possible efficiency of the detectors. The design behaved as expected. A small difference was the small movement on the fibre when changing the loading direction. That is the part from b to c and f to g in the hysteresis graph in Figure 5.11. These were mostly there during the warm test, and very minimal but still present at the cold tests. A possible explanation is because of the stiffer copper frame, but this can be verified with the data. There was also the issue of the system being too warm during the second cold system test. The efficiency of the detector couldn't be tested because of this. A possible reason is the cabling to the motor, which is made of copper and creates a heat load that is too high for the cryostat to maintain a low temperature.

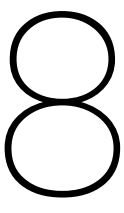
These results of the warm and cold tests verify the accuracy and repeatability of the system. These specifications are in the same order of magnitude as those of the JWST.[41] The largest difference is that this design is fully mechanical and preloaded. The compact design makes it possible to place it inside of the cryostat.

There are three limitations in the results. First, it was shown that the fibre is moving inwards by 25.5 microns when cooling down. This is likely because of the system that is attached to the fibre. This means that the measured absorption of 91.2% during the first cryogenic test after the cooldown is likely influenced by the attached system pushing the fibre inwards. It is possible that the fibre could have been in a more optimal position if the system wasn't attached. Appointing the 5.2% increase in performance of the actuator could be misleading, since the fibre position after the cooldown could have been made worse by the system. Second, the magnitude of the movement of the fibre that is mentioned throughout the report is uncertain. The simulations and the spectra and the results of the spectrometer confirm that it is in the right order of magnitude. Also reproducing an absorption peak at two fibre position that were 1540 nm apart also gave the confirmation that the input distance corresponds to the actual moved fibre distance, but it can't be said with absolute certainty. Lastly, it can be confirmed why the shape of the hysteresis curve appears as it does. The small movement from point b to c and d to d when changing direction of movement could be explained by changing the rotation direction of the screw. And the 2500 nm loss of motion could be explained by the elastic deformations in the system, but this is uncertain.

Some long term issues could also arise. All the lubrication is removed, increasing the wear and reducing the lifetime of the parts. It is recommended to try to add dry lubrication to reduce wear and friction, and also lower the required motor torque. After some time, it would also be possible that the

Loctite could break, that is used to glue the worm on the axle of the gear. It works for now, but the Loctite is not rated for these temperatures and a number of thermal cycles could get it to fail. The same holds for the bolts used in the precision screw clamp. It is unknown what material this is and could fail at some point as its functionality is not guaranteed.

For further development it is recommended to try to lower the temperature inside of the cryostat. This makes it possible to measure the efficiency of detector sensitive to light with a wavelength of 1550 nm. The next step is to see how much the efficiency can be optimized and influenced by the fibre position. The next step is to test a smaller motor on the system so the design can be scaled down and more of them can fit inside of one cryostat.



Conclusion

The goal of this thesis is to design a cryogenic precision actuator able to correct the fibre position. The positioning resolution should be 10 nm and the system should fit inside of the 3 K radiation shield. The final design used a modified Nema 8 stepper motor with step angle of 1.8 degrees in combination with a 80:1 worm gear and a precision screw with 170 treads per inch. This made it theoretically possible to move the fibre with a position resolution of 9.3 nm. The system was tested and it yielded the following results:

- Positioning resolution in the range of 10 nm to 30 nm.
- Motion loss of just 100 nm when unloading and loading.
- Ability to tune the reflected light spectrum very precisely and reproducible.

The foundation for this final design has been laid by first doing a thorough literature study of all current cryogenic precision actuators. Many achieved the required position resolution, but were not suitable for high force applications. It was found that the working principles of the actuator design for the James Webb Space Telescope would work the best for the problem at hand. A Nema 8 stepper motor and a precision screw were cleaned of lubrication and tested cryogenically. Once these crucial parts were functional, the rest of the motion reduction mechanism was designed around it. It was combined with a 80:1 worm gear to reach the required positioning resolution. This design was first tested at room temperature and the design was further improved by iteration. A copper setup was produced and tested cryogenically. It moves predictably along the hysteresis curve that could be derived from its movements for the motion inputs.

The design can be improved by replacing the cabling to the motor with cables that are less thermal conductive than the current ones. The temperature in the cryostat is 3.9 K and to high for a full efficient measurement of the detector. It is also recommended to research the creep that happens in the system. The position of the fibre doesn't settle immediately and can drift up to 50 nm in the next 30 minutes. To be able to scale this design to multiple detectors, the motor needs to be replaced by a compacter motor like the AM1524 that is able to produce enough torque.

It is nonetheless already an accurate and predictable motion in the nanometer range. The ability to manipulate and fine-tune the absorption characteristics of the detector, as demonstrated in this report, promises a much more consistent detection efficiency for Single Quantum's detectors. This has the potential to greatly speed up the production process. After the cooldown the fibre is often too close to the detector, and repositioning the fibre makes it also possible to consistently increase the maximum achievable detector efficiency. The designed actuator offers precision control over the detector absorption and paves the way for Single Quantum to offer more efficient and reliable photon detectors than ever before.

- [1] C. M. Natarajan, M. G. Tanner, R. H. Hadfield, Superconductor Science and Technology 2012, 25, 063001.
- [2] I. E. Zadeh, J. Chang, J. W. Los, S. Gyger, A. W. Elshaari, S. Steinhauer, S. N. Dorenbos, V. Zwiller, *Applied Physics Letters* **2021**, *118*, DOI 10.1063/5.0045990.
- [3] J. Chang, J. W. Los, J. O. Tenorio-Pearl, N. Noordzij, R. Gourgues, A. Guardiani, J. R. Zichi, S. F. Pereira, H. P. Urbach, V. Zwiller, S. N. Dorenbos, I. E. Zadeh, *APL Photonics* **2021**, *6*, DOI 10.1063/5.0039772.
- [4] Interview Hugo Kooiman(SQ employee), Private communication, 2022.
- [5] S. Q. b.v., Single Quantum Eos, https://singlequantum.com/solutions/single-quantum-eos/, [Online; accessed 14-Dec-2022], 2022.
- [6] W. Zhang, L. You, H. Li, J. Huang, C. Lv, L. Zhang, X. Liu, J. Wu, Z. Wang, X. Xie, Science China Physics Mechanics & Astronomy 2017, 60, 120314.
- [7] L. You, Nanophotonics **2020**, 9, 2673–2692.
- [8] G. S. U. HyperPhysics, Critical Magnetic Field, https://www.http://hyperphysics.phy-astr.gsu.edu/hbase/Solids/scbc.html, [Online; accessed 19-Jan-2023], 2023.
- [9] K. M. Rosfjord, J. K. W. Yang, E. A. Dauler, A. J. Kerman, V. Anant, B. M. Voronov, G. N. Goltsman, K. K. Berggren, *Optics Express* **2006**, *14*, 527.
- [10] H. N. bv., LOCTITE STYCAST 2850FT BL, https://www.henkel-adhesives.com/nl/en/product/potting-compounds/loctite_stycast_2850ftbl.html, [Online; accessed 19-Dec-2022], 2022.
- [11] F. Aviles, L. Llanes, A. I. Oliva, J. E. Corona, M. Aguilar-Vega, M. I. Loría-Bastarrachea in *Vol. 13*, (Ed.: F. Avilés), **2009**, pp. 593–594.
- [12] A. Korneev, Y. Vachtomin, O. Minaeva, A. Divochiy, K. Smirnov, O. Okunev, G. Gol'tsman, C. Zinoni, N. Chauvin, L. Balet, F. Marsili, D. Bitauld, B. Alloing, A. Li, A. Fiore, L. Lunghi, A. Gerardino, M. Halder, C. Jorel, H. Zbinden, *IEEE Journal on Selected Topics in Quantum Electronics* 2007, 13, 944–950.
- [13] X. Hu, C. W. Holzwarth, D. Masciarelli, E. A. Dauler, K. K. Berggren, *IEEE Transactions on Applied Superconductivity* **2009**, *19*, 336–340.
- [14] L. Zhang, C. Wan, M. Gu, R. Xu, S. Zhang, L. Kang, J. Chen, P. Wu, *Science Bulletin* **2015**, *60*, 1434–1438.
- [15] S. Miki, T. Yamashita, M. Fujiwara, M. Sasaki, Z. Wang, IEEE Transactions on Applied Superconductivity **2011**, 21, 332–335.
- [16] Interview Harmen Smedes (SQ employee), private communication, 2022.
- [17] A. J. Miller, A. E. Lita, B. Calkins, I. Vayshenker, S. M. Gruber, S. W. Nam, *Optics Express* **2011**, 19, 9102.
- [18] S. N. Dorenbos, R. W. Heeres, E. F. C Driessen, V. Zwiller, 2011.
- [19] I. E. Zadeh, J. W. Los, R. B. Gourgues, V. Steinmetz, G. Bulgarini, S. M. Dobrovolskiy, V. Zwiller, S. N. Dorenbos, *APL Photonics* **2017**, 2, DOI 10.1063/1.5000001.
- [20] S. Miki, M. Takeda, M. Fujiwara, M. Sasaki, Z. Wang, Optics Express 2009, 17, 23557.
- [21] D. V. Reddy, R. R. Nerem, S. W. Nam, R. P. Mirin, V. B. Verma, Optica 2020, 7, 1649.
- [22] J. van der Ende, Photon detector system with distance control, WO2023275390, 2022.
- [23] M. Fouaidy, N. Hammoudi, G Martinet, S Blivet, F Chatelet, M Fouaidy, N Hammoudi, A Olivier, H Saugnac, 2006.

- [24] J. F. Tressler, S. Alkoy, R. E. Newnham, Piezoelectric Sensors and Sensor Materials, 1998.
- [25] R. Changhaii, L. Xinyuu, S. Yuu, Nanopositioning Technologies Fundamentals and Applications, 2016.
- [26] T. Chang, X. Sun, IEEE Transactions on Control Systems Technology 2001, 9, 69–75.
- [27] L. Wang, W. Chen, J. Liu, J. Deng, Y. Liu, Mechanical Systems and Signal Processing 2019, 133, DOI 10.1016/j.ymssp.2019.106254.
- [28] H. J. Lee, S. Woo, J. Park, J. H. Jeong, M. Kim, J. Ryu, D. G. Gweon, Y. M. Choi, *Microsystem Technologies* **2018**, 24, 2653–2662.
- [29] J. Li, H. Huang, T. Morita, Sensors and Actuators A: Physical **2019**, 292, 39–51.
- [30] T. Corperation, https://www.thorlabs.com/, [Online; accessed 22-Dec-2022], 2022.
- [31] G. C. Physik Instrumente (PI), https://www.piceramic.com, [Online; accessed 22-Dec-2022], 2022.
- [32] J. Wang, H. Huang, Z. Wang, T. Liang, H. Zhao, Smart Materials and Structures 2021, 30, DOI 10.1088/1361-665X/ac0399.
- [33] T. R. Hicks, P. D. Atherton, Y. Xu, M. Mcconnell, The NanoPositioning Book, 1997.
- [34] C. Yang, K. Youcef-Toumi, Mechanical Systems and Signal Processing 2022, 171, DOI 10.1016/j. ymssp.2022.108885.
- [35] G. C. Physik Instrumente (PI), Displacement of Piezo Actuators (Stack & Contraction Type), https://www.pi-usa.us/en/products/piezo-flexure-nanopositioners/piezo-motion-control-tutorial/tutorial-4-20/, [Online; accessed 12-Jan-2023], 2023.
- [36] R. G. Gilbertson, J. D. Busch, The Journal of The British Interplanetary Society **1996**, 49, 129–138.
- [37] K. Kim, Y. Lee, I. Llamas-Garro, J. M. Kim, Sensors 2022, 22, DOI 10.3390/s22239490.
- [38] S. Nabavi, M. Menard, F. Nabki, Journal of Microelectromechanical Systems 2022, 31, 820–829.
- [39] Interview Niels Los(SQ employee), Private communication, 2023.
- [40] M. Bendjedia, Y. Ait-Amirat, B. Walther, A. Berthon, *IEEE Transactions on Power Electronics* **2012**, 27, 578–587.
- [41] R. M. Warden', Proceedings of the 38th Aerospace Mechanisms Symposium Langley Research Center **2006**.
- [42] E. Bendek, UNIVERSITY OF ARIZONA COLLEGE OF OPTICAL SCIENCES OPTI 521 2009.
- [43] C. Digest, What is Stepper Motor and How it Works, https://circuitdigest.com/tutorial/what-is-stepper-motor-and-how-it-works, [Online; accessed 1-Feb-2023], 2023.
- [44] K. Uchino, J. R. Giniewicz, Micromechatronics, Marcel Dekker, 2003, p. 489.
- [45] L. Dong, J. Chen, C. Zhang, D. Wu, G. Yu in Institute of Electrical and Electronics Engineers Inc., **2016**, pp. 1997–2002.
- [46] X. M. Feng, Z. J. Duan, Y. Fu, A. L. Sun, D. W. Zhang in **2011**, pp. 892–895.
- [47] JPE, CRYO VOICE COIL ACTUATOR, https://www.jpe-innovations.com/cryo-nano-products/cvca-cryo-voice-coil-actuator/, [Online; accessed 1-Feb-2023], 2023.
- [48] Phytron, LA Linear Actuator, https://www.phytron.eu/fileadmin/user_upload/produkte/motoren_aktuatoren/pdf/ds-la-en.pdf, [Online; accessed 1-Feb-2023], 2023.
- [49] JPE, CRYO LINEAR ACTUATORS, https://www.jpe-innovations.com/cryo-nano-product s/cryo-linear-actuator-piezoknob-claxx01/, [Online; accessed 1-Feb-2023], 2023.
- [50] Attocube, ANPz101eXT12/RES/LT linear z-nanopositioner, https://www.attocube.com/en/products/nanopositioners/low-temperature-nanopositioners/anpz101ext12reslt-linear-z-nanopositioner, [Online; accessed 1-Feb-2023], 2023.
- [51] Q. Design, Renaissance Scientific Cryogenic Nanopositioning Stages, https://qd-uki.co.uk/cryogenics/renaissance-scientific-cryogenic-nanopositioning-stages/, [Online; accessed 1-Feb-2023], 2023.
- [52] Morskate, Stepper Motor VSS (CRYO), https://www.morskatedrivetechnology.com/product s/stepper-motors/stepper-motor-vss-(cryo)/, [Online; accessed 1-Feb-2023], 2023.

[53] JPE, CRM Brochure, https://www.jpe-innovations.com/wp-content/uploads/CRM_Brochure.pdf, [Online; accessed 1-Feb-2023], 2023.

- [54] JPE, CRYO SAMPLE ROTATOR, https://www.jpe-innovations.com/cryo-nano-products/csr-cryo-sample-rotator/, [Online; accessed 1-Feb-2023], 2023.
- [55] K. Mori, T. Miyata, M. Honda, T. Kamizuka, H. Takahashi, S. Sako, R. Ohsawa, K. Okada, M. S. Uchiyama, H. Kataza, H. Ohsaki, T. Hiroe, C. Packham in *Vol. 9912*, SPIE, **2016**, p. 991218.
- [56] J. P. Bugeat, R Petit, D Valentian, 1987.
- [57] Y. K. Yong, S. O. Moheimani, B. J. Kenton, K. K. Leang, *Review of Scientific Instruments* **2012**, *83*, DOI 10.1063/1.4765048.
- [58] Z. Wu, Q. Xu, Actuators 2018, 7, DOI 10.3390/act7010005.
- [59] Z. Qiu, J. Xue, Measurement: Journal of the International Measurement Confederation 2021, 183, DOI 10.1016/j.measurement.2021.109794.
- [60] A. D. Pham, H. J. Ahn, *International Journal of Precision Engineering and Manufacturing Green Technology* **2018**, *5*, 519–533.
- [61] L. V. LaCroix, B. S. Smietanowska, J. K. Campbell, R. M. Yoshikawa, K. M. Morgan, 1990.
- [62] MÄDLER, Spur Gears, Toothed Racks, Internal Gears, Ratchet Wheels, https://www.maedler.de/, [Online; accessed 26-Jan-2023], 2023.
- [63] Precipart, PRECISION GEARS, https://www.precipart.com/products-capabilities/gears-motion-control/precision-gears/, [Online; accessed 26-Jan-2023], 2023.
- [64] D. Collins, What's the difference between backlash and hysteresis in linear systems?, https://www.linearmotiontips.com/whats-the-difference-between-backlash-and-hysteresis-in-linear-systems/, [Online; accessed 26-Jan-2023], 2023.
- [65] PI, P-882 P-888 PICMA Stack Multilayer Piezo Actuators, https://www.pi-usa.us/en/products/piezo-actuators-stacks-benders-tubes/p-882-p-888-picma-stack-multilayer-piezo-actuators-100810, [Online; accessed 1-Feb-2023], 2023.
- [66] C. D. A. Inc., Cryogenic Properties of Copper, https://copper.org/resources/properties/cryogenic/, [Online; accessed 20-Jan-2023], 2023.
- [67] A. J. Fleming, Sensors and Actuators A: Physical **2013**, 190, 106–126.
- [68] Attocube, Displacement Measuring Interferometer, https://www.attocube.com/en/products/laser-displacement-sensor/displacement-measuring-interferometer, [Online; accessed 1-Feb-2023], 2023.
- [69] SmarAct, PICOSCALE Interferometer Controller, https://www.smaract.com/en/picoscale-accessories/product/picoscale-interferometer, [Online; accessed 1-Feb-2023], 2023.
- [70] Interview Lyuben Davidov (ASML employee), private communication, 2023.
- [71] Y. Kim, K. Hibino, N. Sugita, M. Mitsuishi, *Optics Express* **2014**, 22, 18203.
- [72] Attocube, Low Temperature Nanopositioners, https://www.attocube.com/en/products/nanopositioners/low-temperature-nanopositioners, [Online; accessed 1-Feb-2023], 2023.
- [73] PI, P-602 PiezoMove Linear Actuator with High Stiffness, https://www.pi-usa.us/en/products/piezo-actuators-stacks-benders-tubes/p-602-piezomove-high-stiffness-linear-piezo-actuator-202700, [Online; accessed 1-Feb-2023], 2023.
- [74] PI, P-604 Compact PiezoMove Linear Actuator, https://www.pi-usa.us/en/products/piezo-actuators-stacks-benders-tubes/p-604-compact-piezomove-linear-actuator-202820, [Online; accessed 1-Feb-2023], 2023.
- [75] M. J. Grotevent, S. Yakunin, D. Bachmann, C. Romero, J. R. V. de Aldana, M. Madi, M. Calame, M. V. Kovalenko, I. Shorubalko, *Nature Photonics* 2022, DOI 10.1038/s41566-022-01088-7.
- [76] TinyTronics, Nano V3.0 Compatible, https://www.tinytronics.nl/shop/en/development-boards/microcontroller-boards/arduino-compatible/nano-v3.0-compatible, [Online; accessed 12-Aug-2023], 2023.

[77] TWPe-jpc, STEPPER MOTOR VOLTAGE EXPLAINED, https://www.e-jpc.com/stepper-motor-voltage-explained, [Online; accessed 26-april-2023], 2023.

- [78] TinyTronics, A4988 Motor Driver Module, https://www.tinytronics.nl/shop/en/mechanics-and-actuators/motor-controllers-and-drivers/stepper-motor-controllers-and-drivers/a4988-motor-driver-module, [Online; accessed 12-Aug-2023], 2023.
- [79] Allegro, DMOS Microstepping Driver with Translator and Overcurrent Protection, https://www.tinytronics.nl/shop/image/data/product-614/A4988.pdf, [Online; accessed 12-Aug-2023], 2023.
- [80] FAULHABER, Stepper motors, https://www.faulhaber.com/en/products/stepper-motors/, [Online; accessed 26-jun-2023], 2023.
- [81] W. H. Daniel W. Baker, 9.4 Screw Threads, https://engineeringstatics.org/Chapter_09-screw-friction.html, [Online; accessed 27-juni-2023], 2023.
- [82] T. E. Toolbox, Friction Friction Coefficients and Calculator, https://www.engineeringtoolbox.com/friction-coefficients-d_778.html, [Online; accessed 26-Aug-2023], 2023.
- [83] Maedler, Worms Centre Distance in Casing 17 mm + 0,05, https://www.maedler.nl/product/1643/1619/705/743/744/schnecken achsabstand 17 mm, [Online; accessed 8-May-2023], 2023.
- [84] Nanotec, ST2018S0604-A STEPPER MOTOR NEMA 8, https://en.nanotec.com/products/437-st2018s0604-a, [Online; accessed 10-Dec-2022], 2022.
- [85] Faulhaber, Series AM1524, https://www.faulhaber.com/en/products/series/am1524, [Online; accessed 12-July-2023], 2023.
- [86] T. GRADT, Encyclopedia of Tribology **2013**, 641–647.
- [87] Xtrack, Wurth Dry lubricant spray PTFE 300 ML, https://www.xtrack.nl/en/wurth-droogsmeermiddel-ptfe-300-ml, [Online; accessed 25-April-2023], 2023.
- [88] TinyTronics, 100k Ohm Potentiometer Type RV09, https://www.tinytronics.nl/shop/en/components/resistors/potentiometers/100-potentiometer, [Online; accessed 12-Aug-2023], 2023.
- [89] Maedler, Beam coupling KA made from aluminium max. torque 0.9 Nm overall length 19.05mm outer diameter 12.70mm both sides bore 4mm, https://www.maedler.nl/Article/60270800, [Online; accessed 19-May-2023], 2023.
- [90] Misumi, Deep groove ball bearings / single row / MINEBEA, https://uk.misumi-ec.com/vona2/detai1/221004938155/?PNSearch=L-940ZZ&HissuCode=L-940ZZ&searchFlow=suggest2products&Keyword=L-940ZZ, [Online; accessed 19-May-2023], 2023.
- [91] Lagerkoning, SKF Kogellager 618/4 (4x9x2.5mm), https://www.lagerkoning.nl/skf-kogellager-618-4.html, [Online; accessed 19-May-2023], 2023.
- [92] Thorlabs, 1/4"-170 Matched Adjuster/Bushing Pairs, https://www.thorlabs.de/newgrouppage9.cfm?objectgroup_id=13220&pn=F25ES050, [Online; accessed 24-May-2023], 2023.
- [93] ManufacturingET, Unified Thread Standard, http://www.manufacturinget.org/2011/10/unified-thread-standard/, [Online; accessed 25-May-2023], 2023.
- [94] Newport, Adjustment Screw, Hex, 254 TPI, 12.7 mm, 280 nm Sensitivity, https://www.newport.com/p/AJS254-0.5H-NL, [Online; accessed 1-Feb-2023], 2023.
- [95] Rapid, Vishay RTO050F68001FTE1 68K ±1T0-220, https://www.rapidonline.com/vishay-rto050f68001fte1-68k-1-50w-thick-film-resistor-t0-220-51-7350, [Online; accessed 9-May-2023], 2023.
- [96] Misumi, Misumi Catalog, https://us.misumi-ec.com/vona2/detail/221004937457/, [Online; accessed 11-July-2023], 2023.
- [97] W. met Merken, LOCTITE 638, https://www.werkenmetmerken.nl/nl/loctite_638/p/12079, [Online; accessed 15-Aug-2023], 2023.
- [98] H. Soemers, Design principles for precision mechanisms, University of Twente, Netherlands, 2010.

[99] Nedal, -ALLOY DATA SHEET EN-AW 6060[AlMgSi], https://www.nedal.com/wp-content/uploads/2017/11/Nedal-alloy-Datasheet-EN-AW-6060.pdf, [Online; accessed 30-may-2023], 2023.

- [100] D. Pramet, Alles over draadsnijden, https://www.dormerpramet.nl/alles-over-draadsnijden/, [Online; accessed 13-Jun-2023], 2023.
- [101] WTB.ino, As / gat passingen en toleranties, http://werktuigbouw.info/passingen_toleranties.html, [Online; accessed 30-may-2023], 2023.
- [102] T. India, Adjustable Two Bolt Non Rusted Metal Multiple Pipe Clamps For Pipe Fittings, https://www.tradeindia.com/products/adjustable-two-bolt-non-rusted-metal-multiple-pipe-clamps-for-pipe-fittings-7758000.html, [Online; accessed 7-Jun-2023], 2023.
- [103] Takaibane, Spring Design, https://www.tokaibane.com/en/spring-design/disc-springs-formulas, [Online; accessed 8-june-2023], 2023.
- [104] AmaTec, Schotelveren, https://www.amatec.nl/nl/schotelveren/b0281-013.html, [Online; accessed 14-July-2023], 2023.
- [105] suspensionsecrets, coil springs, https://suspensionsecrets.co.uk/how-to-calculate-coil-or-leaf-spring-rates/, [Online; accessed 5-June-2023], 2023.
- [106] TEVEMA, Technical springs in cryogenic environment, https://www.tevema.com/technical-springs-cryogenic-environments/, [Online; accessed 5-juni-2023], 2023.
- [107] J. Castillo, D. Celentano, M. Cruchaga, C. Garcia-Herrera, *Comptes Rendus Mécanique* **2018**, 346, DOI 10.1016/j.crme.2018.05.001.
- [108] Amatec, MW0375-0250-07S, https://www.amatec.nl/nl/multiwave/multiwave-mw0375-0250-07s.html, [Online; accessed 21-July-2023], 2023.
- [109] G. F. Info, Compression springs in space, https://blog.federnshop.com/en/compression-springs-in-space/, [Online; accessed 27-July-2023], 2023.
- [110] J. L. D. Santos, S. N. Monteiro, V. S. Cândido, A. O. D. Silva, F. J. Tommasini in *Vol. 20*, Universidade Federal de Sao Carlos, **2017**, pp. 603–620.
- [111] C. R. Anoop, R. K. Singh, R. R. Kumar, M. Jayalakshmi, T. A. Prabhu, K. T. Tharian, S. V. N. Murty, *Materials Performance and Characterization* **2021**, *10*, DOI 10.1520/MPC20200193.
- [112] J. Childress, S. Liou, C.-L. Chien, http://dx.doi.org/10.1051/jphyscol:1988843 1988, 49, DOI 10.1051/jphyscol:1988843.
- [113] Misumi, Ultra Spring Compression Coil Spring (C264), https://sg.misumi-ec.com/vona2/detail/221000016945/?HissuCode=C264, [Online; accessed 1-Aug-2023], 2023.
- [114] T. E. ToolBox, Euler's Column Formula, https://www.engineeringtoolbox.com/euler-column-formula-d_1813.html, [Online; accessed 11-July-2023], 2023.
- [115] L. Spring Engineers of Houston, AISI 1095 Spring Steel, https://www.springhouston.com/materials/carbon-steel/aisi-1095-spring.html, [Online; accessed 11-July-2023], 2023.
- [116] W. is piping, Guided Cantilever Method, https://whatispiping.com/guided-cantilever-method/, [Online; accessed 13-July-2023], 2023.
- [117] A. Franzen, ComponentLibrary (a vector graphics library for illustrations of optics experiments), https://www.gwoptics.org/ComponentLibrary/, [Online; accessed 21-Aug-2023], 2023.
- [118] Interview Walter Groskamp(SQ employee), Private communication, 2023.
- [119] engineersedge, General ISO Geometrical Tolerances Per. ISO 2768, https://www.engineersedge.com/mechanical,045tolerances/general_iso_tolerance_.htm, [Online; accessed 1-Aug-2023], 2023.
- [120] J. Silge, Poor confused IKEA man... https://www.flickr.com/photos/silgeland/2645819709, [Online; accessed 28-Sep-2023], 2023.



Research Plan

A.1. Plan 1

First experiment set; Proof of concept.

- E.1.1 Put 3 detectors with spacer into the cryostat. One without preload, one without preload, and one attached to the actuator, which is switched off and do a warm measurement.
- E1.2 Cooldown the system of E1.1 and do a cold measurement
- E1.3 Put 3 detectors without spacer into the cryostat. One without preload, one without preload, and one attached to the actuator, which is switched off and do a warm measurement.
- E1.4 Cooldown the system of E1.3 and do a cold measurement. The PCB without pretension is the control group and is free to move during the cooldown. The pretensioned PCB shows the same setup, but now the movement during cooldown is restricted since the fibre is pressed down. The PCB with the actuator should show the influence of the actuator and how the movement in the ferrule could potentially change

Parts that need to be realized before experiments with a stepper motor:

- Test stepper motor at cryogenic temperatures. Do a regular warm test first (E.0.1). Then connect it to the system and test warm(E.0.2), then cool down and do another test(E.0.3).
 - Fix power supply of motor 0.6A, 3.9V
 - Fix code
 - Fix wires
 - Fixed wire tree
- Design a preload mechanism. SQ has some springs, the mount needs to be designed. Can be 3D printed for warm tests. For cold test it needs to be made of copper. CNC of AM(shapeit) (Delivery time, 3-4 weeks) It is nice to do a test first with the 3D printed mount, before ordering.
 - Get CAD models of mushroom mount, ferrule, fibre, etc.
- Design actuation system. There are different elements which need to be combined. The actuator.
 - Check magnification calculation of Hugo.
 - Check lever deformations
 - Select gears that fit in assembly.
 - Resize micro screw if it is too large
 - Design preloading to get rid of backlash.

Second experiment set; Make redesign and continue testing.

This will be relevant depending on future developments.

A.2. Plan 2

A.2. Plan 2

The goal of the experiment is to show a predictable behaviour of the fibre position when actuating it. Channel 3 can be used since this had the highest transmission of 103%. The motor will be actuated and put the fibre in a sequence of positions. The reflected spectrum and later photon counts will be documented to see the predictability and reproducibility of the movement.

- E2.1 Do a quantitative warm test with the PLA model. Export the spectrum for different fibre positions and do some data analysis. Only preform this experiment when the spring arrives before the metal parts. depends on when the springs arrive.
- E2.2 Repeat E2.1, with everything in the cryostat and made from copper, but at room temperature.
- E2.3 Repeat E2.2, with everything in the cryostat and made from copper, but at room 3K.
- E2.4 Repeat E2.3, but now with reading out the counts of the detector.

The initial position is difficult to control. So, the most consistent starting point is on the SNSPD. This position can be found when moving the fibre in, and then starting to move backwards again. Steps of 1 um, or 107 motor steps seem suitable. This doesn't directly transmit the motion since there will be first backlash. The position will move backwards until an undefined point. This would depend on the readout of the graph and the judgement call when it is far enough. A clear shift in the spectrum is needed. Now the fibre is moved back in again. In this way, a hysteresis graph can be produced of the movement. The experiment could be reproduced, to really see how predictable and reproducible the moment really is. The experiment can also potentially confirm if the number of motor steps also corresponds with the corresponding movement of the fibre. -

Python and Arduino Code

B.1. Example code

Example code of a stepper motor used with an A4988 driver.

```
Simple Stepper Motor Control Exaple Code
2
     by Dejan Nedelkovski, www.HowToMechatronics.com
3
5 */
7 // defines pins numbers
8 const int stepPin = 3;
9 const int dirPin = 4;
void setup() {
   // Sets the two pins as Outputs
   pinMode(stepPin,OUTPUT);
13
14
   pinMode(dirPin,OUTPUT);
15 }
16 void loop() {
   digitalWrite(dirPin, HIGH); // Enables the motor to move in a particular direction
    // Makes 200 pulses for making one full cycle rotation
18
    for(int x = 0; x < 200; x++) {
19
      digitalWrite(stepPin,HIGH);
      delayMicroseconds(500);
21
22
      digitalWrite(stepPin,LOW);
     delayMicroseconds(500);
24
    delay(1000); // One second delay
    \label{limit} \mbox{\tt digitalWrite(dirPin,LOW); //Changes the rotations direction}
    // Makes 400 pulses for making two full cycle rotation
    for(int x = 0; x < 400; x++) {
      digitalWrite(stepPin,HIGH);
      delayMicroseconds(500);
      digitalWrite(stepPin,LOW);
32
      delayMicroseconds(500);
34
    delay(1000);
35
```

B.2. 180 degrees turn

Code used to turn the motor for 180 degrees.

```
const int stepPin = 3;
const int dirPin = 2;
const int ENPin = 4;

void setup() {
```

```
// put your setup code here, to run once:
    Serial.begin(9600);
    // Sets the two pins as Outputs
    pinMode(stepPin,OUTPUT);
10
    pinMode(dirPin,OUTPUT);
    pinMode(ENPin,OUTPUT);
13 }
14
void loop() {
    digitalWrite(ENPin,LOW);
    // Serial.println("power on");
18
    digitalWrite(dirPin,LOW); // Enables the motor to move in a particular direction (CCW)
    //digitalWrite(dirPin,HIGH); // Enables the motor to move in a particular direction (CW)
    int b = 100;
    int delaystepper = 500; // needs to be at least 300, at 200 it doesn't rotate
23
    for(int x = 0; x < b; x++) {
24
      digitalWrite(stepPin,HIGH);
      delayMicroseconds(delaystepper);
26
27
      digitalWrite(stepPin,LOW);
      delayMicroseconds(delaystepper);
29
    digitalWrite(ENPin,HIGH);
    // Serial.println("power off");
    // Serial.println();
    while(1) {
34
35
    }
37 }
```

B.3. Read potentiometer

Code used to read the position of the potentiometer

```
int potPin = A0;
const int stepPin = 3;
3 const int dirPin = 2;
4 const int ENPin = 4;
6 void setup() {
   // put your setup code here, to run once:
    Serial.begin(9600);
   pinMode(potPin, INPUT);
   pinMode(stepPin,OUTPUT);
    pinMode(dirPin,OUTPUT);
11
12
    pinMode(ENPin,OUTPUT);
    digitalWrite(ENPin,HIGH); //Turn motor off
14
15 }
void loop() {
   float sensorValue = analogRead(potPin);
    float sensorAngle = sensorValue * 270/1023; //Transfer pot meter output [0-1023] to degrees
20
    Serial.print(sensorAngle)
    delay(100); // delay in between reads for stability
22
23 }
```

B.4. Motor Control

Code used to give feedback to the motor position.

```
int potPin = A0;
const int stepPin = 3;
const int dirPin = 2;
const int ENPin = 4;
```

B.4. Motor Control

```
5
6 void setup() {
    // put your setup code here, to run once:
    Serial.begin(9600);
    pinMode(potPin,INPUT);
10
    pinMode(stepPin,OUTPUT);
11
    pinMode(dirPin,OUTPUT);
12
13
    pinMode(ENPin,OUTPUT);
    Serial.println("---Programm_initiated---");
14
15
   // delay(3000);
17
18 void loop() {
    float targetAngle = 10; // [0=270] Positive is clockwise, seen from looking at the axle
19
    int allowedError = 5; //degrees/
20
21
    // float sensorValue = analogRead(potPin);
22
    // float sensorAngle = sensorValue * 270/1023; //Transfer pot meter output [0-1023] to
23
24
    int count = 100:
25
    float som = 0;
    for (int x=0; x<count; x++) {</pre>
27
28
      som += analogRead(potPin);
     delay(10);
29
30
     // Serial.print(som);
      // Serial.print(", ");
31
32
33
34
    som /= count;
    float sensorAngle = float(som) * 270/1023;
35
37
    if((targetAngle > 270) || (targetAngle < 0)){ //too large OR to small</pre>
38
      Serial.println();
      Serial.println("NOT_A_VALID_TARGET_ANGLE");
40
      Serial.println();
41
      while(1) {
43
    }
44
45
    int error = sensorAngle - targetAngle;
    // Serial.print("Error angle: ");
48
    Serial.print("Error:"); Serial.print(error); Serial.print(",");
49
    // Serial.print("
                           Sensor Angle: ");
    Serial.print("SensorAngle:"); Serial.print(sensorAngle); Serial.print(",");
51
52
53
    if(abs(error) <= allowedError) {</pre>
      Serial.println();
54
      Serial.println("---Reached_position---");
55
      Serial.println();
56
      digitalWrite(ENPin,HIGH); //Turn motor off
57
      while(1) {
59
60
    } else if(error > 0) {
      // Serial.print("
                               too low,");
61
      digitalWrite(dirPin,HIGH); // Enables the motor to move in a particular direction (CW)
62
    } else if(error < 0){</pre>
      // Serial.print("
                               too high,");
64
      digitalWrite(dirPin,LOW); // Enables the motor to move in a particular direction (CCW)
65
66
      Serial.print("Error_in_sensor_reading");
67
    int delaystepper = 500;  // needs to be at least 300, at 200 it doesn't rotate
int steps = abs(error * 5/9); //convert 360 degrees to 200 steps
    Serial.print("Steps:"); Serial.print(steps);
72
    Serial.println();
73
```

B.5. 30 turns 87

```
for(int x = 0; x < steps; x++) {
    digitalWrite(stepPin, HIGH);
    delayMicroseconds(delaystepper);
    digitalWrite(stepPin, LOW);
    delayMicroseconds(delaystepper);
}

delay(1000);
</pre>
delay(1000);
```

B.5. 30 turns

Code used to turn the motor to turn 30 full circles

```
const int stepPin = 3;
const int dirPin = 2;
3 const int ENPin = 4;
5 void setup() {
   // put your setup code here, to run once:
   Serial.begin(9600);
   //Serial.println("Begin setup");
10
11
   // Sets the two pins as Outputs
   pinMode(stepPin,OUTPUT);
12
   pinMode(dirPin,OUTPUT);
13
14
   pinMode(ENPin,OUTPUT);
15
   //Serial.println("end setup");
16
17 }
18
19 void loop() {
   digitalWrite(ENPin,LOW);
   Serial.println("power_on");
21
digitalWrite(dirPin,LOW); // UP
                                            Enables the motor to move in a particular
24
       direction (CCW) (Up)
   // digitalWrite(dirPin,HIGH); // DOWN
                                            Enables the motor to move in a particular
25
       direction (CW) (Down)
   float AantalRondjes = 30 ;
int b = AantalRondjes * 200;
29
   //int b = 650;
30
   int delaystepper = 1000; // needs to be at least 300, at 200 it doesn't rotate
   for(int x = 0; x < b; x++) {
32
      digitalWrite(stepPin,HIGH);
33
      delayMicroseconds(delaystepper);
      digitalWrite(stepPin,LOW);
35
36
      delayMicroseconds(delaystepper);
37
38
   digitalWrite(ENPin,HIGH);
   Serial.print("I've_turned_");
   Serial.print(AantalRondjes);
   Serial.println("_circles");
   //Serial.println("power off");
43
44
   Serial.println();
   while(1) {
45
   }
46
```

B.6. Direct motor control V1.0

Code used to send inputs to the Arduino.

```
# -*- coding: utf-8 -*-
2 """
3 Created on Mon Jul 31 12:37:59 2023
5 @author: rudis
8 import serial
9 import time
10 from pynput import keyboard
11 from pynput.keyboard import Key
12 import numpy as np
13
15 def send_move(steps):
16
                                   #1 equals positive movement
17
      direction = 1
18
      if steps<0:</pre>
          direction = 0
19
      SerialObj.write(bytearray([direction,int(abs(steps))]))
                                                                  #transmit 'A' (8bit) to
21
          micro/Arduino
23 def on_press_init(key):
24
      global state
25
26
     if key == Key.ctrl_l:
          distance = int(input("Move_this_distance_[nm]:_"))
27
          steps = int(round(distance/(149.4/200/80*1000)))
28
          print("I_moved_these_steps", steps)
29
          state.append([steps, steps*149.4/200/80*1000])
          send_move(steps)
31
32
          return
33
     elif key == Key.enter:
34
         print("Continued")
35
          return False
36
37
    elif key == Key.esc:
         print("operation_canceled")
39
          return False
40
41
42 def on_release_init(key):
43
      return
44
45 # def get_statefromstep(step):
                                                               #returns state vector from given
      step position
        state = np.empty(3)
46 #
47
48 #
        state[0] = step
        state[1] = step*np.pi/n_step
                                                                    #Teta
49 #
50 #
        state[2] = np.sin(step*np.pi/n_step)
                                                                    #h
51
52 #
        return(state)
54
55 SerialObj = serial.Serial('COM7') # COMxx format on Windows
57 SerialObj.baudrate = 9600 # set Baud rate to 9600
58 SerialObj.bytesize = 8  # Number of data bits = 8
59 SerialObj.parity = 'N'  # No parity
59 SerialObj.parity ='N'
60 SerialObj.stopbits = 1
                             # Number of Stop bits = 1
n_{step} = 100
63 state = []
                   # Only needed for Arduino,For AVR/PIC/MSP430 & other Micros not needed
65 time.sleep(3)
                   # opening the serial port from Python will reset the Arduino.
                   # Both Arduino and Python code are sharing Com11 here.
67
                   # 3 second delay allows the Arduino to settle down.
68
```

B.7. ByteArray

```
# BytesWritten = SerialObj.write(b'A')  # transmit 'A' (8bit) to micro/Arduino
# Declare A as a Byte (b'A')

# print('BytesWritten = ', BytesWritten)

with keyboard.Listener(on_press=on_press_init, on_release=on_release_init) as listener:
    listener.join()

SerialObj.close()  # Close the port
```

B.7. ByteArray

Code used to receive motor inputs from the python script.

```
1 #define stepPin 3
2 #define dirPin 2
3 #define enPin 4
5 void setup() {
    // put your setup code here, to run once:
    Serial.begin(9600);
    pinMode(stepPin, OUTPUT);
    pinMode(dirPin, OUTPUT);
    pinMode(enPin, OUTPUT);
10
    digitalWrite(enPin, HIGH);
11
12 }
13 byte myArray[2];
14
void loop() {
    // put your main code here, to run repeatedly:
16
    if (Serial.available() > 0) {
17
      Serial.readBytesUntil(255, myArray, 2);
      digitalWrite(enPin, LOW);
19
20
      Serial.print("Received_Data");
21
      int direction = myArray[0];
22
      if (direction==1) {
23
        digitalWrite(dirPin, HIGH);
24
25
26
      if (direction==0) {
        digitalWrite(dirPin, LOW);
27
28
29
      int steps;
30
      steps = myArray[1];
32
      for(int x=0; x<steps; x++) {</pre>
33
          doMotorStep(); //just turn continuously
35
36
      Serial.write(1);
37
38
39
      delay(100); // Keep the motor on to prefent intertia from overshooting its position.
      digitalWrite(enPin, HIGH);
40
41
    }
42 }
44 void doMotorStep(){
    //digitalWrite(6, LOW);
    digitalWrite(stepPin, HIGH);
    delayMicroseconds(500); //lower = faster, but louder
    digitalWrite(stepPin, LOW);
48
49
    delayMicroseconds (500);
    //digitalWrite(6, LOW);
51 }
```

B.8. Direct motor control V1.1

Code used to send inputs to the Arduino.

```
1 # -*- coding: utf-8 -*-5
3 Created on Mon Jul 31 12:37:59 2023
5 @author: rudis
7 #wat ik wil als data [time, distance step, new position] [note]
8 # To do: Write note
10 import serial
11 import time
12 from pynput import keyboard
13 from pynput.keyboard import Key
14 import numpy as np
17 def send_move(steps):
                                   #1 equals positive movement
      direction = 1
18
19
      if steps<0:</pre>
          direction = 0
20
21
     SerialObj.write(bytearray([direction,int(abs(steps))]))
                                                                    #transmit 'A' (8bit) to
          micro/Arduino
23
24 def on_press_init(key):
      global state
25
26
      global position
     global step1
27
28
     if key == Key.ctrl_l:
         distance = int(input("Move_this_distance_[nm]:_"))
30
31
          steps = int(round(distance/step1))
          print("Ready")
32
          position += np.round(steps*step1,2)
33
          state.append([get_time(t0), position, np.round(steps*step1,2)])
          send_move(steps)
35
36
          return
      elif key == Key.up:
38
          fixed_move(2000) #1867 for one rotation
39
          return
41
     elif key == Key.down:
42
         fixed_move(-2000) #1867 for one rotation
43
44
          return
     elif key == Key.left:
          fixed_move(-200) #1867 for one rotation
47
48
49
      elif key == Key.right:
          fixed_move(200) #1867 for one rotation
51
52
          return
      elif key == Key.insert:
54
          note = str(input("Write_note:"))
55
          state.append([note])
          return
57
      elif key == Key.home:
          position = 0
60
          state.append(["Position_Reset"])
          print("Position_Reset")
62
63
          return
64
      elif key == Key.enter:
65
         print("Continued")
```

```
67
          return False
68
       elif key == Key.esc:
69
          print("operation_canceled")
           return False
71
73 def on_release_init(key):
      return
74
75
76 def get_time(t0):
       dt = time.time() - t0
77
       m = int(dt//60)
       s = int(round(dt\%60,0))
79
      return str(m) + ":" + str(s)
81
82 def fixed_move(distance):
       global state
83
       global position
84
       global step1
85
       steps = int(round(distance/(step1)))
87
       # print("I moved this distance:", distance)
88
       position = np.round((position + steps*step1),2)
       state.append([get_time(t0), np.round(steps*step1,2), position])
90
91
       send_move(steps)
       print(state[-1])
92
93
      return
94
# def get_statefromstep(step):
                                                               #returns state vector from given
       step position
         state = np.empty(3)
97 #
99
         state[0] = step
         state[1] = step*np.pi/n_step
100 #
                                                                   #Teta
         state[2] = np.sin(step*np.pi/n_step)
                                                                   #h
102
103 #
        return(state)
105
106 SerialObj = serial.Serial('COM7') # COMxx format on Windows
108 SerialObj.baudrate = 9600 # set Baud rate to 9600
109 SerialObj.bytesize = 8
                              # Number of data bits = 8
SerialObj.parity ='N'
                              # No parity
serialObj.stopbits = 1
                              # Number of Stop bits = 1
n_{step} = 100
114 state = []
115 position = 0
116 t0 = time.time()
117 step1 = 149.4/200/80*1000
                                    #distance in nm of 1 motor step
118
119
120 time.sleep(3)
                   # Only needed for Arduino, For AVR/PIC/MSP430 & other Micros not needed
                   # opening the serial port from Python will reset the Arduino.
121
122
                   # Both Arduino and Python code are sharing Com11 here.
                   # 3 second delay allows the Arduino to settle down.
123
124
                                                # transmit 'A' (8bit) to micro/Arduino
# BytesWritten = SerialObj.write(b'A')
                                              # Declare A as a Byte (b'A')
126
127
# print('BytesWritten = ', BytesWritten)
129
130 print("arrow_up_and_down,_+-2000;_arrow_left_and_right,_+-200;_ctrl_1,_input_distance_+-_
       2000; _home,_set_new_base_position; _instert__, _make_note; _esc_&_enter, _cancle_opperation")
# print("give a distance between +-2000nm")
132 with keyboard.Listener(on_press=on_press_init, on_release=on_release_init) as listener:
       listener.join()
133
print(state)
```

135 SerialObj.close() # Close the port



Mail contact

C.1. Mail Send to Thorlabs

To: techsupport@thorlabs.com Subject: F25ES050 Question

Dear Sir/Madam,

We are currently working with the 1/4"-170 Adjuster to achieve a position resolution of 10nm for positioning an optical fiber. One of the design options we currently have in mind is using a drive train with a stepper motor, a worm gear, and the 1/4"-170 adjuster to achieve the positioning resolution. We are wondering what linear position resolution is achievable with this adjuster. The product pages mentions that the tolerances are tighter than the ASME/ANSI Class 3 UTS standard, but not the specific tolerances. That rases for us two questions.

What are the exact tolerances? And is there information regarding the maximum linear position resolution of this adjuster?

Thanks in advance.

Kind regards,
Rudi Smits

C.2. Reply from Thorlabs

Subject: RE: F25ES050 Question | CAS-555616-W7B4K8

Dear Mr. Smits,

Thank you for your e-mail and your interest in our actuators. The F25ES050 has a lead screw with an 1/4-170-3A thread while the bushing is 1/4-170-3B. The thread specs are as follows:

```
1/4-170-3A:
```

```
max. major diameter: 0.2500"
min. major diameter: 0.2480"
max. pitch diameter: 0.2462"
min. pitch diameter: 0.2449"
max. minor diameter: 0.2432"
min. minor diameter: 0.2410"
```

1/4-170-3B:

max. major diameter: 0.2526"
min. major diameter: 0.2505"
max. pitch diameter: 0.2479"
min. pitch diameter: 0.2462"
max. minor diameter: 0.2440"
min. minor diameter: 0.2438"

We define the resolution of the actuator as the travel per revolution, which is 25.4 mm / 170 = 149.4 μm .

Mit freundlichen Grüßen / With kind regards Bettina Wünsch

C.3. Mail received to Amatec

Beste Rudi,

Het is erg lastig materiaal te vinden wat geschikt is voor minus 270°C waar ook nog veren van gemaakt kunnen worden. Hieronder een overzicht van materialen waar wij veren van maken.

Whether in cooling systems, in space or other low temperature applications. Metal springs often have to withstand temperatures of up to - 200 degrees. Despite rising tensile strength low temperatures have an unfavorable effect on the material, as the toughness decreases and brittle fractures can occur. For low-temperature applications, stainless spring steels, copper and nickel alloys are preferable to the patented spring wires and valve spring wires. The following table shows the limit temperatures.

Spring material Lowest working temperature in ° C Patented drawn spring steel wire according to EN 10270-1 -60 Oil tempered valve spring wire according to EN 10270-2 -60 X10CrNi 18.8 (1.4310) -200 X7CrNiAl 17.7 (1.4568) -200 -200 X5CrNiMo 17-12-2 (1.4401) CuSn6 -200 CuZn36 -200 CuBe2 -200

Table C.1: Recommendations for use at low temperatures.

Met vriendelijke groet, Kind regards, Remo Schrama

C.4. Reply Send to Amatec

Beste Remo,

CuNi18Zn20

Inconel X750

Nimonic90

Bedankt voor je mail en het uitzoeken. Dat de limiet temperaturen van veermaterialen relatief warm is klinkt niet veel beloven voor onze toepassen. We hebben de paper "A Review on Steels for Cryogenic Applications" gevonden, waar stainless steel 1.4301 wel positief uit komt. Onze toepassing heeft minder dan 50 load cycles op cryogene temperaturen, dus we hebben hoop dat een veer uit dit materiaal gaat werken.

-200

-100

-100

Met vriendelijke groeten, Rudi Smits

C.5. Reply received from Amatec

Hoi Rudi,

Rvs 304 (1.4301) is echter zacht materiaal en hier worden normaliter geen veren van gemaakt. Wel draadvormen en dergelijke.

Met vriendelijke groet, Kind regards, Remo Schrama

ISO 2768 Tolerances

Machining parts isn't perfect. There are general geometrical tolerances defined in ISO 2768. The permissible deviations are different, depending in the size of the part, and the chosen accuracy, which can either be Very coarse, Coarse, Medium, and Fine. The Medium tolerance class was deemed to the best option for the design. Not too expensive in production, but still accurate enough. This means that certain margins need to be taken in to account in the design. The linear and angular displacements are shown in Table D.1 and Table D.2 respectively. These deviations needed to be taking in to account in the design.

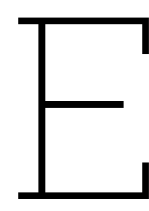
Holes that needed to be aligned with a threaded hole, were given an extra 0.2-0.5mm margin, depending on their size and allowed tolerances. One thing that also should have received a change in dimension are the parts mounted on the inside of the frame. This outer diameter matches the extra inner diameter of the frame and could be difficult to assemble when their just slightly too large, or that the frame is too small. It is made out of copper which is a relatively soft material. So if there are really issue, a bit of sandpaper could remove enough material to improve the fit of the parts.

Table D.1: Permissible Linear Deviations for Medium ISO 2768.[119]

Range Nominal length [mm]	Allowed error [mm]		
0.5-6	0.1		
6-30	0.2		
0-120	0.3		
120-400	0.5		

Table D.2: Permissible Angular Deviations for Medium ISO 2768.[119]

Range Nominal length [mm]	Allowed error [deg and minutes]		
< 10	1°		
10-50	0° 30′		
50-120	0° 20′		



Fibre Position

Here is the input position data for the different experiment that were preformed.

E.1. Second Warm Test

Here is the list of motor inputs for the second warm test. It is a list of action, where the first item is the number of steps, and the second item is the corresponding steps in nanometers. [[214, 1998.22], [54, 504.22], [54, 504.22], [214, 1998.22], [214, 1998.22], [214, 1998.22], [214, 1998.22], [214, 1998.22], [214, 1998.22], [214, 1998.22], [54, 504.22], [11, 102.71], [11, 102.71], [11, 102.71], [11, 102.71], [11, 102.71], [11, 102.71], [11, 102.71], [11, 102.71], [-54, -504.22], [-54, -5[-214, -1998.22], [-214, -1998. -1998.22], [-214, -1998. -1998.22], [-214, -1998.22], [214, 1998.22], [2 1998.22], [214, 1998.22], [54, 504.22], [54, 50 504.22], [11, 102.71], [21, 196.09], [21, 196.09], [21, 196.09], [54, 504.22], [54, 504.22], [54, 504.22], [54, 504.22], [11, 102.71], [11, 102.71], [32, 298.8], [32, 298.8], [32, 298.8], [32, 298.8], [32, 298.8], [32, 298.8], [32, 298.8], 504.22], [32, 298.8 298.8], [32, 298.8], [-32, -298.8], [-32, -298.8], [-32, -298.8], [-32, -298.8], [-54, -504.22], [-54, -504.22], [-54, -504.22], [-214, -1998.22], [-2 [-214, -1998.22], [-214, -1998. -1998.22], [-214, -1998.22], [-214, -1998.22], [-214, -1998.22], [-214, -1998.22], [-214, -1998.22], [-214, -1998.22], [214, 1998.22], [54, 504.22], [54, 504.22], [54, 504.22], [32, 298.8], [32, 298.8], E.2. Third Warm Test 1 98

[32, 298.8], [32, 298.8], [64, 597.6], [-214, -1998.22], [-139, -1297.91], [-214, -1998.22], [-214, -1998. -1998.22], [-214, -1998.22], [-[214, 1998.22], [-214, -1998.22], [214, 1998.22], [54, 504.22], [-32, -298.8], [-107, -999.11], [-107, -999.11], [-107, -999.11], [-214, -1998.22], [-214, -19 -1998.22], [-214, -1998.22], [-214, -1998.22], [-214, -1998.22], [-107, -999.11], [-10[-107, -999.11], [-10[-107, -999.11], [-10[-107, -999.11], [-54, -504.22], [-54, -504.22], [-32, -298.8], [-32, -298.8], [-32, -298.8], [-32, -298.8], -298.8], [-32, -298.8] -298.8], [-32, -298.8] -298.8], [-32, -298.8]

E.2. Third Warm Test 1

[['Time', 'Moved Steps', 'Moved Distance', 'Steps Position', 'Theoretical Linear Postion'], ['0:8', 11, 102.71, 11, 102.71], ['0:12', 214, 1998.22, 225, 2100.94], ['0:14', 214, 1998.22, 439, 4099.16], ['0:15', 214, 1998.22, 653, 6097.39], ['0:20', 214, 1998.22, 867, 8095.61], ['0:20', 214, 1998.22, 1081, 10093.84], ['0:21', 214, 1998.22, 1295, 12092.06], ['0:21', 214, 1998.22, 1509, 14090.29], ['0:21', 214, 1998.22, 1723, 16088.51], ['0:27', 214, 1998.22, 1937, 18086.74], ['0:29', 214, 1998.22, 2151, 20084.96], ['0:32', 214, 1998.22, 2365, 22083.19], ['0:37', 214, 1998.22, 2579, 24081.41], ['0:53', -214, -1998.22, 2365, 22083.19], ['0:54', 214, 1998.22, 2579, 24081.41], ['0:58', 214, 1998.22, 2793, 26079.64], ['1:1', -214, -1998.22, 2579, 24081.41], ['1:2', -214, -1998.22, 2365, 22083.19], ['1:3', 214, 1998.22, 2579, 24081.41], ['1:3', 214, 1998.22, 2793, 26079.64], ['1:4', 214, 1998.22, 3007, 28077.86], ['1:37', 214, 1998.22, 3221, 30076.09], ['1:42', 214, 1998.22, 3435, 32074.31], ['1:43', -214, -1998.22, 3221, 30076.09], ['2:14', -214, -1998.22, 3007, 28077.86], ['2:15', -214, -1998.22, 2793, 26079.64], ['2:15', -214, -1998.22, 2579, 24081.41], ['2:16', 214, 1998.22, 2793, 26079.64], ['2:16', 214, 1998.22, 3007, 28077.86], ['2:17', 214, 1998.22, 3221, 30076.09], ['2:18', 214, 1998.22, 3435, 32074.31], ['2:18', 214, 1998.22, 3649, 34072.54], ['2:20', 214, 1998.22, 3863, 36070.76], ['2:20', 214, 1998.22, 4077, 38068.99], ['2:21', 214, 1998.22, 4291, 40067.21], ['2:22', 214, 1998.22, 4505, 42065.44], ['2:25', 214, 1998.22, 4719, 44063.66], ['2:32', 214, 1998.22, 4933, 46061.89], ['2:35', 214, 1998.22, 5147, 48060.11], ['2:39', 214, 1998.22, 5361, 50058.34], ['2:42', 214, 1998.22, 5575, 52056.56], ['2:42', 214, 1998.22, 5789, 54054.79], ['2:45', 214, 1998.22, 6003, 56053.01], ['2:46', 214, 1998.22, 6217, 58051.24], ['2:46', 214, 1998.22, 6431, 60049.46], ['2:47', 214, 1998.22, 6645, 62047.69], ['2:47', 214, 1998.22, 6859, 64045.91], ['2:47', 214, 1998.22, 7073, 66044.14], ['2:48', 214, 1998.22, 7287, 68042.36], ['2:58', 214, 1998.22, 7501, 70040.59], ['2:59', 214, 1998.22, 7715, 72038.81], ['2:60', 214, 1998.22, 7929, 74037.04], ['3:0', 214, 1998.22, 8143, 76035.26], ['3:0', 214, 1998.22, 8357, 78033.49], ['3:7', 214, 1998.22, 8571, 80031.71], ['3:7', 214, 1998.22, 8785, 82029.94], ['3:8', 214, 1998.22, 8999, 84028.16], ['3:8', 214, 1998.22, 9213, 86026.39], ['3:14', 214, 1998.22, 9427, 88024.61], ['3:14', 214, 1998.22, 9641, 90022.84], ['3:15', 214, 1998.22, 9855, 92021.06], ['3:15', 214, 1998.22, 10069, 94019.29], ['3:19', 214, 1998.22, 10283, 96017.51], ['3:20', 214, 1998.22, 10497, 98015.74], ['3:20', 214, 1998.22, 10711, 100013.96], ['3:20', 214, 1998.22, 10925, 102012.19], ['3:26', 214, 1998.22, 11139, 104010.41], ['3:26', 214, 1998.22, 11353, 106008.64], ['3:26', 214, 1998.22, 11567, 108006.86], ['3:31', 214, 1998.22, 11781, 110005.09], ['3:39', 11, 102.71, 11792, 110107.8], ['3:40', 11, 102.71, 11803, 110210.51], ['3:43', 11, 102.71, 11814, 110313.22], ['3:43', 11, 102.71, 11825, 110415.94], ['3:43', 11, 102.71, 11836, 110518.65], ['3:44', 11, 102.71, 11847, 110621.36], ['3:44', 11, 102.71, 11858, 110724.08], ['3:49', 11, 102.71, 11869, 110826.79], ['3:50', 11, 102.71, 11880, 110929.5], ['3:50', 11, 102.71, 11891, 111032.21], ['3:50', 11, 102.71, 11902, 111134.92], ['3:50', 11, 102.71, 11913, 111237.64], ['3:60', 11, 102.71, 11924, 111340.35], ['4:0', 11, 102.71, 11935, 111443.06], ['4:1', 11, 102.71, 11946, 111545.78], ['4:1', 11, 102.71, 11957, 111648.49], ['4:1', 11, 102.71, 11968, 111751.2], ['4:6', 11, 102.71, 11979, 111853.91], ['4:6', 11, 102.71, 11990, 111956.62], ['4:6', 11, 102.71, 12001, 112059.34], ['4:6', 11, 102.71, 12012, 112162.05], ['4:10', 11, 102.71, 12023, 112264.76], ['4:11', 11, 102.71, 12034, 112367.48], ['4:19', 11, 102.71, 12045, 112470.19], ['4:20', 11, 102.71, 12056, 112572.9], ['4:25', 11, 102.71, 12067, 112675.61], ['4:26', 11, 102.71, 12078, 112778.32], ['4:34', 11, 102.71, 12089, 112881.04], ['4:40', 11, 102.71, 12100, 112983.75], ['6:22', 11, 102.71, 12111, 113086.46], ['6:28', 11, 102.71, 12122, 113189.18], ['6:45', 11, 102.71, 12133, 113291.89], ['6:51', E.3. Third Warm Test 2

11, 102.71, 12144, 113394.6], ['6:58', 11, 102.71, 12155, 113497.31], ['7:10', 11, 102.71, 12166, 113600.02], ['7:20', 11, 102.71, 12177, 113702.74], ['7:26', 11, 102.71, 12188, 113805.45], ['7:32', 11, 102.71, 12199, 113908.16], ['7:39', 11, 102.71, 12210, 114010.88], ['7:46', 11, 102.71, 12221, 114113.59], ['8:0', 11, 102.71, 12232, 114216.3], ['8:6', 11, 102.71, 12243, 114319.01], ['8:11', 11, 102.71, 12254, 114421.72], ['8:16', 11, 102.71, 12265, 114524.44], ['8:23', 11, 102.71, 12276, 114627.15], ['8:31', 11, 102.71, 12287, 114729.86], ['hier te dicht bij'], ['Position Reset'], ['10:8', -11, -102.71, -11, -102.71], ['10:13', -11, -102.71, -22, -205.42], ['10:18', -11, -102.71, -33, -308.14], ['10:42', -11, -102.71, -44, -410.85], ['10:49', -11, -102.71, -55, -513.56], ['11:6', -11, -102.71, -66, -616.28], ['11:8', -11, -102.71, -77, -718.99], ['11:8', -11, -102.71, -88, -821.7], ['11:12', -214, -1998.22, -302, -2819.92], ['hier al beweging'], ['11:46', -11, -102.71, -313, -2922.64], ['11:52', -11, -102.71, -324, -3025.35], ['11:58', -11, -102.71, -335, -3128.06], ['11:59', -11, -102.71, -346, -3230.78], ['Dit lijkt optimaal'], ['13:1', -1, -9.34, -347, -3240.11], ['13:16', -3, -28.01, -350, -3268.12], ['13:24', -3, -28.01, -353, -3296.14], ['Position Reset'], ['hier echt optimaal op 1550, zie foto 1], ['17:4', -214, -1998.22, -214, -1998.22], ['17:12', -214, -1998.22, -428, -3996.45], ['17:17', -214, -1998.22, -642, -5994.68], ['17:27', 214, 1998.22, -428, -428, -428]-3996.45], ['17:32', 214, 1998.22, -214, -1998.22], ['17:38', 214, 1998.22, 0, 0.0], ['17:51', 11, 102.71, 11, 102.71], ['17:53', 11, 102.71, 22, 205.42], ['17:53', 11, 102.71, 33, 308.14], ['17:58', 11, 102.71, 44, 410.85], ['17:58', 11, 102.71, 55, 513.56], ['17:58', 11, 102.71, 66, 616.28], ['18:4', 11, 102.71, 77, 718.99], ['18:7', 11, 102.71, 88, 821.7], ['18:8', 11, 102.71, 99, 924.41], ['18:12', 11, 102.71, 110, 1027.12], ['18:18', 11, 102.71, 121, 1129.84], ['18:24', 11, 102.71, 132, 1232.55], ['18:28', 11, 102.71, 143, 1335.26], ['18:33', 11, 102.71, 154, 1437.98], ['18:38', 11, 102.71, 165, 1540.69], ['18:42', 11, 102.71, 176, 1643.4], ['18:47', 11, 102.71, 187, 1746.11], ['18:48', 11, 102.71, 198, 1848.82], ['19:15', 5, 46.69, 203, 1895.51], ['19:27', 5, 46.69, 208, 1942.2], ['19:48', 11, 102.71, 219, 2044.91], ['19:53', 11, 102.71, 230, 2147.62], ['19:58', 11, 102.71, 241, 2250.34], ['20:3', 11, 102.71, 252, 2353.05], ['20:8', 11, 102.71, 263, 2455.76], ['20:13', 11, 102.71, 274, 2558.48], ['hier zit ie er weer op, zie foto 2'], ['21:51', 5, 46.69, 279, 2605.16], ['22:1', 5, 46.69, 284, 2651.85], ['22:9', 5, 46.69, 289, 2698.54], ['22:18', 5, 46.69, 294, 2745.22], ['22:49', 5, 46.69, 299, 2791.91], ['23:4', 11, 102.71, 310, 2894.62], ['23:11', 11, 102.71, 321, 2997.34], ['23:16', 11, 102.71, 332, 3100.05], ['weer te dicht bij. Word meer vlak'], ['23:48', -11, -102.71, 321, 2997.34], ['23:60', -11, -102.71, 310, 2894.62], ['24:6', -11, -102.71, 299, 2791.91], ['24:7', -11, -102.71, 288, 2689.2], ['24:12', -11, -102.71, 277, 2586.49], ['24:12', -11, -102.71, 266, 2483.78], ['24:16', -11, -102.71, 255, 2381.06], ['24:17', -11, -102.71, 244, 2278.35], ['24:22', -11, -102.71, 233, 2175.64], ['24:22', -11, -102.71, 222, 2072.93], ['24:22', -11, -102.71, 211, 1970.21], ['24:27', -11, -102.71, 200, 1867.5], ['24:27', -11, -102.71, 189, 1764.79], ['24:27', -11, -102.71, 178, 1662.08], ['24:32', -11, -102.71, 167, 1559.36], ['24:32', -11, -102.71, 156, 1456.65], ['24:32', -11, -102.71, 145, 1353.94], ['24:37', -11, -102.71, 134, 1251.23], ['24:37', -11, -102.71, 123, 1148.51], ['24:37', -11, -102.71, 112, 1045.8], ['24:42', -11, -102.71, 101, 943.09], ['24:42', -11, -102.71, 90, 840.38], ['24:42', -11, -102.71, 79, 737.66], ['24:47', -11, -102.71, 68, 634.95], ['24:47', -11, -102.71, 57, 532.24], ['24:52', -11, -102.71, 46, 429.52], ['24:52', -11, -102.71, 35, 326.81], ['hier begint hij weer wat te bewegen'], ['25:17', -11, -102.71, 24, 224.1], ['25:18', -11, -102.71, 13, 121.39], ['25:27', -11, -102.71, 2, 18.68], ['25:27', -11, -102.71, -9, -84.04], ['Hier zit hij weer op het optimum, zie foto 3'], ['Extra diode boven aan de PCB mount. er zijn M3 diodes'], ['40:22', 11, 102.71, 2, 18.68], ['Hem optillen laat hem ook bewegen. Trillingen hebben effect'], ['48:33', 0, 0.0, 2, 18.68]]

E.3. Third Warm Test 2

[[Time', Moved Steps', Moved Distance', Steps Position', Theoretical Linear Postion'], ['0:18', -214, -1998.22, -214, -1998.22], ['0:25', -214, -1998.22, -428, -3996.45], ['0:26', -214, -1998.22, -642, -5994.68], ['0:36', -214, -1998.22, -856, -7992.9], ['0:51', 11, 102.71, -845, -7890.19], ['0:54', -11, -102.71, -856, -7992.9], ['0:56', 214, 1998.22, -642, -5994.68], ['1:1', 214, 1998.22, -428, -3996.45], ['1:1', 214, 1998.22, -214, -1998.22], ['1:8', 11, 102.71, -203, -1895.51], ['1:11', 11, 102.71, -192, -1792.8], ['1:12', 11, 102.71, -181, -1690.09], ['1:13', 11, 102.71, -170, -1587.38], ['1:16', 11, 102.71, -159, -1484.66], ['1:16', 11, 102.71, -148, -1381.95], ['1:17', 11, 102.71, -137, -1279.24], ['1:21', 11, 102.71, -126, -1176.53], ['1:22', 11, 102.71, -115, -1073.81], ['1:22', 11, 102.71, -104, -971.1], ['1:27', 11, 102.71, -93, -868.39], ['1:27', 11, 102.71, -82, -765.68], ['1:32', 11, 102.71, -71, -662.96], ['1:32', 11, 102.71, -60, -560.25], ['1:37', 11, 102.71, -49, -457.54], ['1:37', 11, 102.71, -38, -354.82], ['1:43', 11, 102.71, -27, -252.11], ['1:43', 11, 102.71, -16, -149.4], ['1:47', 11, 102.71, -5, -46.69], ['1:52', 11, 102.71, 6, 56.03], ['1:57', 11, 102.71, 17, 158.74], ['2:2', 11, 102.71, 28, 261.45], ['2:7', 11, 102.71, 39, 364.16], ['2:12', 11, 102.71, 50, 466.88], ['2:19', 11, 102.71, 61, 569.59], ['2:27', 11, 102.71, 72, 672.3], ['2:34', 11, 102.71, 183, 775.01], ['2:43', 11, 102.71, 94, 877.72], ['2:48', 11, 102.71, 105, 980.44], ['2:53', 11, 102.71, 116, 1083.15], ['2:57', 11, 102.71, 127, 1185.86], ['3:2', 11, 102.71, 138, 1288.58], ['3:8', 11, 102.71, 149, 1391.29], ['3:13', 11, 102.71, 160, 1494.0], ['3:43', 11, 102.71, 171, 1596.71], ['3:47', 11, 102.71, 182, 1699.42], ['3:52', 11, 102.71, 193, 193.71], ['2:43', 11, 102.71, 171, 1596.71], ['3:47', 11, 102.71, 182, 1699.42], ['3:52', 11, 102.71, 193, 193.71], ['1:102.71, 193, 193.71], ['1:102.71, 193, 193.71], ['1:102.71, 193, 193.71], ['1:102.71, 193, 193.71], ['1:102.71, 193, 193.71], ['1:102.71, 193, 193.71], ['1:102.71, 193,

E.3. Third Warm Test 2

1802.14], ['3:58', 11, 102.71, 204, 1904.85], ['4:3', 11, 102.71, 215, 2007.56], ['4:8', 11, 102.71, 226, 2110.28], ['4:24', 3, 28.01, 229, 2138.29], ['4:38', 3, 28.01, 232, 2166.3], ['Hier zit hij er redelijk op. Begin experiment hier'], ['Position Reset'], ['6:36', 0, 0.0, 0, 0.0], ['6:46', 3, 28.01, 3, 28.01], ['6:58', 3, 28.01, 6, 56.03], ['7:8', 3, 28.01, 9, 84.04], ['7:19', 3, 28.01, 12, 112.05], ['7:48', 3, 28.01, 15, 140.06], ['7:58', 5, 46.69, 20, 186.75], ['9:2', 1, 9.34, 21, 196.09], ['9:52', 0, 0.0, 21, 196.09], ['10:0', 1, 9.34, 22, 205.42], ['10:13', 11, 102.71, 33, 308.14], ['10:23', 11, 102.71, 44, 410.85], ['10:31', 11, 102.71, 55, 513.56], ['tweede foto genomen, nu weer terug'], ['11:57', -11, -102.71, 44, 410.85], ['12:4', -11, -102.71, 33, 308.14], ['12:11', -11, -102.71, 22, 205.42], ['12:15', -11, -102.71, 11, 102.71], ['12:18', -11, -102.71, 0, 0.0], ['12:19', -11, -102.71, -11, -102.71], ['12:20', -11, -102.71, -22, -205.42], ['12:23', -11, -102.71, -33, -308.14], ['12:23', -11, -102.71, -44, -410.85], ['12:23', -11, -102.71, -55, -513.56], ['12:43', -11, -102.71, -66, -616.28], ['12:43', -11, -102.71, -77, -718.99], ['12:44', -11, -102.71, -88, -821.7], ['12:48', -11, -102.71, -99, -924.41], ['12:48', -11, -102.71, -110, -1027.12], ['12:49', -11, -102.71, -121, -1129.84], ['12:53', -11, -102.71, -132, -1232.55], ['12:53', -11, -102.71, -143, -1335.26], ['12:54', -11, -102.71, -154, -1437.98], ['12:58', -11, -102.71, -165, -1540.69], ['12:58', -11, -102.71, -176, -1643.4], ['12:59', -11, -102.71, -176, -1643.4], ['12:59', -11, -102.71, -176, -1643.4], ['12:59', -11, -102.71, -176, -1643.4], ['12:59', -11, -102.71, -176, -1643.4], ['12:59', -11, -102.71, -176, -1643.4], ['12:59', -11, -102.71, -176, -1643.4], ['12:59', -11, -102.71, -176, -1643.4], ['12:59', -11, -102.71, -176, -1643.4], ['12:59', -11, -102.71, -176, -1643.4], ['12:59', -11, -102.71, -176, -1643.4], ['12:59', -11, -102.71, -176, -1643.4], ['12:59', -11, -102.71, -176, -1643.4], ['12:59', -11, -102.71, -176, -1643.4], ['12:59', -11, -102.71, -176, -1643.4], ['12:59', -11, -102.71, -176, -1643.4], ['12:59', -11, -102.71, -176, -1643.4], ['12:59', -11, -102.71, -176, -1643.4] -11, -102.71, -187, -1746.11], ['13:4', -11, -102.71, -198, -1848.82], ['13:8', -11, -102.71, -209, -1951.54], ['13:8', -11, -102.71, -220, -2054.25], ['Hier begint hij te bewegen'], ['13:33', -11, -102.71, -231, -2156.96], ['13:39', -11, -102.71, -242, -2259.68], ['13:44', -11, -102.71, -253, -2362.39], ['14:5', -5, -46.69, -258, -2409.08], ['14:13', -5, -46.69, -263, -2455.76], ['14:24', -5, -46.69, -268, -2502.45], ['14:34', -5, -46.69, -273, -2549.14], ['14:44', -5, -46.69, -278, -2595.83], ['3e foto genomen. Hier zit hij weer op de grafiek'], ['15:59', -11, -102.71, -289, -2698.54], ['16:8', -11, -102.71, -300, -2801.25], ['16:11', -11, -102.71, -311, -2903.96], ['16:20', -11, -102.71, -322, -3006.68], ['16:28', -11, -102.71, -333, -3109.39], ['16:34', -11, -102.71, -344, -3212.1], ['16:42', -11, -102.71, -355, -3314.81], ['16:42', -11, -102.71, -366, -3417.52], ['16:43', -11, -102.71, -377, -3520.24], ['200 nm hiervoor zat hij er echt precies helemaal op'], ['18:0', -11, -102.71, -388, -3622.95], ['18:1', -11, -102.71, -399, -3725.66], ['18:10', -11, -102.71, -410, -3828.38], ['18:11', -11, -102.71, -421, -3931.09], ['18:40', -11, -102.71, -432, -4033.8], ['18:40', -11, -102.71, -443, -4136.51], ['18:41', -11, -102.71, -454, -4239.23], ['18:41', -11, -423, -4239.23], ['18:41', -11, -423, -4239.23], ['18:41', -11, -423, -4239.23], ['18:41', -11, -423, -4239.23], ['18:41', -11, -423, -4239.23], ['18:41', -423, -4239.23], ['18:41', -423, -4239.23], ['18:41', -423, -4239.23], ['18:41', -423, -4239.23], ['18:41', -423, -4239.23], ['18:41', -4239.23], ['18:41', -4239.23], ['18:41', -4239.23], ['18:41', -4239.23], ['18:41', -4239.23], ['18:41', -4239.23], ['18:41', -4239.23], ['18:41', -4239.23], ['18:41', -4239.23], ['18:41', -4239.23], ['18:41', -4239.23], ['18:41', -4239.23], ['18:41', -4239.23], ['18:41', -4239.23], ['18:41', -4239.23], ['18:41', -4239.23], [' -465, -4341.94], ['18:41', -11, -102.71, -476, -4444.65], ['18:52', -11, -102.71, -487, -4547.36], ['18:52', -11, -102.71, -498, -4650.08], ['18:52', -11, -102.71, -509, -4752.79], ['18:53', -11, -102.71, -520, -4855.5], ['18:53', -11, -102.71, -531, -4958.21], ['18:60', -11, -102.71, -542, -5060.92], ['18:60', -11, -102.71, -553, -5163.64], ['19:0', -11, -102.71, -564, -5266.35], ['19:0', -11, -102.71, -575, -5369.06], ['19:1', -11, -102.71, -586, -5471.78],['19:8', -11, -102.71, -597, -5574.49], ['19:8', -11, -102.71, -608, -5677.2], ['19:8', -11, -102.71, -619, -5779.91],['19:9', -11, -102.71, -630, -5882.62], ['19:9', -11, -102.71, -641, -5985.34], ['Hier er weer naar toe'], ['20:21', 11, 102.71, -630, -5882.62], ['20:28', 11, 102.71, -619, -5779.91], ['20:33', 11, 102.71, -608, -5677.2], ['20:38', 11, 102.71, -597, -5574.49], ['20:43', 11, 102.71, -586, -5471.78], ['20:47', 11, 102.71, -575, -5369.06], ['Weer de eerste 200-300 veranderingen in het spectrum, daarna niet meer'], ['21:8', 11, 102.71, -564, -5266.35], ['21:8', 11, 102.71, -553, -5163.64], ['21:14', 11, 102.71, -542, -5060.92], ['21:14', 11, 102.71, -531, -4958.21], ['21:18', 11, 102.71, -520, -4855.5], ['21:18', 11, 102.71, -509, -4752.79], ['21:23', 11, 102.71, -498, -4650.08], ['21:24', 11, 102.71, -487, -4547.36], ['21:28', 11, 102.71, -476, -4444.65], ['21:28', 11, 102.71, -465, -4341.94], ['21:33', 11, 102.71, -454, -4239.23], ['21:33', 11, 102.71, -443, -4136.51], ['21:38', 11, 102.71, -432, -4033.8], ['21:38', 11, 102.71, -421, -3931.09], ['Hier komen er veranderingen in het spectrum'], ['22:0', 11, 102.71, -410, -3828.38], ['22:4', 11, 102.71, -399, -3725.66], ['22:4', 11, 102.71, -388, -3622.95], ['22:9', 11, 102.71, -377, -3520.24], ['22:9', 11, 102.71, -366, -3417.52], ['22:13', 11, 102.71, -355, -3314.81], ['22:14', 11, 102.71, -344, -3212.1], ['22:19', 11, 102.71, -333, -3109.39], ['22:20', 11, 102.71, -322, -3006.68], ['22:24', 11, 102.71, -311, -2903.96], ['22:24', 11, 102.71, -300, -2801.25], ['22:33', 11, 102.71, -289, -2698.54], ['22:34', 11, 102.71, -278, -2595.83], ['22:39', 11, 102.71, -267, -2493.11], ['22:39', 11, 102.71, -256, -2390.4], ['22:45', 11, 102.71, -245, -2287.69], ['22:45', 11, 102.71, -234, -2184.98], ['22:49', 11, 102.71, -223, -2082.26], ['22:49', 11, 102.71, -212, -1979.55], ['22:54', 11, 102.71, -201, -1876.84], ['22:54', 11, 102.71, -190, -1774.12], ['22:59', 11, 102.71, -179, -1671.41], ['22:59', 11, 102.71, -168, -1568.7], ['23:4', 11, 102.71, -157, -1465.99], ['23:4', 11, 102.71, -146, -1363.28], ['23:14', 11, 102.71, -135, -1260.56], ['23:14', 11, 102.71, -124, -1157.85], ['23:24', 11, 102.71, -113, -1055.14], ['23:24', 11, 102.71, -102, -952.42], ['23:30', 11, 102.71, -91, -849.71], ['23:30', 11, 102.71, -80, -747.0], ['23:34', 11, 102.71, -69, -644.29], ['23:34', 11, 102.71, -58, -541.58], ['Hier lijkt hij er zo goed als weer op te zitten. Zie foto '], ['24:40', 11, 102.71, -47, -438.86], ['24:47', 11, 102.71, -36, -336.15], ['24:55', 11, 102.71, -25, -233.44], ['25:2', 11, 102.71, -14, -130.72], ['25:10', 11, 102.71, -3, -28.01], ['25:16', 11, 102.71, 8, 74.7], ['25:21', 11, 102.71, 19, 177.41], ['laatste foto, niet ena laatste']]

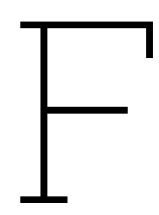
E.4. First Cold System Test, Test 1 Motor Inputs

[Time, Moved Steps, Moved Distance, Steps Position, Theoretical Linear Postion] ['0:60', -11, -102.71, -11, -102.71] ['1:0', -11, -102.71, -22, -205.42] ['1:1', -11, -102.71, -33, -308.14] ['1:1', -11, -102.71, -44, -410.85] ['1:17', 11, 102.71, -33, -308.14] ['1:17', 11, 102.71, -22, -205.42] ['1:18', 11, 102.71, -11, -102.71] ['1:18', 11, 102.71, 0, 0.0] ['1:25', 11, 102.71, 11, 102.71] ['1:26', 11, 102.71, 22, 205.42] ['1:31', -11, -102.71, 11, 102.71] ['1:31', -11, -102.71, 0, 0.0] ['1:32', -11, -102.71, -11, -102.71] ['1:32', -11, -102.71, -22, -205.42] ['1:33', -214, -1998.22, -236, -2203.65] ['1:39', -214, -1998.22, -450, -4201.88] ['1:47', -214, -1998.22, -664, -6200.1] ['1:52', -214, -1998.22, -878, -8198.33] ['1:57', -214, -1998.22, -1092, -10196.55] ['2:2', -214, -1998.22, -1306, -12194.78] ['3:35', -214, -1998.22, -1520, -14193.0] ['3:46', -214, -1998.22, -1734, -16191.22] ['3:55', -214, -1998.22, -1948, -18189.45] ['4:23', -11, -102.71, -1959, -18292.16] ['4:27', -11, -102.71, -1970, -18394.88] ['4:28', -11, -102.71, -1981, -18497.59] ['4:28', -11, -102.71, -1992, -18600.3] Position Reset Write note: Here it has the same shape as the optimal shape in previous plots during the warm experiments. Picture taken ['10:21', -214, -1998.22, -214, -1998.22] ['10:34', -214, -1998.22, -428, -3996.45] ['11:5', -214, -1998.22, -642, -5994.68] Write note:Foto gemaakt. Er was wat creep en bewoog wat terug. Dit is de uiteindelijke vorm van de graph. Andere grafiek verborgen ['16:6', -214, -1998.22, -856, -7992.9] ['16:45', -214, -1998.22, -1070, -9991.12] Write note:Foto gemaakt. Nu duidelijk resultaat. vanaf hier weer terug ['20:39', 11, 102.71, -1059, -9888.41] ['20:39', 11, 102.71, -1048, -9785.7] ['21:35', 11, 102.71, -1037, -9682.99] ['21:36', 11, 102.71, -1026, -9580.28] ['22:2', 11, 102.71, -1015, -9477.56] ['22:2', 11, 102.71, -1004, -9374.85] ['22:3', 11, 102.71, -993, -9272.14] ['22:11', 11, 102.71, -982, -9169.43] ['22:15', 11, 102.71, -971, -9066.71] ['22:15', 11, 102.71, -960, -8964.0] Write note: Eerste paar 200-400nm had hij beweging, nu niet meer ['24:52', 11, 102.71, -949, -8861.29] ['24:52', 11, 102.71, -938, -8758.58] ['24:57', 11, 102.71, -927, -8655.86] ['24:58', 11, 102.71, -916, -8553.15] ['24:58', 11, 102.71, -905, -8450.44] ['25:2', 11, 102.71, -894, -8347.72] ['25:3', 11, 102.71, -883, -8245.01] ['25:23', 11, 102.71, -872, -8142.3] ['25:27', 11, 102.71, -861, -8039.59] ['25:32', 11, $102.71, -850, -7936.88] \ ['25:33', 11, 102.71, -839, -7834.16] \ ['25:47', 11, 102.71, -828, -7731.45] \ ['25:48', 11, 102.$ 102.71, -817, -7628.74] ['26:2', 11, 102.71, -806, -7526.02] ['26:3', 11, 102.71, -795, -7423.31] ['26:8', 11, 102.71, -784, -7320.6] ['26:8', 11, 102.71, -773, -7217.89] ['26:13', 11, 102.71, -762, -7115.18] ['26:13', 11, 102.71, -751, -7012.46] ['26:18', 11, 102.71, -740, -6909.75] ['26:19', 11, 102.71, -729, -6807.04] Write note: Vanaf hier kleine beweging ['26:48', 11, 102.71, -718, -6704.32] ['26:48', 11, 102.71, -707, -6601.61] ['26:53', 11, 102.71, -696, -6498.9] ['26:53', 11, 102.71, -685, -6396.19] ['26:59', 11, 102.71, -674, -6293.48] ['26:59', 11, 102.71, -663, -6190.76] Write note: Hier de eerste grote shift in het spectrum ['27:28', 11, 102.71, -652, -6088.05] ['27:28', 11, 102.71, -641, -5985.34] ['27:43', 11, 102.71, -630, -5882.62] ['27:43', 11, 102.71, -619, -5779.91] ['27:50', 11, 102.71, -608, -5677.2] ['27:50', 11, 102.71, -597, -5574.49] ['27:58', 11, 102.71, -586, -5471.78] ['27:59', 11, 102.71, -575, -5369.06] ['27:59', 11, 102.71, -564, -5266.35] ['28:8', 11, 102.71, -553, -5163.64] ['28:9', 11, 102.71, -542, -5060.92] ['28:9', 11, 102.71, -531, -4958.21] ['29:39', 11, 102.71, -520, -4855.5] ['29:39', 11, 102.71, -509, -4752.79] ['29:39', 11, 102.71, -498, -4650.08] ['29:45', 11, 102.71, -487, -4547.36] ['29:45', 11, 102.71, -476, -4444.65] ['29:45', 11, 102.71, -465, -4341.94] ['29:50', 11, 102.71, -454, -4239.23] ['29:50', 11, $102.71, -443, -4136.51] \ ['29:50', 11, 102.71, -432, -4033.8] \ ['29:59', 11, 102.71, -421, -3931.09] \ ['29:59', 11, 102.71, -432, -432] \ ['29:59', 11, 102.71, -432, -432] \ ['29:59', 11, 102.71, -432] \ ['29:59', 11, 102.71, -432] \ ['29:59', 11, 102.71, -432] \ ['29:59', 11, 102.71, -432] \ ['29:59', 11, 102.71, -432] \ ['29:59', 11, 102.71, -432] \ ['29:59', 11, 102.71, -432] \ ['29:59', 11, 102.71, -432] \ ['29:59', 11, 102.71, -432] \ ['29:59', 11, 102.71, -432] \ ['29:59', 11, 102.71, -432] \ ['29:59', 11, 102.71, -432] \ ['29:59', 11, 102.71, -432]$ 102.71, -410, -3828.38] ['29:60', 11, 102.71, -399, -3725.66] ['30:9', 11, 102.71, -388, -3622.95] ['30:9', 11, 102.71, -377, -3520.24] ['30:10', 11, 102.71, -366, -3417.52] ['30:22', 214, 1998.22, -152, -1419.3] ['30:34', 214, 1998.22, 62, 578.93] Write note: Hij zit er hier al basically op. Zelfs al een stukje er over heen. Foto is gemaakt ['32:23', 11, 102.71, 73, 681.64] ['32:30', 11, 102.71, 84, 784.35] ['32:30', 11, 102.71, 95, 887.06] ['32:50', 11, 102.71, 106, 989.78] ['32:51', 11, 102.71, 117, 1092.49] Write note:Foto gemaakt, dit is te ver operation canceled (And restarted) Write note:Perongelijk beeindigd, Zonder dat ie aangesloten is weer op zelfde uitgangspunt gezet ['1:22', -11, -102.71, 106, 989.78] ['1:27', -11, -102.71, 95, 887.06] ['1:32', -11, -102.71, 84, 784.35] ['1:32', -11, -102.71, 73, 681.64] ['1:37', -11, -102.71, 62, 578.93] ['1:37', -11, -102.71, 51, 476.21] ['1:42', -11, -102.71, 40, 373.5] ['1:42', -11, -102.71, 29, 270.79] ['1:42', -11, -102.71, 18, 168.08] ['1:47', -11, -102.71, 7, 65.36] ['1:47', -11, -102.71, -4, -37.35] Write note: Deze keer geen beweging bij de eerste paar honderd nm ['4:30', -11, -102.71, -15, -140.06] ['4:31', -11, -102.71, -26, -242.78] ['6:36', -11, -102.71, -37, -345.49 ['6:39', -11, -102.71, -48, -448.2]'(6:39', -11, -102.71, -59, -550.91]'(6:39', -11, -102.71, -70, -653.62] [7:46', -11, -102.71, -81, -756.34] [7:46', -11, -102.71, -92, -859.05] [7:55', -11, -102.71, -103, -961.76] [8:9', -11, -102.71, -103, -961.76]-214, -1998.22, -317, -2959.99 ['8:28', -11, -102.71, -328, -3062.7] ['8:31', -11, -102.71, -339, -3165.41] ['8:32', -11, -102.71, -350, -3268.12] ['8:37', -214, -1998.22, -564, -5266.35] Write note:Hij zat vast, en hier schoot hij ineens er te ver voorbij. Voor de laatste inputwas ie nog steeds te dichtbij. Toen schoot ie veel te ver. Continued

E.5. First Cold System Test, Test 2 Motor Inputs

[Time, Moved Steps, Moved Distance, Steps Position, Theoretical Linear Postion] ['0:11', 214, 1998.22, 214, 1998.22] ['0:19', 214, 1998.22, 428, 3996.45] ['0:24', 214, 1998.22, 642, 5994.68] ['0:24', 214, 1998.22, 856, 7992.9] ['0:29', 214, 1998.22, 1070, 9991.12] ['0:35', 214, 1998.22, 1284, 11989.35] ['0:44', 214, 1998.22, 1498, 13987.58] ['0:54', 214, 1998.22, 1712, 15985.8] ['1:0', 11, 102.71, 1723, 16088.51] ['1:1', 11, 102.71, 1734, 16191.22] ['1:1', 11, 102.71, 1745, 16293.94] ['1:1', 11, 102.71, 1756, 16396.65] ['1:1', 11, 102.71, 1767, 16499.36] ['1:10', 11, 102.71, 1778, 16602.08] ['1:10', 11, 102.71, 1789, 16704.79] ['1:10', 11, 102.71, 1800, 16807.5] ['1:10', 11, 102.71, 1811, 16910.21] ['1:10', 11, 102.71, 1822, 17012.92] ['1:26', 11, 102.71, 1833, $17115.64]\ ['1:27',\ 11,\ 102.71,\ 1844,\ 17218.35]\ ['1:27',\ 11,\ 102.71,\ 1855,\ 17321.06]\ ['1:27',\ 11,\ 102.71,\ 1866,\ 17321.06]$ 17423.78] ['1:27', 11, 102.71, 1877, 17526.49] ['1:36', 11, 102.71, 1888, 17629.2] ['1:43', 11, 102.71, 1899, 17731.91] Position Reset Write note:Foto gemaakt. Heeft nu een dal op 1550 ['4:24', 11, 102.71, 11, 102.71] ['4:29', 11, 102.71, 22, 205.42] ['4:33', 11, 102.71, 33, 308.14] ['4:34', 11, 102.71, 44, 410.85] ['4:39', 11, 102.71, 55, 513.56] ['4:39', 11, 102.71, 66, 616.28] ['4:53', 11, 102.71, 77, 718.99] ['4:54', 11, 102.71, 88, 821.7] ['5:3', 11, 102.71, 99, 924.41] ['5:3', 11, 102.71, 110, 1027.12] Write note:Foto, hier is ie duidelijk te ver. Vanaf hier weer terug ['6:32', -11, -102.71, 99, 924.41] ['6:39', -11, -102.71, 88, 821.7] ['6:44', -11, -102.71, 77, 718.99] ['6:44', -11, -102.71, 66, 616.28] ['6:45', -11, -102.71, 55, 513.56] ['6:49', -11, -102.71, 44, 410.85] ['6:49', -11, -102.71, 33, 308.14 ['6:50', -11, -102.71, 22, 205.42] ['6:54', -11, -102.71, 11, 102.71] ['6:54', -11, -102.71, 0, -102.71, 11, 102.71] ['6:54', -11, -102.71, 0, -102.71, 11, 102.71] 0.0] ['6:55', -11, -102.71, -11, -102.71] ['6:59', -11, -102.71, -22, -205.42] ['6:59', -11, -102.71, -33, -308.14] [6:60', -11, -102.71, -44, -410.85] [7:4', -11, -102.71, -55, -513.56] [7:5', -11, -102.71, -66, -616.28] [7:5', -11, -102.71, -66, -616.28]-102.71, -77, -718.99 ['7:10', -11, -102.71, -88, -821.7] ['7:10', -11, -102.71, -99, -924.41] ['7:10', -11, -102.71, -99, -924.41] ['7:10', -11, -102.71, -99, -924.41] -110, -1027.12] [7:15', -11, -102.71, -121, -1129.84] [7:15', -11, -102.71, -132, -1232.55] [7:15', -11, -102.71, -132, -1232.55] -143, -1335.26] ['7:20', -11, -102.71, -154, -1437.98] ['7:20', -11, -102.71, -165, -1540.69] ['7:20', -11, -102.71, -102-176, -1643.4] ['7:24', -11, -102.71, -187, -1746.11] ['7:25', -11, -102.71, -198, -1848.82] ['7:25', -11, -102.71, -198, -1848.82] -209, -1951.54] ['7:30', -11, -102.71, -220, -2054.25] ['7:30', -11, -102.71, -231, -2156.96] ['7:30', -11, -102.71, -102-242, -2259.68] ['7:35', -11, -102.71, -253, -2362.39] ['7:35', -11, -102.71, -264, -2465.1] ['7:35', -11, -102.71, $-275, -2567.81] \ ['7:40', -11, -102.71, -286, -2670.52] \ ['7:40', -11, -102.71, -297, -2773.24] \ ['7:40', -11, -102.71, -277, -2773.24] \ ['7:40', -11, -102.71, -277, -2773.24] \ ['7:40', -11, -102.71, -277, -2773.24] \ ['7:40', -11, -10$ -308, -2875.95] [7:45', -11, -102.71, -319, -2978.66] [7:45', -11, -102.71, -330, -3081.38] [7:45', -11, -102.71, -310-341, -3184.09] ['7:50', -11, -102.71, -352, -3286.8] ['7:50', -11, -102.71, -363, -3389.51] ['7:50', -11, -102.71, -374, -3492.22] Write note: Hier de eerste beweging in het spectrum ['8:20', 11, 102.71, -363, -3389.51] ['8:25', 11, 102.71, -352, -3286.8] Write note:En ineens zat ie volledig op het optimale spectrum die eerder was opgeslagen. En dat met 1 100nm stap. Foto gemaakt ['10:17', -11, -102.71, -363, -3389.51] ['10:22', -11, -102.71, -374, -3492.22] ['10:27', -11, -102.71, -385, -3594.94] ['10:32', -11, -102.71, -396, -3697.65] ['10:32', -11, -102.71, -407, -3800.36 ['10:38', -11, -102.71, -418, -3903.08] ['10:39', -11, -102.71, -429, -4005.79] ['10:43', -11, -102.71, -407, -3800.36] ['10:38', -11, -102.71, -407, -3800.36] ['10:38', -11, -102.71, -418, -3903.08] ['10:39', -11, -102.71, -429, -4005.79] ['10:43', -11, -102.71, -407, -3800.36] ['10:38', -11, -102.71, -418, -3903.08] ['10:39', -11, -102.71, -429, -4005.79] ['10:49', -11, -102.71, -418, -3903.08] ['10:39', -11, -102.71, -429, -4005.79] ['10:49', -11, -102.71, -418, -3903.08] ['10:39', -11, -102.71, -419, -4005.79] ['10:49', -11, -102.71, -419, -4005.79] ['10:49', -11, -102.71, -419, -4005.79] ['10:49', -11, -102.71, -419, -4005.79] ['10:49', -11, -419,-102.71, -440, -4108.5] ['10:43', -11, -102.71, -451, -4211.21] Write note: Nu verschuift hij niet meer. Hij zit nu wel mooier op het spectrum van eerder ['11:18', -11, -102.71, -462, -4313.92] ['11:18', -11, -102.71, -473, -4416.64] ['11:23', -11, -102.71, -484, -4519.35] ['11:24', -11, -102.71, -495, -4622.06] ['11:28', -11, -102.71, -506, -4724.78 ['11:28', -11, -102.71, -517, -4827.49 ['11:28', -11, -102.71, -528, -4930.2 ['11:29', -11, -102.71, -539, -5032.91 ['11:29', -11, -102.71, -550, -5135.62] ['11:33', -11, -102.71, -561, -5238.34] ['11:33', -11, -102.71, -572, -5341.05] ['11:33', -11, -102.71, -583, -5443.76] ['11:33', -11, -102.71, -594, -5546.48] ['11:34', -11, -102.71, -605, -5649.19] Write note: Nu is ie verschoven Write note: Foto is gemaakt Write note: Vanaf hier weer terug ['14:14', 11, 102.71, -594, -5546.48] ['14:14', 11, 102.71, -583, -5443.76] ['14:14', 11, 102.71, -572, -5341.05] ['14:24', 11, 102.71, -561, -5238.34] ['14:24', 11, 102.71, -550, -5135.62] ['14:29', 11, 102.71, -539, -5032.91] ['14:29', 11, 102.71, -528, -4930.2] ['14:44', 11, 102.71, -517, -4827.49] ['14:44', 11, 102.71, -506, -4724.78] ['16:20', 11, 102.71, -495, -4622.06] ['16:20', 11, 102.71, -484, -4519.35] ['16:20', 11, 102.71, -473, -4416.64] ['16:25', 11, 102.71, -462, -4313.92] ['16:25', 11, 102.71, -451, -4211.21] ['16:25', 11, 102.71, -440, -4108.5] ['16:30', 11, 102.71, -429, -4005.79] ['16:30', 11, 102.71, -418, -3903.08] ['16:30', 11, 102.71, -407, -3800.36]['16:30', 11, 102.71, -396, -3697.65] ['16:35', 11, 102.71, -385, -3594.94] ['16:35', 11, 102.71, -374, -3492.22]['16:35', 11, 102.71, -363, -3389.51] ['16:35', 11, 102.71, -352, -3286.8] ['16:40', 11, 102.71, -341, -3184.09] ['16:40', 11, 102.71, -330, -3081.38] ['16:40', 11, 102.71, -319, -2978.66] ['16:45', 11, 102.71, -308, -2875.95]['16:45', 11, 102.71, -297, -2773.24] ['16:45', 11, 102.71, -286, -2670.52] ['16:45', 11, 102.71, -275, -2567.81]['16:50', 11, 102.71, -264, -2465.1] ['16:51', 11, 102.71, -253, -2362.39] ['16:51', 11, 102.71, -242, -2259.68] $['16:51', 11, 102.71, -231, -2156.96] \ ['16:55', 11, 102.71, -220, -2054.25] \ ['16:55', 11, 102.71, -209, -1951.54]$ ['16:55', 11, 102.71, -198, -1848.82] ['16:56', 11, 102.71, -187, -1746.11] ['16:60', 11, 102.71, -176, -1643.4] ['16:60', 11, 102.71, -165, -1540.69] ['17:5', 11, 102.71, -154, -1437.98] Write note:Laatste 100nm schoot ie hem ineens voorbij. Hij zat er bij de eerste sweep er op, maar toen ie er nog een keer overheen en toen was ie te ver. Foto gemaakt ['20:31', 11, 102.71, -143, -1335.26] ['20:33', 11, 102.71, -132, -1232.55] ['20:39',

11, 102.71, -121, -1129.84] ['20:39', 11, 102.71, -110, -1027.12] ['20:44', 11, 102.71, -99, -924.41] ['20:44', 11, 102.71, -88, -821.7] ['20:44', 11, 102.71, -77, -718.99] ['20:48', 11, 102.71, -66, -616.28] ['20:49', 11, 102.71, -55, -513.56] ['20:49', 11, 102.71, -44, -410.85] ['20:58', 11, 102.71, -33, -308.14] ['20:58', 11, 102.71, -12, -205.42] ['21:19', 11, 102.71, -11, -102.71] ['21:28', 11, 102.71, 0, 0.0] ['21:34', 11, 102.71, 11, 102.71] Write note:De Andere was een fringe. Hij zit er hier 100Write note:Ging er eerst best ver vanaf, maar toen ging ie er helemaal naar toe Continued



Quick User Manual of System

This manual will explain you how to use the setup for anyone who will use it in the future.

The wiring Copy the wire diagram from subsection 3.1.2, minding to connect the right driver pins to the right arduino pins. The motor is controlled by jumper cables and custom wires are made to converge from a SMA connector at the bottom of the cyrostat, to 4 pins jumper cables halfway the cryostat. The motor is connected to this. Mind the color of the wires, since connecting it the opposite way will cause the motor to rotate in the opposite directing for the input that it is given.

The red and black wires from the driver will be attached to the 12V adapter, minding to connect the red wire in the centre of the connector pin. Connect the 4 jumper cables coming from the driver to the connectors coming from the SMA connector outputs of the cryostat. Once again mind the colors of the wires. Plug the arduino in the computer and the hardware is ready to go.

Setting up the code An Arduino nano clone is used. An extra drives needs to be installed to be able to use it. The drives can be found *here on the tinytronic site*. The Arduino IDE also needs to be installed, *and can be found here*. Also python is required. Spyder in Anaconda3 can be recommended.

Plug the Arduino in the computer you have the IDE and python installed on. In Device Manager you can find the port the Arduino is put in to, and take note of this. In IDE under Tools > Port set it to the right port. And set Tools > board > Arduino AVR Board to 'Arduino Nano'. And Tools > Processor needs to be set to 'ATmega328P (Old Bootloader)'. Copy Paste the code from section B.7 in Appendix B. Upload the code to the Arduino.

Open the python code from section B.8 in Appendix B and set on line 106 the SerialObj to the 'COM#' to the same port you've connected the Arduino to. Also make sure you have the packages serial, time, pynput and numpy installed. Run the code and you can now control the motor with keyboards inputs. The printed instructions will tell you what keyboard inputs to use.

The disassembly The starting point is a fully assembled system. It can either be in the cryostat of standing on the table. The fibre is spring loaded in the system with 3 kg of force (so 30 N). Mind this when taking it apart.

- 1. Remove the 3 screws that hold the frame and the bottom mount together. Lift it up vertically. There is some resistance since the worm gear needs to 'pop out' of the slightly concave worm wheel. This part is not spring loaded.
- 2. At this point it is easier to put the system upside down, so with the PCB closest to the table and the precision screw upwards. Next the clamp of the precision screw bushing will be removed. There is 3 kg of force on this parts, so I recommend to first removed two screws that are diagonal across each other. Carefully remove the last two screws while pressing down on the bottom of the precision screw. NB: Do not press down on the worm wheel, since this is not firmly attached to the precision screw. If the screws are out, slowly let the spring push the part upwards. The fibre now will come out of the sleeve.

- 3. Take the fibre mount out of the spring also pull the spring out of the system if you want to change the PCB
- 4. Removed the PCB Spacer carefully not to damage the bonding wires and sleeve.

The assembly This is roughly the same procedure as the disassembly, but in reverse order. A few different things need to be notes. Also the hygiene needs to be taken in to account, since the contact surfaces between different copper parts need to stay clean to keep the thermal conductivity high.

- 1. First put the PCB mount in the frame. 1 of the threads is broken, so only 3 screw can go in.
- 2. Place the PCB and the PCB spacer on the PCB, being careful not to touch the bonding wires.
- 3. Clamp the spring in the PCB spacer. It is tricky and a bit painful for the fingers to deform the lower coil winding enough. Ask your local Sloper for help if it is not working out. Mind the end of the spring just rests on the PCB mount. This makes sure the spring is vertical since it only rests on the ground surfaced.
- 4. Put the fibre in the fibre mount. Mind that the M2 crews are resting on the metal brim and not on the two cutouts to make sure it is firmly attached. Mind that the orientation of a PM fibres relative to the PCB maters. The line through the two cut outs need to be parallel to the short edge of the detector.
- 5. The clamp for the bushing can be attached in two different orientation, and only one will fit. The head of the bolt is sunken in to the parts. This is done so the edge of the stepper motor doesn't conflict. The other side has a thread sticking out, so mind to put the clamp on it in the right orientation.
- 6. Put the fibre mount in the spring. Keep in mind that it is nicer to have the fibre non on the side of the motor, since the fibre could end up inbetween the gears. Put the clamp and the precision screw above it and carefully press it down by applying force on only the backside of the precision screw. Keep it straight as the fibre needs to go in the sleeve. Once the fibre is in the sleeve is save to press it down all the way. Attached the screw while keeping the precision screw pressed down. Mind that the fiber should still be in the right orientation.
- 7. The worm wheel, if not already attached, needs to be in the right position on the precision screw. There needs to be a 1.3 mm margin between the bushing and the worm wheel when the fibre is on the detector. So first press the fibre mount downwards by hand, and then screw the precision screw downwards until you feel resistance. There is a 3D printed 'spacer' of 1.3 mm thick that can be put between the bushing and the worm wheel while tightening the setscrew.
- 8. Attach the motor with the spacer to the bottom mount, and place it on the cryostat if needed.
- 9. Place the frame on the bottom mount. There is some resistance since the worm gear needs to 'pop in' the slightly concave worm wheel. Attach the three screws to keep everything in place.
- 10. Connect and thermalize all wires, minding the the coax cable to the detectors won't touch the radiation shield.

The setup is now ready for usage.



Figure F.1: If confused, contact Hugo or Rudi.[120]

CAD Drawings

